5-2018

Analysis of Slope Failure on Cochrane Road, Dominica Prior to Hurricane Maria

Audrey Fisher
Clemson University, crafton.audrey@gmail.com

ANALYSIS OF SLOPE FAILURE ON COCHRANE ROAD, DOMINICA PRIOR TO HURRICANE MARIA

A Thesis
Presented to
the Graduate School of
Clemson University

In Partial Fulfillment
of the Requirements for the Degree
Master of Science
Hydrogeology

---

by
Audrey Fisher
May 2018

Accepted by:
Dr. Stephen Moysey, Committee Chair
Scott Brame
Dr. Larry Murdoch

ABSTRACT

The volcanic island Dominica is one of the Windward Islands located near the center of the Lesser Antilles. It contains rugged peaks with steep slopes and has a humid tropical climate. Dominica has four distinct soil types (kandoid, smectoid, allophane latosolic, and allophane podzolic). The distribution of these soils is dictated by climatic factors that influence the degree and depth of leaching. Along with the geology and climate of Dominica, these soils play a large role in determining the prevalence of landslides in different portions of the island. The landslides are typically triggered by high intensity rainfall during tropical storms and hurricanes and since the soil types have varying porosity and permeability, they will react differently to the high rainfall levels.

Several recent slope failures were investigated in January 2017 to gain insights into the nature of landslides in tropical settings on island arcs that are experiencing rapid uplift due to their active subduction zone setting. The area selected for investigation is representative of many sites on the island that have roads cutting into slopes at the angle of repose. The roads are often buried and damaged by material from slope failures. The selected slope failure sites are located along a ½ mile section of road and share similar climate, associated soil types, and topographic setting. The two sites selected for further investigations (Forested Site and Lemongrass Site) differ in their vegetative cover (forested vs covered in lemongrass). This investigation analyzed the similarities and differences between the selected sites in order to make a comparison between the failure mechanisms at each site. The Forested Site consists of slope failures CR2 and CR3, while the Lemongrass Site consists of slope failure CR6 and stable slope LG. At these sites, soil

cores were collected and taken to the laboratory for soil characterization (plasticity, soil color, and soil name), XRD analysis, and direct shear strength testing. A slope stability analysis was conducted using a limit equilibrium approach. Soil characterization was conducted using the USDA Soil Texturing Field Flow Chart.

Results indicate that the two sites are underlain by sandy to silty clay soils with a medium high to high plasticity. XRD analysis revealed a halloysite rich matrix, which is indicative of kandoid soils. Kandoid soils are highly permeable soils found in the oldest volcanic areas and in areas of high rainfall (2100-3750mm) where leaching is moderate but continuous. Drained direct shear tests were completed to determine the effective friction angle and cohesion. The LG sample had a 32 degree friction angle and a value of 128 psf for cohesion. The CR6 sample had a 26 degree friction angle and a value of 159 psf for cohesion. The CR2 sample had a 47 degree friction angle and a value of 320 psf for cohesion. The CR3 sample had a 47 degree friction angle with a value of 0 psf for cohesion after correcting for a calculated negative cohesion which is not possible. These values served as the basis for inputs into a limit equilibrium slope stability analysis using the infinite slope method.

Two different types of calculations can be done using the infinite slope method: forward calculations and back calculations. Forward calculations are used to find the factor of safety for slopes that haven't failed before. For slopes that have failed before, two different back calculations can be done by rearranging the original formula to solve for 1) the friction angle needed for the current slope to stay stable under different conditions, and 2) the height above or below the failure surface that the water table

reached when the initial failure occurred. The forward calculations for the slope stability analysis of slope LG at the Lemongrass Site produced a factor of safety greater than 1 which indicates that slope LG is predicted to remain stable. Results of the back calculation analysis determined that at CR2 and CR3 the water table was located an average of 1 ft above the failure surface at the time the slope failed. This means that failure occurred before seepage conditions (seepage conditions occur when the water table is located at the ground surface due to prolonged and heavy rainfall conditions) were fully reached. For slope failure CR6, the water table was calculated at 4.3 ft below the failure surface at the time of failure, which implies that failure occurred before general conditions (general conditions occur when the water table is at the same elevation as the failure surface) were reached. The back calculation analysis also revealed that the slopes must have an effective friction angle of at least 36˚ (measured from horizontal) to remain stable under general conditions (where the water table is at the failure surface) and a friction angle greater than 62˚ for seepage conditions. Slopes with friction angles less than 36˚ will be more likely to fail under general conditions, while those with friction angles less than 62˚ will be more likely to fail under seepage conditions. Since most clays and silty clays have friction angles with maximum values around 30˚, it is anticipated that these slopes would fail under seepage conditions.

ACKNOWLEDGMENTS

A special thanks goes out to Dr. Ronald D. Andrus and his student Barnabas Bwambale of the Glenn Department of Civil Engineering at Clemson University. Without their guidance and knowledge of direct shear testing and limit equilibrium analysis, this study would not have been possible. I would also like to thank Nancy Osler, the managing director of the Archbold Tropical Research and Education Center, for directing us to the sites on Cochrane Road and for assisting with logistics during our stay on Dominica.

TABLE OF CONTENTS

Table of Contents (Continued)

Page

LIST OF TABLES

List of Tables (cont'd)

Table Page

LIST OF FIGURES

List of Figures (cont'd)

Figure Page

List of Figures (cont'd)

Figure Page

List of Figures (cont'd)

Figure Page

List of Figures (cont'd)

Figure Page

List of Figures (cont'd)

Figure Page

List of Figures (cont'd)

Figure Page

CHAPTER ONE

INTRODUCTION

The volcanic island Dominica is one of the Windward Islands and is located near the center of the Lesser Antilles (Figure 1.1). It is 785 km^2 of andesitic and dacitic volcanic deposits that form rugged peaks with many slopes steeper than 40 degrees (Rouse et al., 1986). In general, the climate is humid tropical but it varies with location

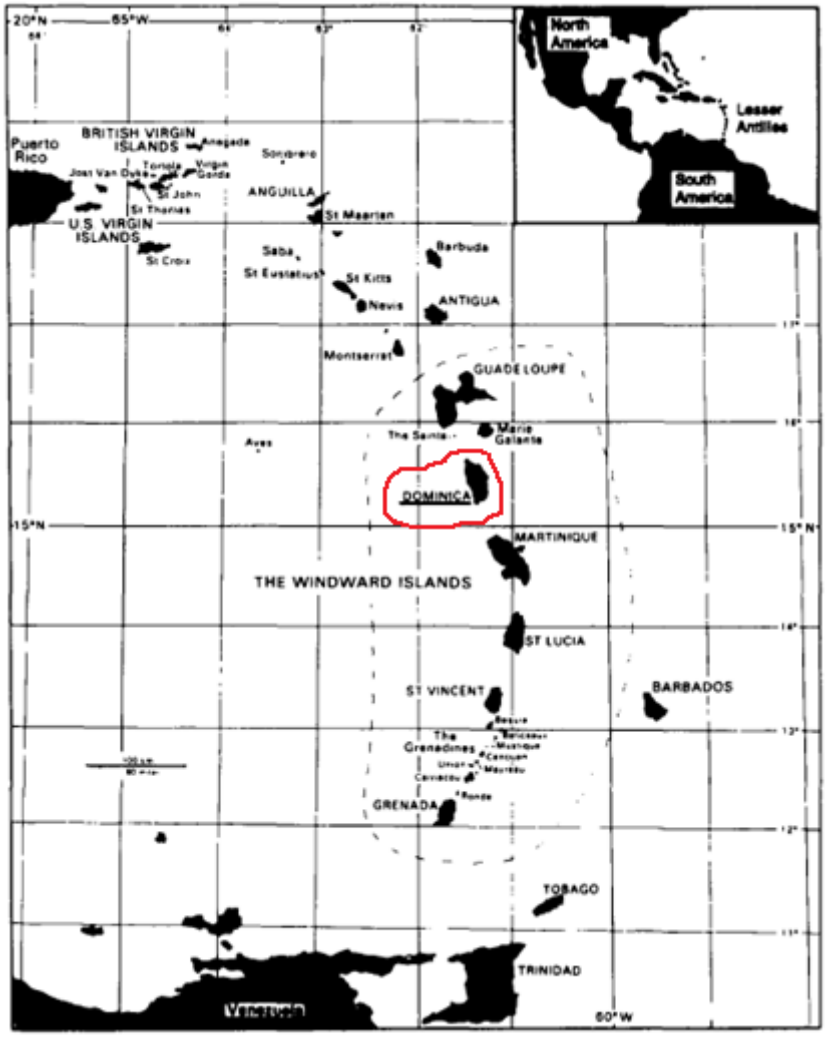

Figure 1.1: Location of Dominica (Modified from Reading, 1991)

due to orographic uplift and rain shadow effects. The western coast receives ~1000 mm/yr rainfall, the eastern coast receives ~2000 mm/yr rainfall and the interior receives up to 10,000 mm/yr rainfall (Reading, 1991) (Figure 1.2b). The vegetation consists of tropical rain forest and dry scrub woodland (Rouse et al., 1986) (Figure 1.2d).

There are four distinct types of soils on Dominica (kandoid, smectoid, allophane latosolic, and allophane podzolic). The distribution of these soils is affected by climatic factors that influence the degree and depth of leaching (Rouse et al., 1986) (Figure 1.2c). Leaching is the loss of soluble components, such as mineral and organic solutes, from the soil caused by percolating water. Effects of leaching include soil acidification and increased opportunities for erosion. Kandoid soils are highly permeable soils found in the oldest volcanic areas and in areas of high rainfall (2100-3750mm) where leaching is moderate but continuous. Smectoid soils have low porosities and very low permeability when wet. They occur on the western coastlands where there is less than 2100 mm of rainfall and leaching rates are low. Allophane latosolic soils are highly porous and are the most abundant soils. They occur in areas of high annual rainfall (3750 mm) with no dry season, which causes intense and uninterrupted leaching (Rouse, 1990). Allophane podzolic soils are the result of extremely high leaching and occur in areas with over 7000 mm of annual rainfall (Rouse et al., 1986).

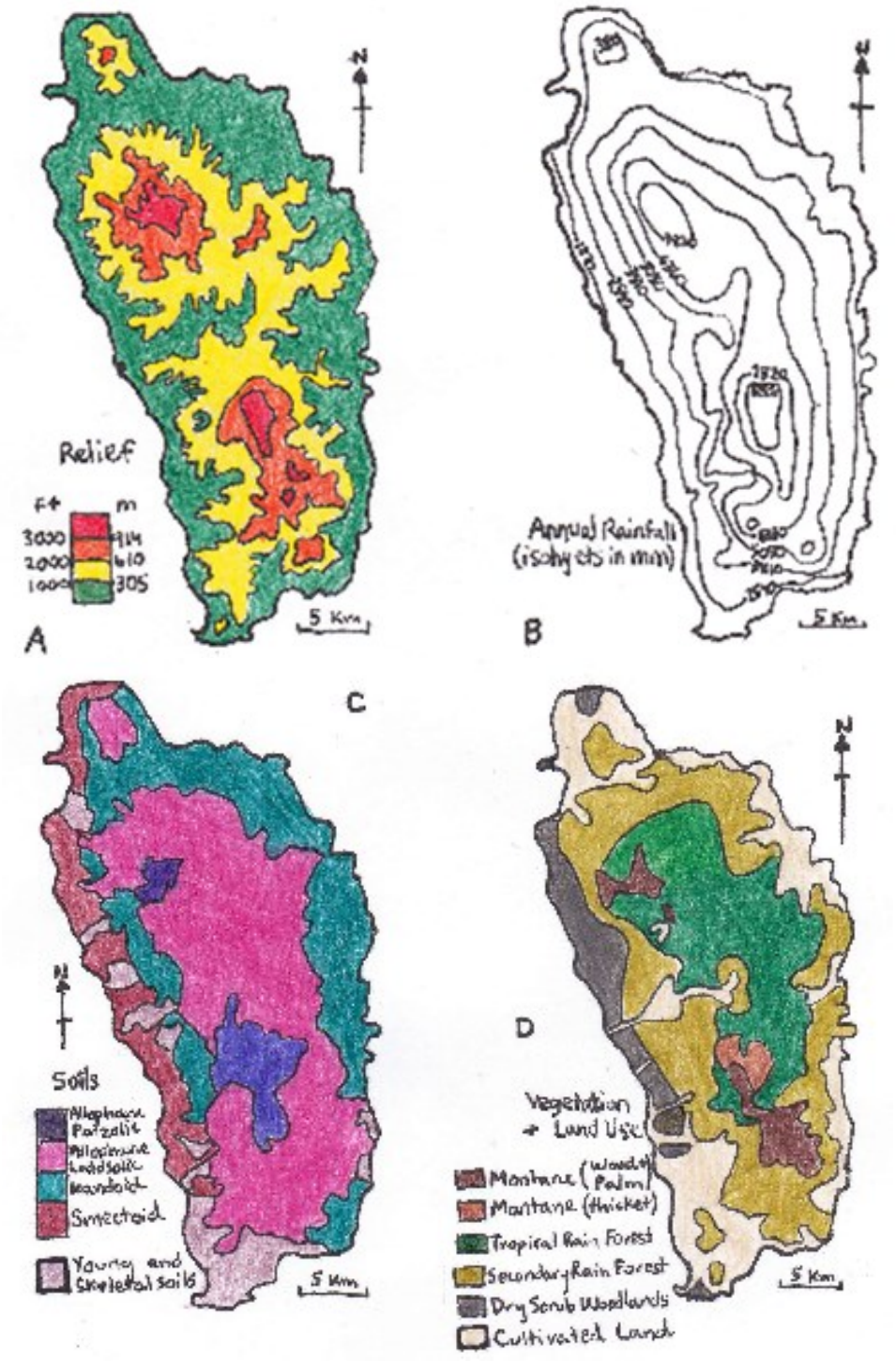

Figure 1.2: Relief, vegetation, rainfall, and soils of Dominica (Modified from Rouse et al., 1986).

The soils and climate described above play a large role in the occurrence of landslides on Dominica. A landslide is a movement of soil, rock, or debris down a slope (Crunden, 1991) (Figure 1.3). The landslides on Dominica are typically triggered by high

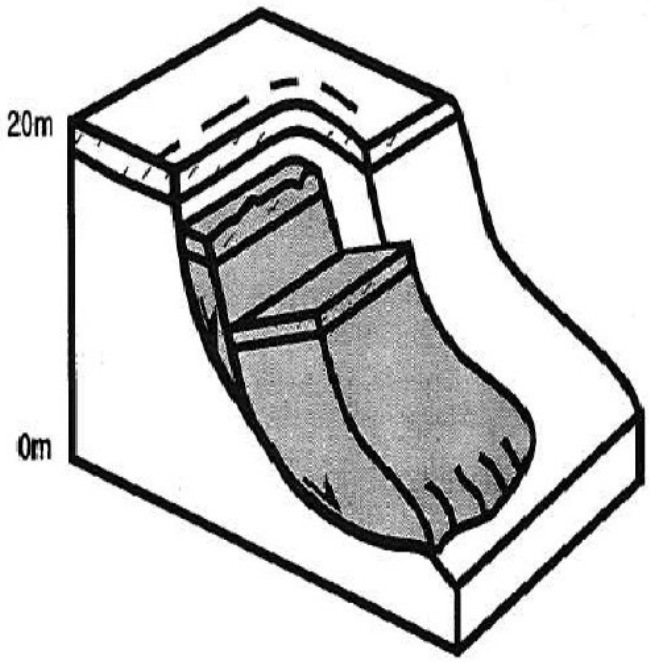

Figure 1.3: A schematic diagram of a landslide (Cooper, 2007).

intensity rainfall during tropical storms and hurricanes (DeGraff et al., 1989), but they can also be triggered by human activity such as deforestation and road cuts (Anderson et al., 2011). Tropical cyclone tracks have shifted southward into the more central and southern islands of the Lesser Antilles since 1959, and the potential for landslides has increased as a result (Rouse et al., 1986). In 1979, Dominica was devastated by Hurricane David (August 29th) and Hurricane Frederic (September 4th). These two storms laid waste to the island's vegetation and resulted in numerous landslides. Hurricane David had winds up to 200 mph and produced rainfall of 105-210 mm. Less than a week later

Hurricane Frederic contributed rainfall of up to 300mm in a day (Rouse et al., 1986). The most recent hurricane prior to this research that impacted the island was Tropical Storm Erika in 2015. During that event Dominica received over 500 mm of rainfall in 10 hours, which produced the most significant flooding since Hurricane David (Ogden, 2016). High rainfall in short periods of time increases pore-water pressure and reduces shear strength in soils. The loss of shear strength, along with the added weight of the water creates the potential for slope failure in shallow soil (DeGraff et al., 1989).

Several recent slope failures were investigated in January 2017 to gain insights into the nature of landslides in tropical settings on island arcs that are experiencing rapid uplift due to their location on an active subduction zone. The area selected for investigation is representative of many sites on the island that have roads cutting into slopes at the angle of repose. The roads are often buried and damaged by material from slope failures. The selected slope failure sites are located along a ½ mile section of road and share similar climate, associated soil types, and topographic setting. The two sites selected for further investigations (Forested Site and Lemongrass Site) differ in their vegetative cover. This investigation analyzed the similarities and differences between the selected sites in order to make a comparison between the failure mechanisms at each site.

CHAPTER TWO

LITERATURE REVIEW

This chapter will review and explain the relevance of the research objectives in the context of prior work and literature, as well as outline the specifics of the topics and methods addressed in the objectives in order give a better understanding of slope failures. Soils are an important component in the slope failure process due to the effects that characteristics like soil structure, composition, and consolidation can have on the shear strength of a slope. Therefore, a portion of this chapter will discuss tropical soil characteristics and shear strength determination from direct shear testing. Other topics include landslide characteristics in tropical settings and slope stability analysis using the limit equilibrium method.

Characteristics of Landslides in the Caribbean

The combination of geologic setting, climate, and slopes in the Caribbean region create conditions suitable for most types of landslides. For the Windward Islands, the common types of landslides are debris flows, debris slides, rockslides, rockfalls, and slumps (Figure 2.1). A slide is a mass movement where there is a distinct zone of weakness that separates the slide material from more stable underlying material. A flow is a rapid mass movement in which a combination of rock, loose soil, organic matter, and water mobilize as a slurry flowing downslope. A fall is an abrupt movement of material, such as rocks or boulders, which becomes detached from slopes or cliffs. A slump is a type of slide where there is rotational failure with parallel curved planes of movement.

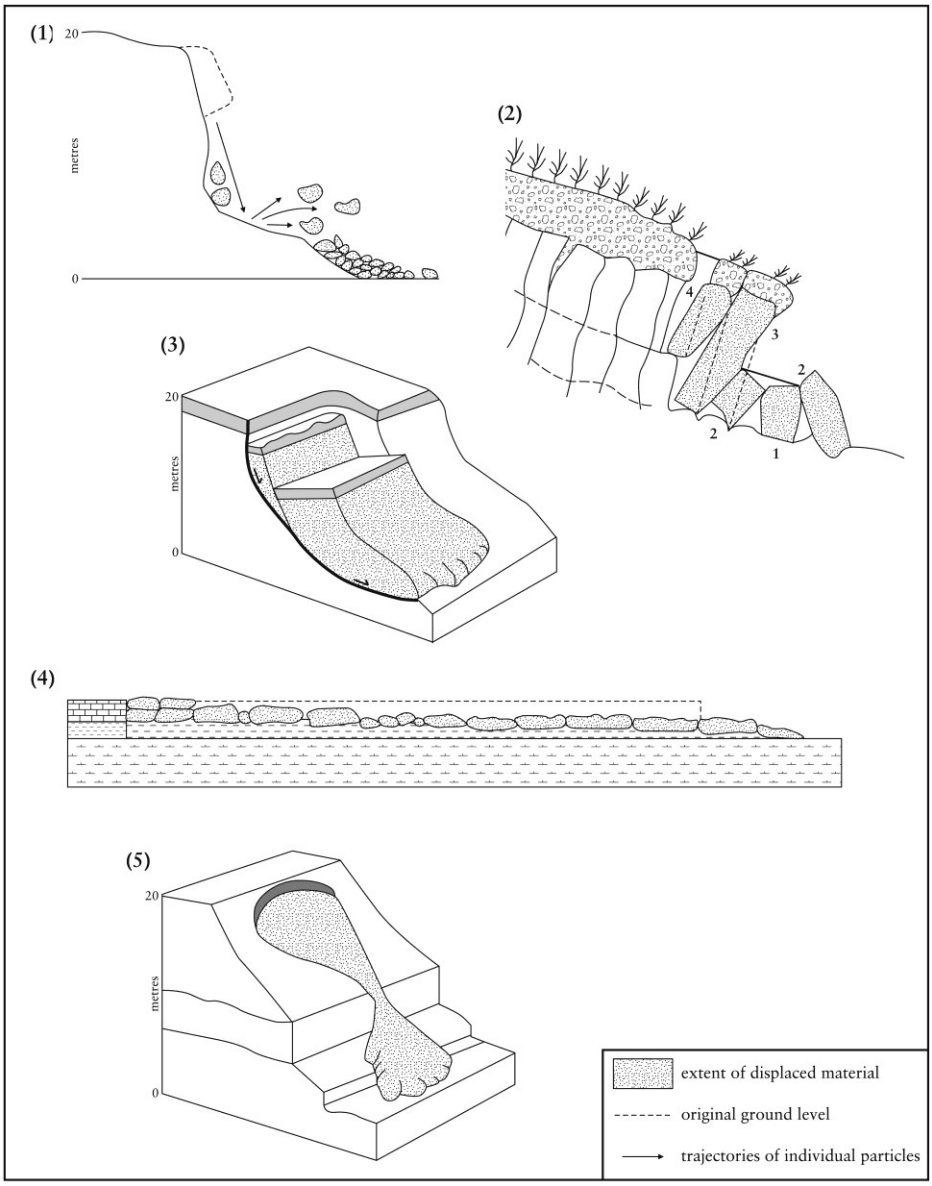

Figure 2.1: Different types of landslides. The types shown are a fall (1), a topple (2), a slide (3), a spread (4), and a flow (5) (Cooper, 2007).

In a comparison of landslides on Dominica, St. Vincent, and St. Lucia, DeGraff et al. (1989) found that the majority of slides were debris flows which are common on the many mountainous slopes in the Windward Islands. In DeGraff's landslide inventories of the three islands, Dominica had the highest total number of landslides and the largest

average size of landslide (Table 2.1). He estimated that almost two percent of Dominica's land surface has been disturbed by landslides. The next most common landslide types in the Windward Islands are rockslides and rockfalls, and the least common are slumps and rotational failures, which are a type of slide where the failure surface is curved concavely upward. The rotational failures are generally small and limited to areas with cultivated slopes or road cuts (DeGraff, 1989).

Island	Number of landslides	Landslide size (in hectacres)		Landslide Density (per sq. km)	Terrain Disturbed (in percent)
		Average	Largest		
St. Vincent	475	0.5	4.0	1.4	1
St. Lucia	430	3.0	5.0	0.7	2
Dominica	980	4.0	12.5	1.2	2

Table 2.1: Number, size, and distribution by past landslides on St. Vincent, St. Lucia, and Dominica (Modified from DeGraff et al., 1989).

The geology and materials of the slopes on Windward Islands play a big role in the development of the landslides (Yifru, 2015). Slopes are close to the angle of repose for underlying materials and only small changes in stability conditions would be needed for the slopes to become close to failure. The volcanic deposits within the slopes are usually thick and are made of alternating layers of ash, lava, or breccia (DeGraff et al., 1989). Volcanic bedrock is more susceptible to deep weathering due to tropical climates and produces weathered volcanic soil that is weaker than the original bedrock (Van Westin, 2016). The failure plane commonly coincides with contacts between soil and underlying bedrock, and in these instances the failure plane is defined by the surface of

the bedrock (DeGraff et al., 1989). Shallow depth failures of 2 meters or less were noted on Martinique and Dominica by Walsh (1985) and Faugeres (1966). On St. Lucia, Prior and Ho (1972) found that the debris slides with failure depths of 2 meters or less typically occur on slopes steeper than 35 percent. The soil overlying the bedrock in St. Lucia is commonly found to contain large amounts of clay including kaolinite, montmorillonite, and occasionally chlorite and illite. On Dominica, the clays can influence the intensity of rainfall that is needed to induce landslides due to differences in porosity and permeability (Rouse et al., 1986).

DeGraff et al. (1989), Rouse (1990), and Rouse et al. (1986) all agree that the most efficient means for triggering the landslides in the Caribbean are the large and intense prolonged rainfall events from tropical storms and hurricanes. For example, during tropical storm Erica Dominica received over 500mm of precipitation in 10 hours and hundreds of landslides were triggered on the island (Ogden, 2016; Van Westin, 2016). Intense rainfall over a short period of time can cause the soil to become oversaturated. This condition increases the pore-water pressure within discontinuities decreasing shear strength. The loss in strength in addition to the added weight of the water forms a zone of weakness, such as at the soil bedrock interface or discontinuities within the bedrock, where the mass destabilizes and it is here that the slope failure will most likely occur (DeGraff et al., 1989; Van Westin, 2016).

In 2014, the World Bank initiated the Caribbean Hazard and Risk Information Program, also known as CHARIM. Their aim was to provide landslide and flood hazard and risk information. They could then apply this information to reduce disaster risk for

		Landslide susceptibility			Triggering Event
Source	**Characteristics**	**Low**	**Moderate**	**High**	**Event**
Susceptibility map	Area (km^2)	392	169	192	
	% of total area	52.0	22.4	25.5	
DeGraff 1987	Landslide area (m^2)	$6.99x10^4$	$1.48x10^5$	$5.62x10^6$	Klaus (Nov. 6, 1984)
	Number of landslides	17	35	838	
	Landslide density (%)	0.018	0.088	2.93	
	Landslide density (nr/km^2)	0.043	0.208	4.37	
DeGraff 1990	Landslide area (m^2)	7507	$8.88x10^4$	$8.35x10^5$	Hugo (Sept. 17, 1989)
	Number of landslides	7	21	155	
	Landslide density (%)	0.002	0.053	0.436	
	Landslide density (nr/km^2)	0.018	0.125	0.808	
Andereck 2007	Landslide area (m^2)	$1.13x10^4$	$3.26x10^4$	$2.77x10^5$	Rain & earthquake (Nov. 21, 2004) Only for area of 22 km^2
	Number of landslides	9	17	135	
	Landslide density (%)	0.003	0.019	0.145	
	Landslide density (nr/km^2)	0.023	0.101	0.704	
This study 2014	Landslide area (m^2)	$6.41x10^4$	$1.77x10^5$	$4.91x10^6$	Accumulation of many Events
	Number of landslides	33	86	777	
	Landslide density (%)	0.016	0.105	2.56	
	Landslide density (nr/km^2)	0.084	0.51	4.05	
Tropical storm Erika August, 2015	Landslide area (m^2)	$3.46x10^4$	$1.41x10^5$	$1.65x10^6$	Tropical storm Erika (Aug. 27, 2015)
	Number of landslides	69	188	$1.21x10^3$	
	Landslide density (%)	0.009	0.084	0.861	
	Landslide density (nr/km^2)	0.176	1.12	6.34	

Table 2.2: Summary information of landslide inventories for the final landslide susceptibility map of Dominica (found in Figure 2.2). About half of the map contains low susceptibility areas, a quarter contains moderate susceptibility areas, and another quarter contains high susceptibility areas. By looking at the number of landslides from each source, you'll see that a large number of landslides occur in the high susceptibility areas. (Modified from Van Westin, 2016).

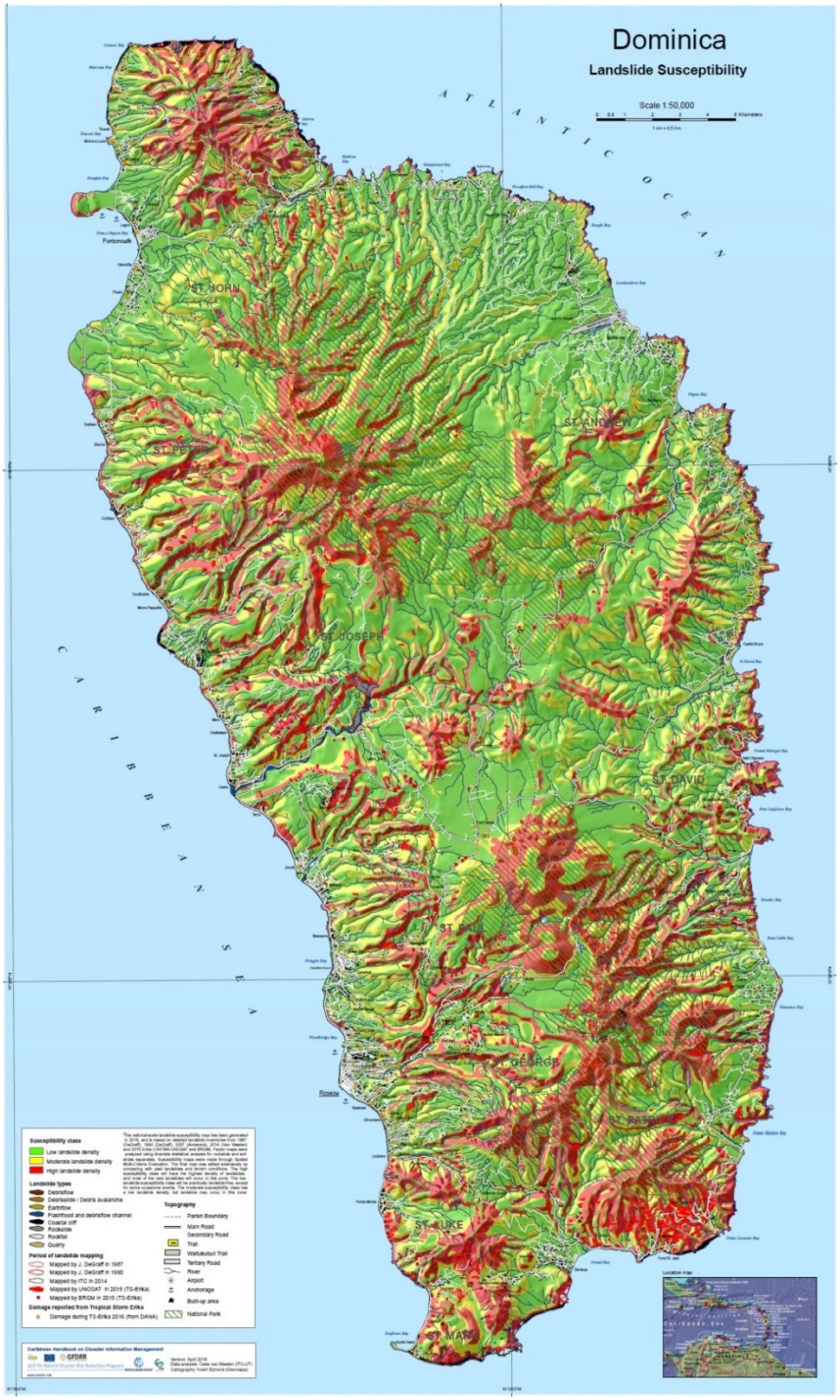

Figure 2.2: Landslide susceptibility map for Dominica. A larger legend for this figure can be found in Figure 2.3. The red, yellow, and green areas correspond to high, moderate, and low susceptibility classes. (Van Westin, 2016).

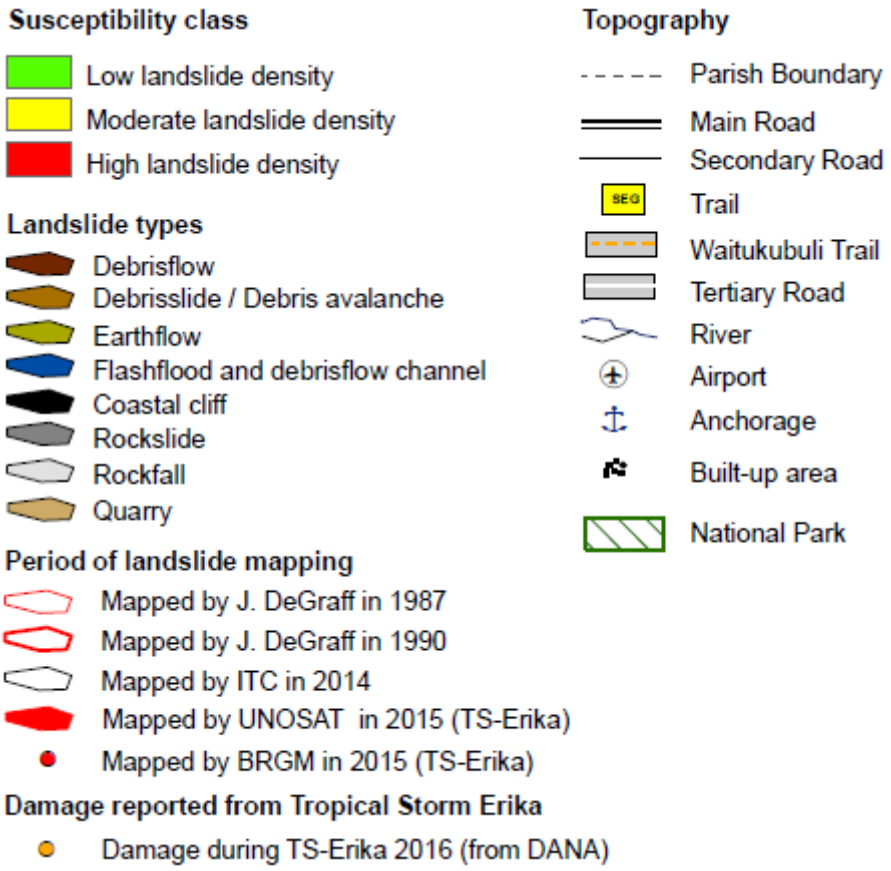

Figure 2.3: Legend for the landslide susceptibility map found in Figure 2.2 (Modified from Van Westin, 2016).

future infrastructure related to health, education, and government (Van Westin, 2016). The study generated a national-scale landslide susceptibility map for Dominica that included landslide inventories. A landslide susceptibility map indicates the likelihood that landslides may occur and should include zones where landslides have occurred in the past and where they may occur in the future (Van Westin, 2016). In their final map for Dominica, 52% of the total area occurs in the low susceptibility category, 22% in

moderate, and 26% in high susceptibility (Table 2.2, Figure 2.2). A larger view of the legend for Figure 2.2 is show in Figure 2.3.

Tropical Soil Characteristics

Dominica contains variable soil types that correspond to regions of the island that experience climatic differences due to orographic uplift and rain shadow effects (Figure 1.2). The four soil types on the island (smectoid, kandoid, allophane latosolic, and allophane podzolic) are each rich in certain clay minerals. Rouse et al. (1986) found that the smectoids are rich in montmorillonite which is a 2:1 expanding lattice clay mineral. The kandoids are rich in the 1:1 lattice clay minerals kaolin and halloysite. Both the allophane latosolic and allophane podzolic are rich in the silica-depleted clay mineral allophane as indicated by their name. However, continuous leaching of allophane latosolic soils produces gibbsite when the silica is depleted.

Consistent high temperatures and abundant moisture, along with a young parent material and high rates of slope erosion, create conditions that limit the time for soil development on the island. As a result, the clay minerals halloysite, allophane, and montmorillonite are more abundant than the kaolinites and gibbsite (Reading, 1991). Reading (1991) and Rouse et al. (1986) categorize Dominica's soils as residual tropical soils which are soils that form in situ by chemical weathering of rocks under humid tropical condition. Rouse et al. found that a prominent feature of Dominica's clay soils is their high porosity. They also reported that topsoil infiltration capacities were very high, which minimized overland flow due to rapid infiltration, and that rainfall easily entered

the soil adding to the overall weight of the soil column. This condition has implications for slope stability during extended or heavy rainfall events.

Shear Strength and Direct Shear Testing

When analyzing the stability of slopes it is a necessity to determine shear strength which is a material's resistance to shearing (A Dictionary of Earth Sciences, 2017). For soils, shear strength is normally expressed on a Mohr-Coulomb diagram and can be plotted in terms of either total normal stress, σ, or effective normal stress, σ' (Wright, 2005). Effective normal stress is the difference between the total normal stress and pore water pressure, u.

$$\sigma' = \sigma - u \tag{2.1}$$

The equations for shear strength, s, in terms of total stress and effective stress are defined as follows:

$$s = c + \sigma \tan\phi \tag{2.2}$$

$$s = c' + \sigma' \tan\phi' \tag{2.3}$$

where c and ϕ are the cohesion and friction angle related to total stress, and c' and ϕ' are the cohesion and friction angle related to effective stress (Wright, 2005).

The type of test used to define the shear strength is what determines whether to use effective or total strength. Common laboratory tests for measuring the shear strength of soils include direct shear, unconfined compression, and triaxial compression. Huang (2014) states that direct shear tests are simple to conduct and typically determine effective shear strength using drained (long-term) conditions. Direct shear tests can determine two different types of shear strength: peak strength and residual strength. Peak

shear strength is the peak load that a soil can carry under drained conditions. Residual strength is a term applied to shear strength developed at large strains and is applicable to slides where there is a pre-existing shear plane from either a previous failure or geologic process (Wright, 2005). When looking at a graph of shear stress versus displacement, the peak shear strength is the largest strength reached, while the residual strength is the constant strength value that is reached after the peak (Figure 2.4). Triaxial compression can be used to determine either total or effective shear strength and for drained or undrained (short-term) conditions. Unconfined compression determines total shear strength and can only be used for undrained tests. They are only applicable to soils with a low enough permeability that prevents the sample from expelling or taking up water during loading (Wright, 2005). Due to the presence of previous failures at the study site, the type of test used must be one that determines residual strength. The most common method for determining residual strength of clays is a drained multiple reversal (cyclic) direct shear test (Mesri & Huvaj-Sarihan, 2012), so that is the test that will be used in this study.

In a direct shear test samples are sheared inside a metal box that is divided into top and bottom halves. The box consists of a circular shear ring with porous plates or stones at the top and bottom (Figure 2.5). The soil sample is mounted between the two porous stones which allows the sample to drain. Locking bolts and set screws help control interactions between the top and bottom portions of the shear ring. The locking bolts keep the two halves connected while the set screws can be used to create a gap.

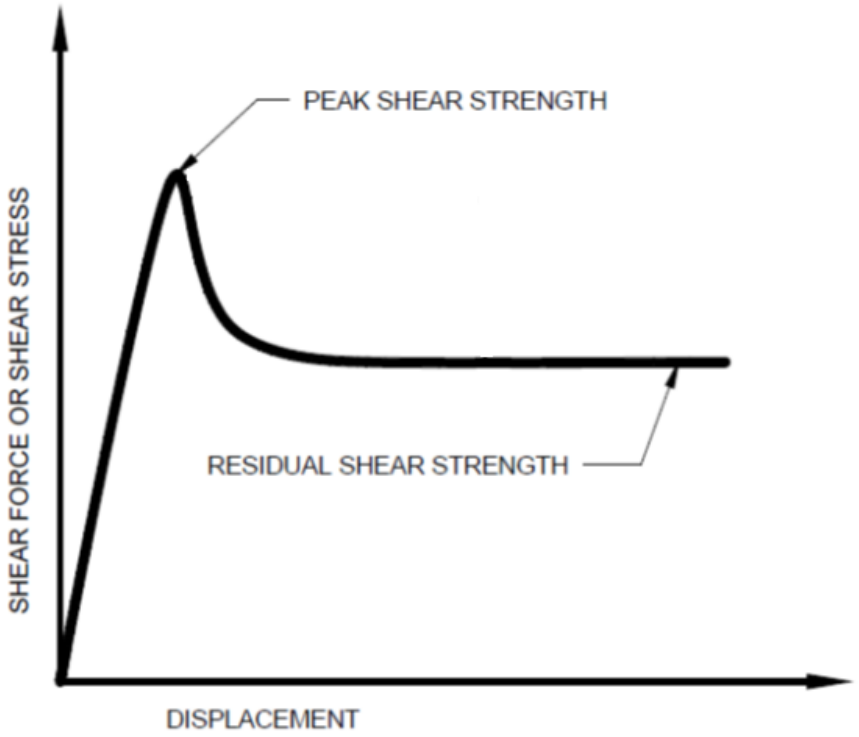

Figure 2.4: Example graph displaying peak shear strength and residual strength (Modified from Thiel, 2001).

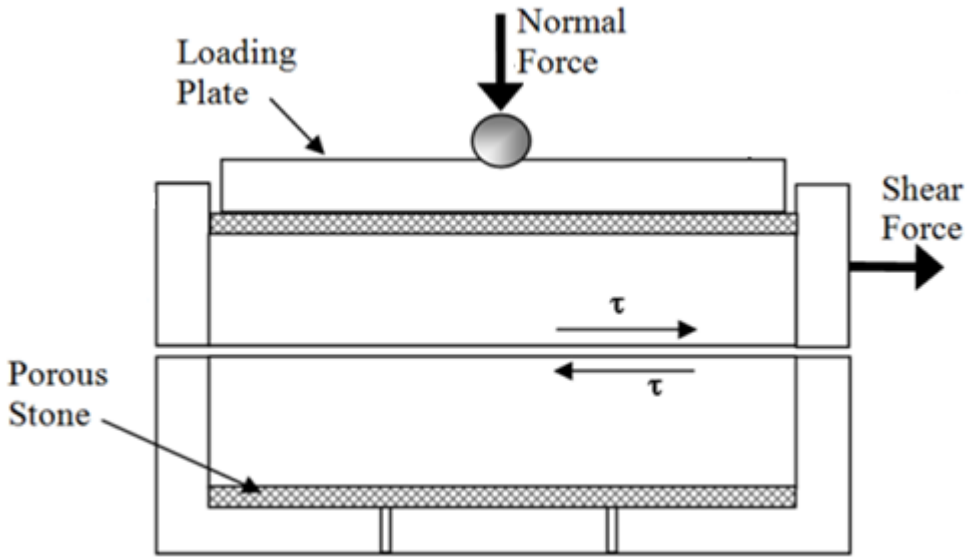

Figure 2.5: Schematic diagram of a direct shear box (Modified from IIT Gandhinagar, n.d.)

A vertical load is applied to the plate on top of the sample. Consolidation is measured over time and once the plot of deformation versus time reaches a constant value, horizontal shearing begins and produces a plot of shear stress versus horizontal displacement. For proper measurements of drained shear strength, the loading rates have to be slow enough to allow full draining of the specimen after the application of the vertical load and the soil needs a sufficient period of time to consolidate fully before shearing. The shear load must also be applied at a slow enough rate so that excess pore water pressures generated during shear dissipate, otherwise the soil tends to expand and shear strength is overestimated (Wright, 2005). If the loads are indeed applied slowly enough, then the effective stress can be calculated and strength can be plotted (Figure 2.6). The parameters determined from the plotted results are the effective stress cohesion c' (y-intercept from Figure 2.6) and the effective friction angle ϕ' (slope of the line in Figure 2.6) (Wright, 2005).

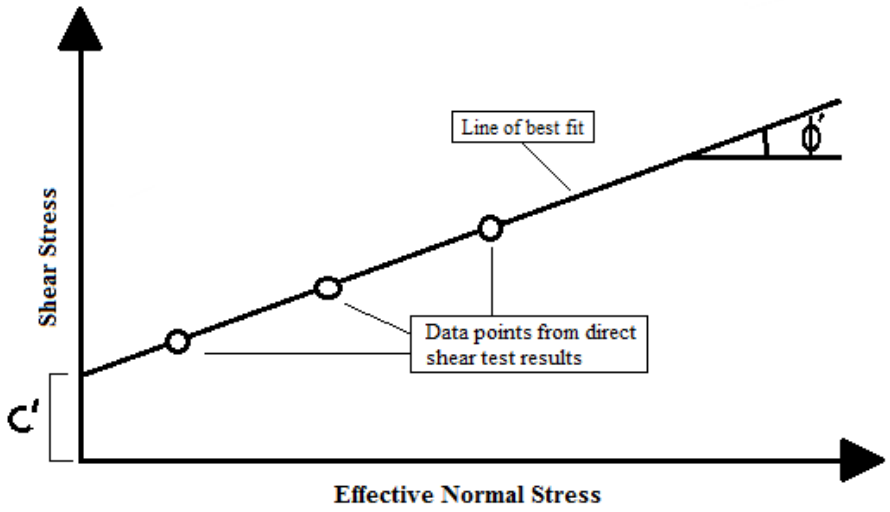

Figure 2.6: Results from a direct shear test are plotted on a graph of effective normal stress vs shear stress. The y-intercept is the effecting cohesion and the slope of the line is the effective friction angle.

In their studies on Dominica, Rouse et al. (1986), Rouse (1990), and Reading (1991) discuss direct shear tests as well as ring shear tests. A ring shear test is a torsional shear test where rotational shearing action is applied continuously until constant residual shear strength is reached. Rouse et al. (1986) and Reading (1991) found that shear strength results are affected by which apparatus is used. Ring shear tests produce consistently lower ϕ' values (by about eight to ten degrees) for the Dominican allophane soils than for the direct shear test, while results for kandoid soils were similar for both tests. They noted that sample preparation and test methodology affect the results. They, along with Rouse (1990) and Wesley (1977), found that pre-test air drying affects ϕ' values for kandoid soils, but not allophane or smectoid soils. Wallace (1973) tested allophane soils from Papua New Guinea with a direct shear box and obtained similar ϕ' results to Rouse et al. (1986). Wesley (1977) tested allophane soils from Indonesia with a ring shear test, but his ϕ' results were much higher than those of Rouse et al. (1986) and more similar to direct shear test results.

Limit Equilibrium Method

Using the results of direct shear testing, a slope stability analysis can be done using the limit equilibrium approach. This is the most common method for stability analysis and has been used since the 1930's (Huang, 2014; Matthews et al., 2014). It is done by expressing shear stress along a failure surface as

$$\tau = \frac{s}{FS} \quad \text{or} \quad FS = \frac{s}{\tau} \tag{2.5}$$

where τ is shear stress, s is shear strength, and FS is factor of safety. Note that s is defined in 2.2 and 2.3. The factor of safety is defined as the ratio between the resisting force due to shear strength and the driving force due to weight.

$$FS = \frac{Resisting\ force\ along\ failure\ surface}{Driving\ force\ along\ failure\ surface} \tag{2.6}$$

When the two are equal, the factor of safety is one and failure is predicted (Huang, 2014). If the resisting force is greater than the driving force, than FS is greater than one and the slope is predicted to remain stable.

There are three types of failure surfaces one must consider when using the limit equilibrium approach. They are circular, composite, and noncircular (Figure 2.7). Circular failure surfaces, also called cylindrical failure surfaces, often form if the slope's materials are homogeneous with no apparent weak layers. Composite failure surfaces are initially circular, but when a circle cuts into a weak layer, the failure surface will then follow the bottom of the weak layer and become a plane failure surface. Noncircular failure surfaces, also called plane failure surfaces, are when the failure surface is made up of a series of planes. They form if there are weak layers that begin or end near the slope's surface (Huang, 2014).

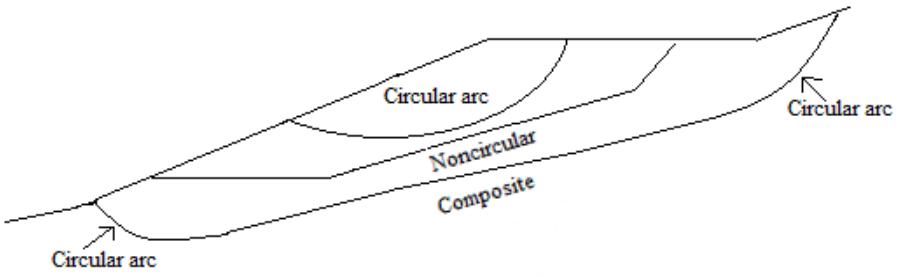

Figure 2.7: The three types of failure surfaces (Modified from Huang, 2014).

When using the limit equilibrium approach, certain conditions must be considered to select the correct method. The conditions to be considered are: a) the type of stress analysis: total or effective, b) slope material: homogeneous or layered, and c) failure surface: circular, composite, or noncircular. For example, Huang (2014) stated that for a total stress analysis with a circular failure surface, the Fellenius method is most suitable, whereas the sliding block analysis could be used for one with a noncircular surface.

Rouse et al. (1986), Rouse (1990), and Reading (1991) stated the slides on Dominica are commonly shallow and translational (noncircular), with the key failure plane at the base of the subsoil at a depth of about 0.5 to 2 meters and roughly parallel to the ground surface. Rotational (circular) slides do occur there as well, but they are small and less common than translational slides (DeGraff et al., 1989). In all three of their studies they say the infinite slope model is appropriate for the translational slides. The infinite slope model assumes that the slope is elongate and that the failure surface is parallel to the ground surface.

Since a drained shear test is performed, the infinite slope equation for effective stress will be used and is as follows:

$$FS = \frac{c'}{\gamma z}\frac{2}{\sin(2\beta)} + \left[cot\beta - \frac{u}{\gamma z}(cot\beta + tan\beta)\right] tan\phi' \qquad (2.7)$$

where FS is factor of safety, *c'* is effective cohesion, γ is soil density, β is slope angle, u is pore pressure, z is depth of failure, and ϕ' is effective friction angle. A derivation of this formula can be seen below.

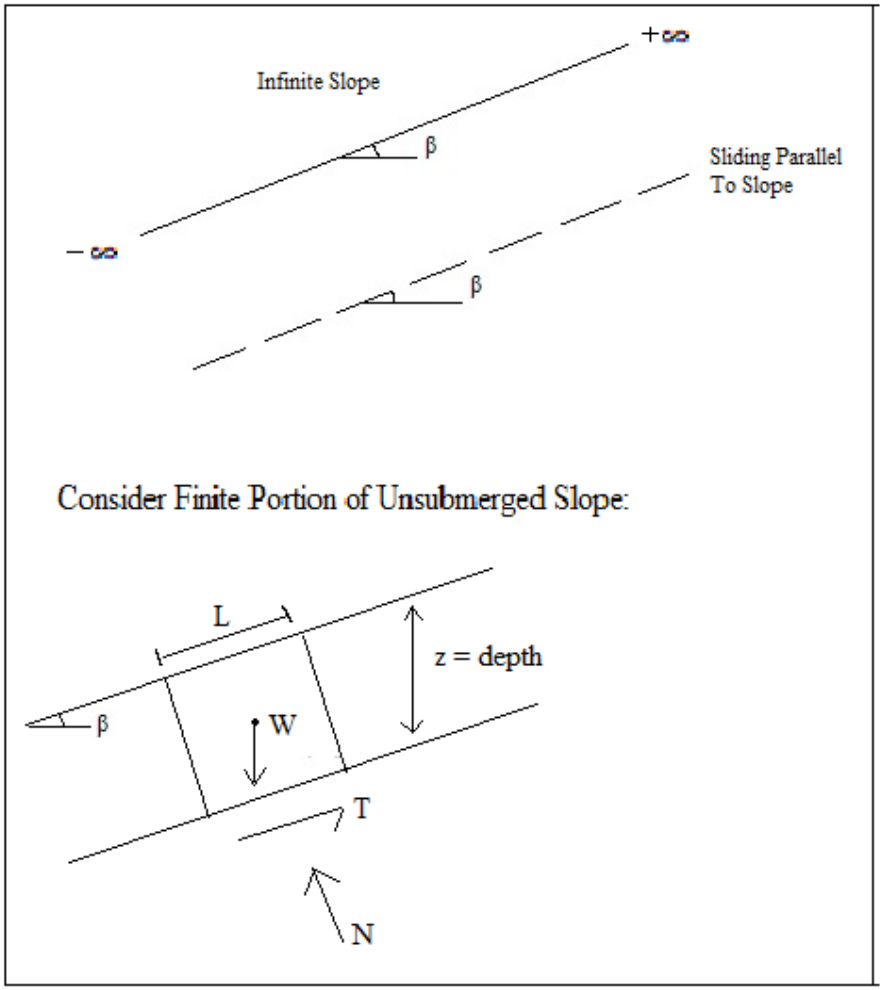

Figure 2.8: An infinite slope shown with a finite unsubmerged portion of the slope.

Using Figure 2.8, the derivation begins by considering a finite portion of an unsubmerged slope:

$$\sigma = \frac{N}{L \cdot 1} = \frac{W cos\beta}{L \cdot 1} = \frac{\gamma L z cos\beta}{L \cdot 1} = \gamma z cos^2\beta$$

$$\tau = \frac{T}{L \cdot 1} = \frac{W sin\beta}{L \cdot 1} = \gamma z cos\beta sin\beta$$

The effective stress analysis equation is then $FS = \frac{c' + (\gamma z cos^2\beta - u) tan\phi'}{\gamma z cos\beta sin\beta}$, which rearranges to $FS = \frac{c'}{\gamma z cos\beta sin\beta} + \left(\frac{\gamma z cos^2\beta - u}{\gamma z cos\beta sin\beta}\right) tan\phi'$. Since $\frac{1}{cos\beta sin\beta} = \frac{2}{\sin(2\beta)}$, the formula can be simplified to $FS = \frac{c'}{\gamma z}\frac{2}{\sin(2\beta)} + \left[cot\beta - \frac{u}{\gamma z}(cot\beta + tan\beta)\right] tan\phi'$ (Formula 2.7).

Forward calculations for slopes that haven't failed can be done using Formula 3.3 to find the factor of safety. If the factor of safety is greater than 1, the slope is predicted to remain stable. If the factor of safety is less than or equal to 1, failure is predicted. If a slope has already failed, two different back calculations can be done. These calculations, which involve rearranging Formula 2.7, will determine the friction angle needed for the current slope to stay stable under different conditions and the depth above or below the failure surface that the water table reached before the initial failure occurred (z_w). A more detailed description of the calculations done using the infinite slope method is presented in the methodology chapter.

Rouse (1990) and Reading (1991) used the back calculation method to find the friction angle needed for the slopes in their studies to remain stable. Rouse (1990) found that for dry slopes, the maximum angle that a dry slope could remain stable ranged from 29 degrees to 41 degrees (Table 2.3), while Reading (1991) found that it ranged from 29 to 38 degrees.

Measurement:	**Sample Name:**					
	Attley	Bells	Carhome	FWL	Rosalie	Calibishie
Soil type	Allophane	Allophane	Allophane	Allophane	Allophane	Kandoid
Sat. Weight (kN/m^2)	14.16	14.78	13.35	13.94	14.33	15.98
Laboratory Shear - mean ϕ'	35.5	35.6	38.4	34.3	35.0	29.1
Strength -max ϕ'	41.2	38.0	39.2	34.9	38.0	29.5
Field Slope Angle (degrees)	43.0	40.0	35.0	50.0	35.0	30.0
Maximum Stable Slope (degrees)	35.5	35.6	38.4	34.3	35.0	29.1

Table 2.3: Results from an infinite slope stability analysis of Dominican landslides (Modified from Rouse, 1990).

CHAPTER THREE

METHODOLOGY

The sites in this study are located on Cochrane Road in Dominica. Cochrane Road is located on the western side of the island, northeast of the capital city of Roseau and in close proximity to Clemson University's Springfield Field Station and the Archbold Tropical Research and Education Center (ATREC) (Figures 3.1 and 3.2).

Figure 3.1: Location of the Archbold Tropical Research and Education Center (ATREC) on Dominica (Google Maps, 2017).

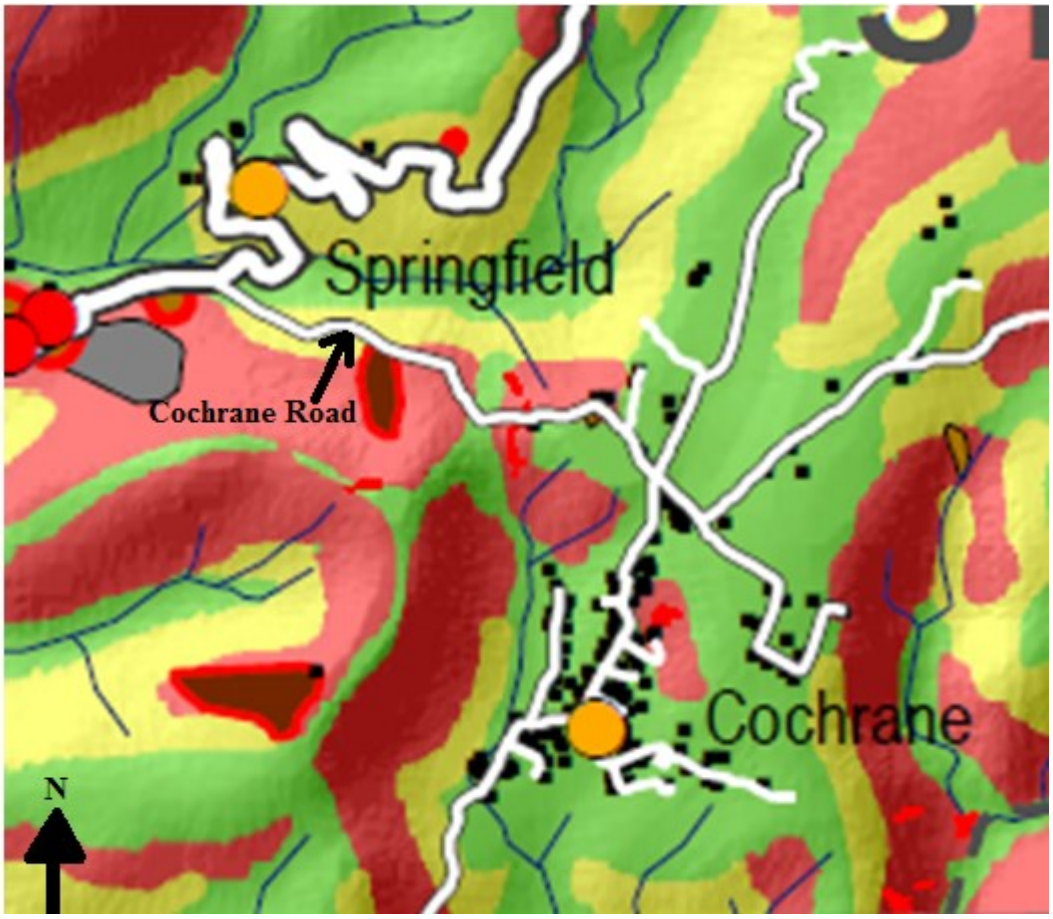

Figure 3.2: Location of the study area taken from the landslide susceptibility map shown in Figure 2.1. The yellow dots signify the locations of Springfield and the town of Cochrane. The red, yellow, and green colors show the susceptibility of the area to landslides. The red coloring signifies areas of high susceptibility, the yellow area signifies moderate susceptibility, and the green area signifies low susceptibility. The brown areas outlined in bright red are debris flows mapped by DeGraff in 1990. The grey area outlined in black is a rockslide mapped by ITC in 2014. A detailed legend for this figure can be found in Figure 2.2 (Modified from Van Westin, 2016).

Cochrane Road climbs a mountain side and contains steep hills on one side and steep drop offs on the other. Many of these areas contain previous slope failures. The vegetation on these slopes ranges from areas of tropical forest in the lower parts to fields of lemongrass where the road is on ridge at the top of the mountain. The CHARIM

landslide susceptibility map for Dominica shows many areas along Cochrane Road that are highly susceptible to landslides (Figure 3.2). Some of these areas contain slope failures that were either absent or were not identified when the CHARIM database and map were published. When the slopes in this area fail, the debris are either deposited onto the road (and later bulldozed away) or they keep moving downslope until reaching rivers and streams where they can be washed away. A conceptual model for the landslides can be seen in Figures 3.3 and 3.4. Figure 3.3 shows a slide with an un-vegetated failure surface at a depth of z and a vertical head scarp with roots hanging out at the top. The failed material is deposited further downhill. This material could have kept the original vegetation in place as it traveled downhill. Commonly, the failure occurs at a depth below the roots. Figure 3.4 shows models with the ground surface, water table, and failure surface. The water table can be in a number of locations when failure occurs, but for seepage conditions, the water table is at the ground surface and for general conditions the water table is at the failure surface. During seepage conditions, water is flowing above the failure surface when failure occurs. During general conditions, the water is flowing at and below the failure surface. As in Figure 3.3, the failure generally occurs beneath the roots of the vegetation.

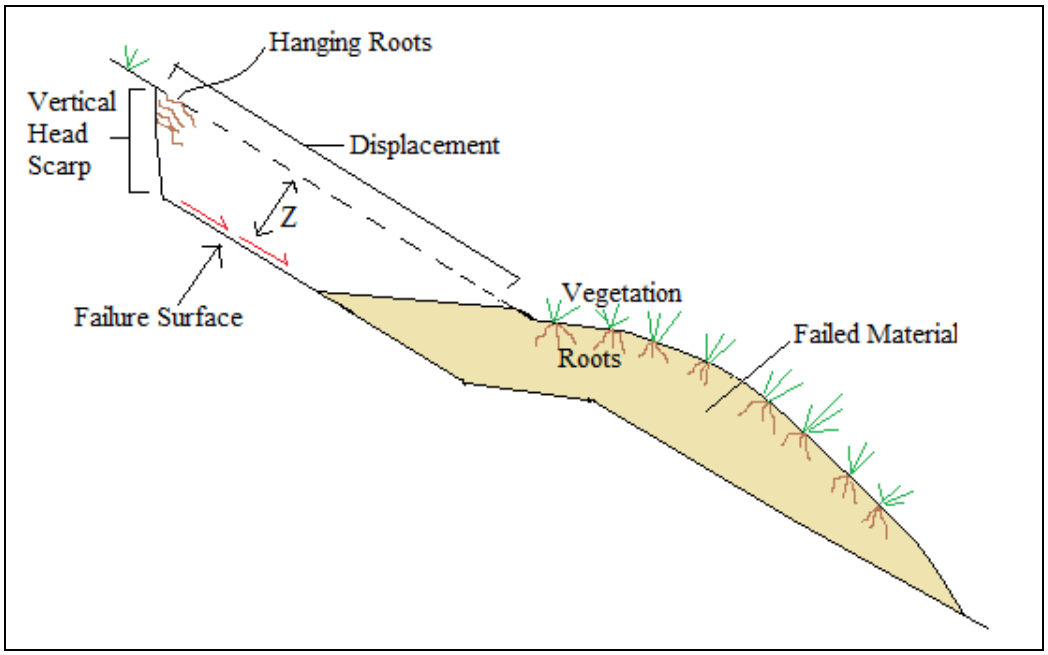

Figure 3.3: Conceptual model for the landslides on Cochrane Road.

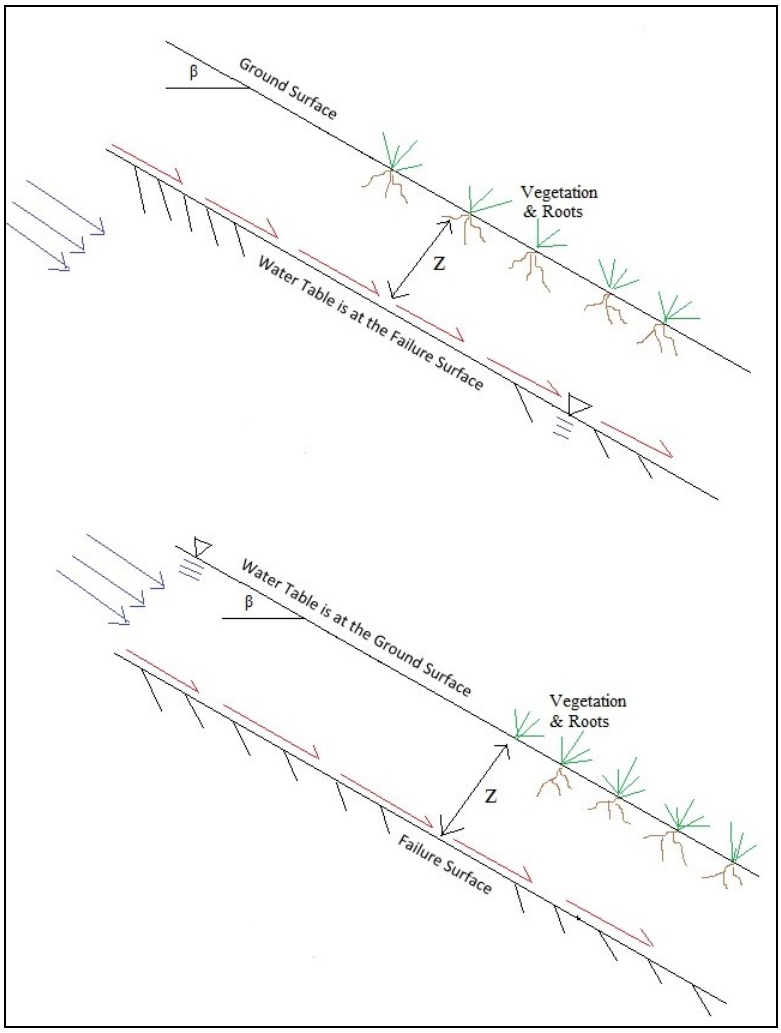

Figure 3.4: Conceptual model showing the locations of the failure plane, water table, and ground surface.

Landslide Characteristics

Slope failures adjacent to Cochrane Road were identified from the bottom of the hill where it terminates at Imperial Road to a house at the apex of the hill that is adjacent to a tall cell tower (Figure 3.5). Along this distance of 0.56 miles (about 900 meters) a total of eight pre-existing slope failures were mapped. Each of the sites, with exception to

one due to accessibility issues (too dangerous to descend the slope), were described using photographs and measurements of slope angles, widths, and heights.

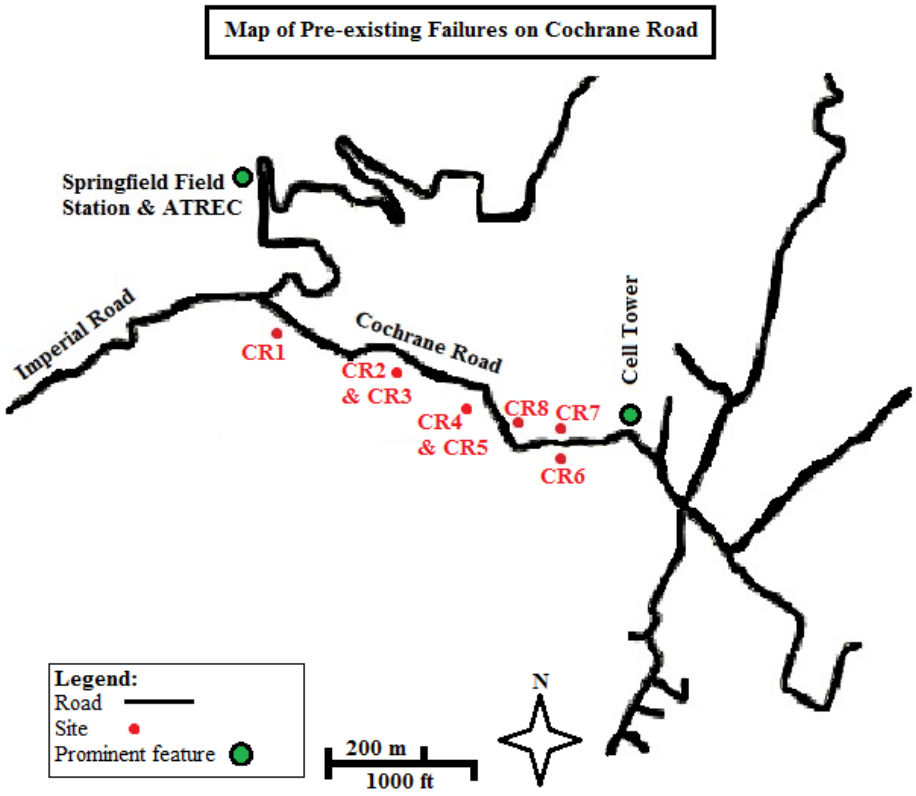

Figure 3.5: Map of pre-existing failures on Cochrane road.

Starting at the intersection with the Imperial Road and heading uphill, CR1 was the first slide encountered. Its width was measured at the bottom near the road as 131 feet wide with a length of 53 feet along the slope using the highest point (Figure 3.6 and Figure 3.7). The slope angle was 40 to 45 degrees. About 2 to 3 feet of material had been removed during the failure. The top and sides of the slide consisted of small overhangs with hanging roots. The slope was un-vegetated with a variety of material ranging from large boulders to clay-sized ash (Figure 3.8). Due to its fresh and un-vegetated appearance, it is assumed this slope failed during Hurricane Erica in 2015.

Figure 3.6: Slide CR1 is shown with a man at the top of the slide measuring the length from the base to the highest point. The top of the slide is at the boundary between the vegetated and un-vegetated areas. At the base of the picture is the curb of the road with large boulders resting just above it.

Figure 3.7: View of CR1 from the far right side of the slide. CR1 is the un-vegetated surface. In the top left of the picture there are small overhangs with roots and in the mid-right of the picture are the large boulders that were shown in Figure 3.6. They are partially buried in the soil.

Figure 3.8: Range of CR1 material pictured with a 3 by 6 inch scale (outline of the card) The top photo shows cobbles surround by clay sized ash. The bottom photo shows the large boulders at the bottom of the slope.

CR2 and CR3 are slides about 1000 ft (305 m) further up the road from CR1. CR2 is a more recent slide that occurred on the older CR3 slide (Figure 3.9). CR2 had an un-vegetated failure surface which implies it failed during Hurricane Erica in 2015 (Figure 3.10). In contrast, the vegetation on CR3 (Figure 3.11) had completely grown back. Thus CR3 predates Hurricane Erika. CR2 had a length of 43 feet from the base to the highest point and a width of 18 feet at its widest point, which was about 15 feet above the bottom of the slide surface. The depth of the landslide was approximately 3 feet at the top and then reduced to 2 feet over the remaining failure surface. The slope angle at both sites is 36 degrees, with a 30 degree angle at the bottom where the failure surface ended. The material on CR2 and CR3 ranges from clay size to cobble (Figure 3.12).

Slides at sites CR4 and CR5 (Figure 3.13) are located about 700 feet (213 m) up the road from CR2 and CR3. CR4 (Figure 3.14) is a recent failure that occurred as a result of Hurricane Erika that had cut into the older and vegetated CR5 failure (Figure 3.15). The failed material from these slides had been deposited in the roadway and been bulldozed into piles on the downslope side of the road (Figure 3.16). This pile consisted of cobbles less than 20 cm and clay clasts of 5 cm or less in diameter (Figure 3.17). The bottom width of CR4 is 19 ft and the angle of the slope is 40-45 degrees. The slide was too steep to climb, so a length measurement was not taken but is estimated at 20 ft. CR5 had large amounts of tall brush and fallen trees on it, so an accurate slope angle could not be taken, but it is estimated that it was close to that of CR4 around 40 to 45 degrees.

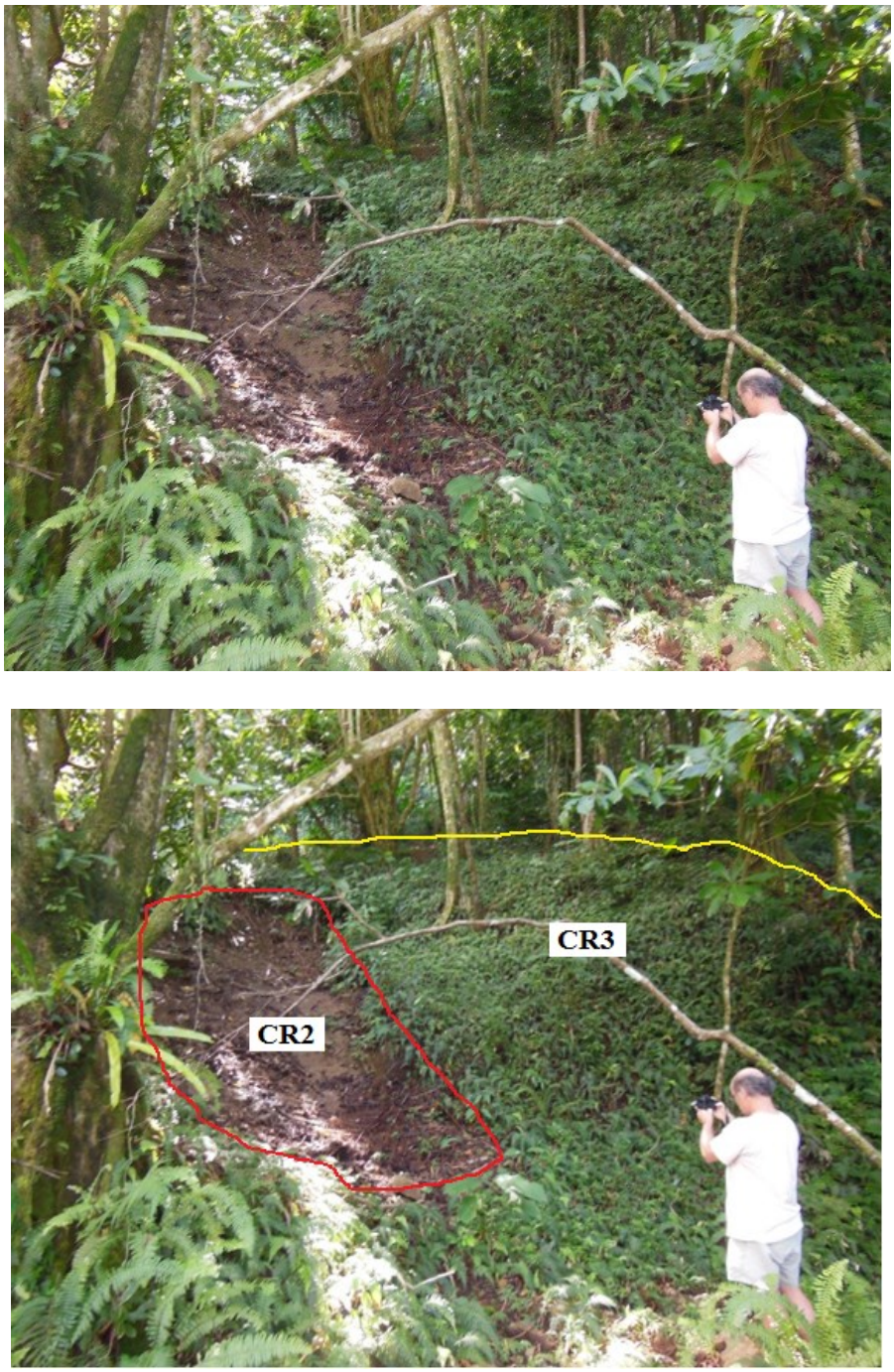

Figure 3.9: Slides CR2 (un-vegetated area on the left) and CR3 (vegetated area on the right, top of the scarp outline in yellow) shown with a person for scale. The bottom photograph is an annotated version of the top photograph to show where CR2 and CR3 are positioned. CR3 has a small scarp further uphill.

Figure 3.10 Direct view of slide CR2. Slide CR2 is the un-vegetated surface. The top photo is the original photograph while the bottom photo is an annotated version showing the outline (red) of the CR2 slide surface.

Figure 3.11 Slide CR3 covered in vegetation consisting of tropical brush and trees. There is a small scarp further uphill (yellow) completely covered in brush.

Figure 3.12: Clay sized to cobble material found on slide CR2 pictured with a 3x6 inch scale (outline of card). The leaves cover much of the clay sized material.

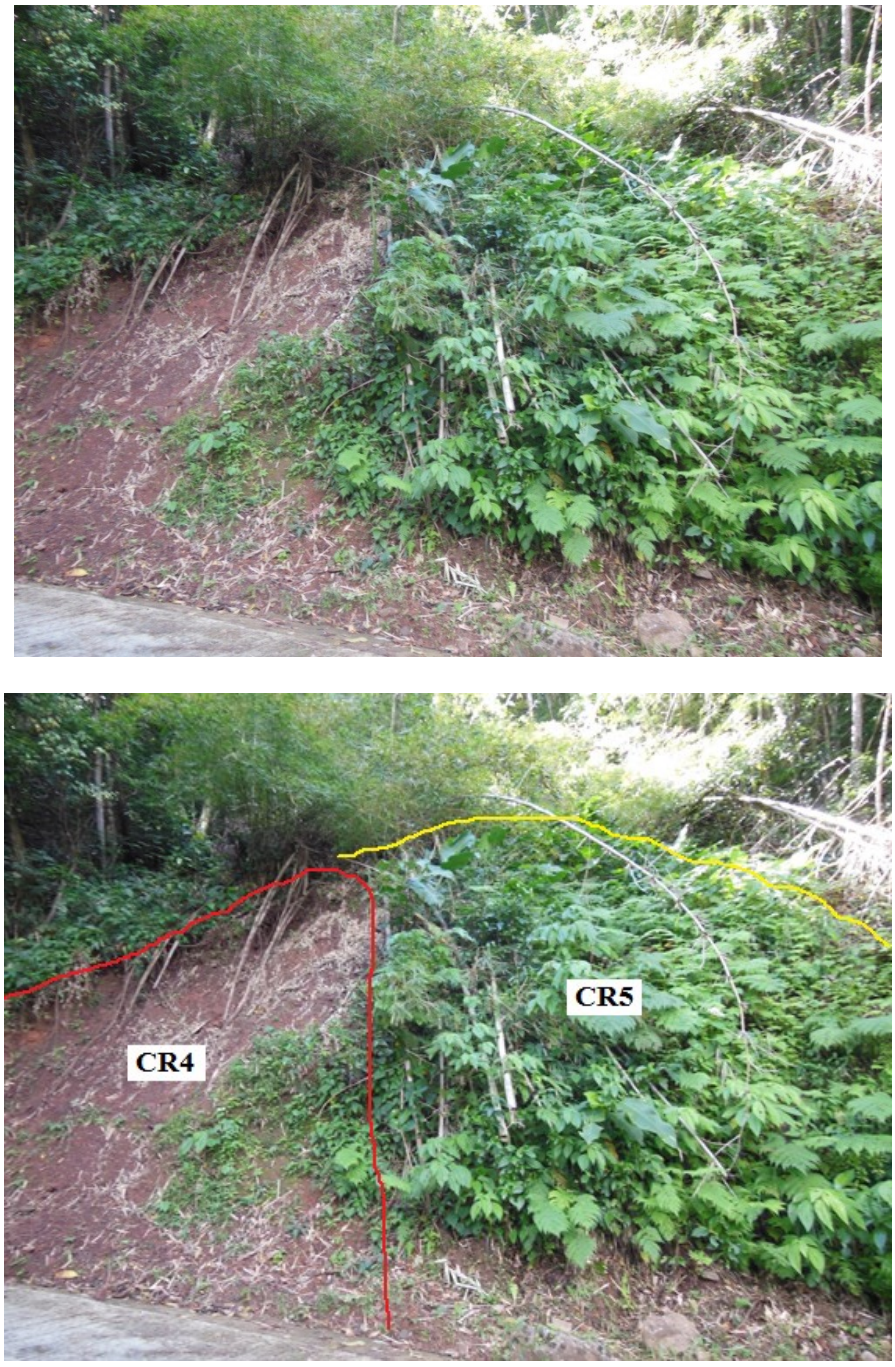

Figure 3.13: Slide CR4 on the left with a non-vegetated, fresh dirt surface (outlined in red) and slide CR5 on the right with a vegetated surface (outlined in yellow). CR4 has hanging roots and the top and a small area of regrowth on the right. CR5 is covered in tall leafy brush and some skinny trees that had fallen down.

Figure 3.14 Un-vegetated slide surface of CR4 (outlined in solid red). At the top of the slide there is a small scarp (between the solid and dashed red lines) with long hanging roots and on the right most portion of the slide there is a small area of regrowth.

Figure 3.15: Slide CR5 covered in tall leafy brush. The vegetation on this slope is markedly different than what is found on the surrounding slopes, suggesting that this slope failed, lost its vegetation, and then regrew new vegetation

Figure 3.16: Pile of material from slides CR4 and CR5 that was bulldozed across the road.

Figure 3.17: CR4 and CR5 material consisting of cobbles less than 20 cm and clay clasts of 5 cm or less in diameter pictured with a 3x6 inch scale (outline of card).

CR8 is the next slide encountered. Unlike the other failures so far, this failure occurred on the left and downslope side of the road. As a result, the scarp of the slide coincided with the road and actually undermined the asphalt surface. The nature of this condition limited access and it was deemed unsafe to climb down for photos or measurements. From the road side, loose material and soil was visible, but no boulders or cobbles. The slope angle was estimated to be 50 degrees with a 4 to 5 foot vertical head scarp.

Further up the road about 300 feet (90 m) is a section where the road is on a narrow ridge with steep sides and there are slope failures on both sides (Figure 3.18). This condition threatens to undermine the road leading to catastrophic failure. It appeared as if the road could crumble at any minute and made driving over that section, which is reduced to barely one lane, nerve wracking. The two failures that flank the road are CR6 on the right and CR7 on the left. CR6 is a translational slide about 44 ft long and 70 ft wide (Figure 3.19). The slope angle was 36 degrees except for a 5 foot high vertical scarp at the top that starts at the edge of the road. The failed material at the bottom of the CR6 slope was composed of clay clasts and rocks about 3 cm or less in diameter (Figure 3.20). The surface of the CR6 slope was 5 ft below the surrounding intact slopes (Figure 3.21) so the failure surface was considered to be 5 ft deep. Lemongrass covered much of the area to the left, right, and bottom of the fresh failure surface.

Across the road from CR6, CR7 had a scarp height of 5 to 6 ft, a length of 64 ft, and a width of 48 ft (Figure 3.22). The head scarp at the top undermined the road and the pavement overhangs the failure surface by about 1 ft. CR7 had a vertical scarp at the top and a slope angle of 52 degrees with an angle of 22 degrees lower down the slope near the toe of the slide. The failed material at the bottom of the slope is composed of clay clasts and rocks about 3 cm or less in diameter (Figure 3.23), similar to that observed on CR6. Note that CR6 and CR7 both failed in deeply weathered soils found on a ridgetop which contrasts to the much rockier material found down the hill at sites CR1, CR2, CR3, CR4, and CR5.

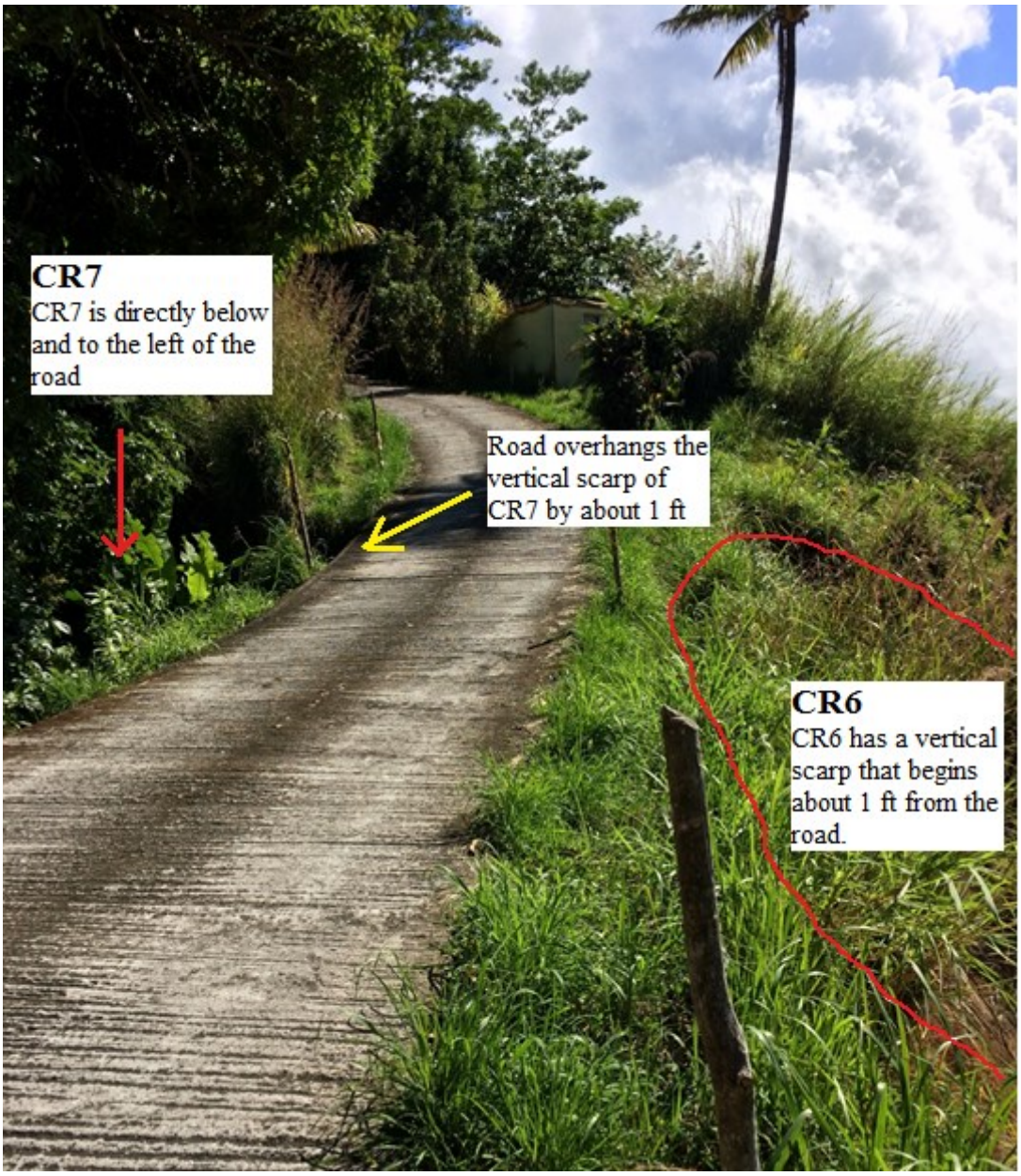

Figure 3.18: Portion of Cochrane Road that is on a narrow ridge with slope failures on either side. CR6 is located on the right side of the road and begins about 1 ft from the road. CR7 is located on the left side of the road. A portion of the road overhangs CR7's scarp by about 1 ft.

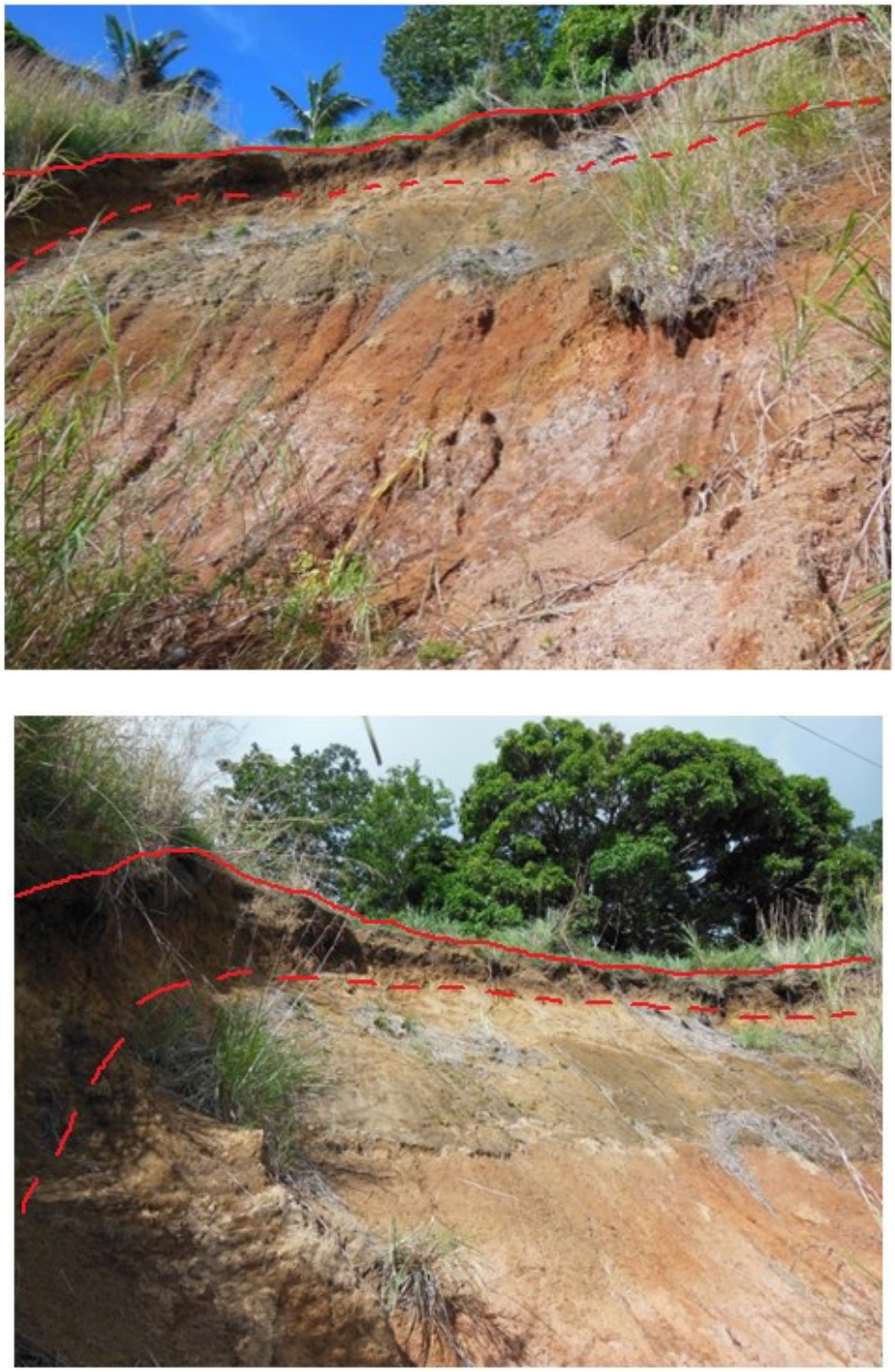

Figure 3.19: Views of CR6 taken from the bottom right (top photo) and bottom left (bottom photo) of the slide. There is a 5 ft vertical scarp (outlined in red) at the top of the slide. Lemongrass is present at the top, sides, and bottom of the slide. Cochrane Road is located about 1 ft back from the top of the slide.

Figure 3.20: Material from CR6 consisting of clay clasts and rocks about 3 cm or less in diameter shown with a 3x6 inch scale (outline of card).

Figure 3.21: Left side of the CR6 failure surface shown 5 ft below the intact slope to the left of the slide.

Figure 3.22: View of the CR7 slide surface with the road overhanging at the top. Portions of the slide surface are revegetated.

Figure 3.23: Material from CR7 consisting of small rocks and clay clasts about 3 cm or less in diameter shown with a 3x6 inch scale (outline of card).

Selected Site Characterization

After investigating the sites above, two sites were chosen for further analysis and will be referred to as the Forested Site and the Lemongrass Site. The Lemongrass Site consists of CR6 and LG. LG refers to the slope adjacent and to the right of CR6 if looking down from the road. At the time of the study, LG was stable, completely covered in lemongrass, and had a slope of 36 degrees. The Forested Site consists of CR2 and CR3. When choosing the sites, ease of access had to be considered as not all of the areas by the previous slides were climbable. While conducting field work at these two sites, ropes were used for stability when ascending and descending as the slopes were quite slick. These conditions made it challenging to take measurements and collect samples.

At the Lemongrass Site, ½ inch diameter soil cores were collected from the surface to a depth of 8 ft at the top of the slope near the road (LGa) and at three other locations in a transect down the slope named LGb, LGc, and LGd (Figure 3.24). These locations were approximately 20 feet apart as measured along the slope. These soil cores were bagged and taken back to Clemson for soil characterization and XRD analysis. Soil cores were attempted at the Forested Site, but due to high rock density and tree roots it was impossible to penetrate more than a few inches. Samples were instead collected from close to the surface.

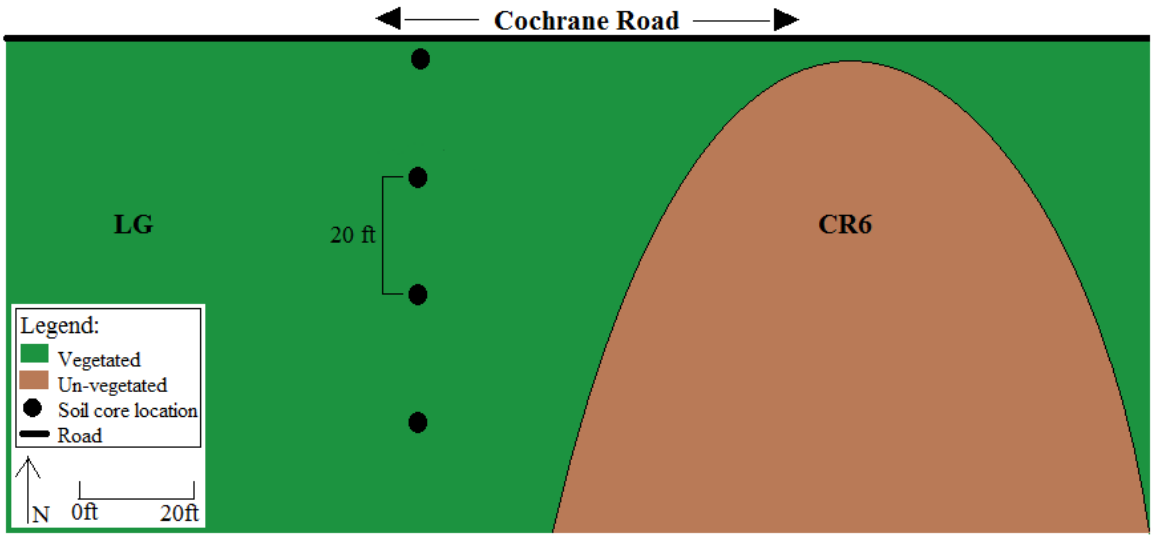

Figure 3.24: Location of the ½ inch diameter soil cores in relation to LG and CR6.

At all four locations (CR6, LG, CR2, and CR3), 3 inch diameter soil cores were collected in 1 ft long hollow PVC tubes and brought back to Clemson for direct shear testing. This was done by digging out a flat surface on the slope at the desired sample depth (Figure 3.25). The tubes were hammered into the soil (Figure 3.26) with a mallet and a piece of wood placed on top to prevent the PVC from breaking when hammered. The tubes were dug out with a shovel (Figure 3.27), capped at both ends, and bagged for travel. The samples for CR6 were collected near the left side of the slide, about 9.3 ft from the top of the slide, and at a depth of about 1.5 ft. The LG samples were collected about 20 ft downslope from the road, 11 ft from the edge of the CR6 slide, and at a depth of 2.5 ft (Figure 3.28). CR2 samples were taken 15 ft below the scarp at a depth of 0.8 ft. CR3 samples were taken about 15 ft to the right of the CR2 samples at a depth of 1.4 ft (Figure 3.29).

Figure 3.25: Digging out a flat surface to collect cores for direct shear testing.

Figure 3.26: Core tube that has been hammered into the ground.

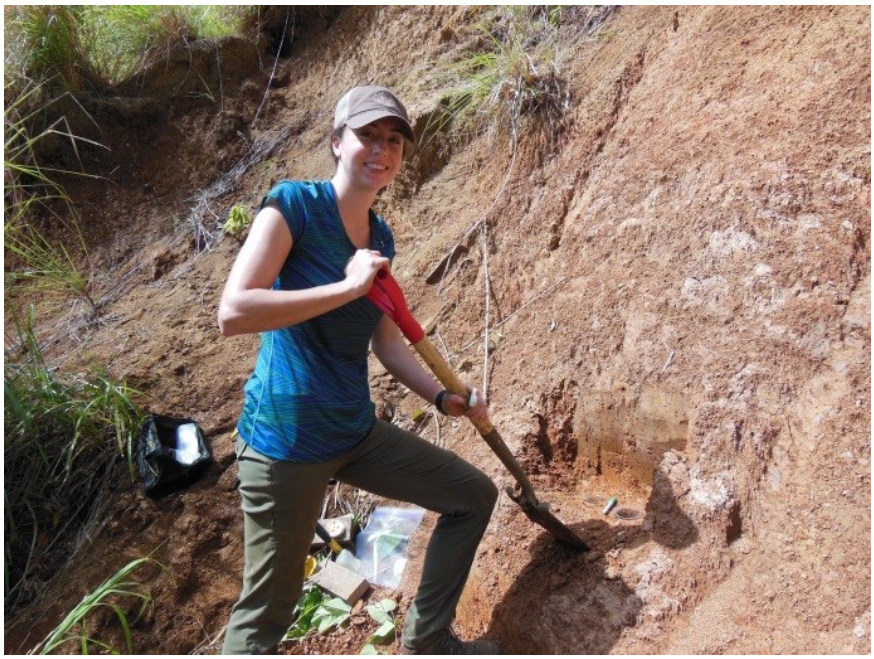

Figure 3.27: Digging the core tube out of the ground after it has been hammered down.

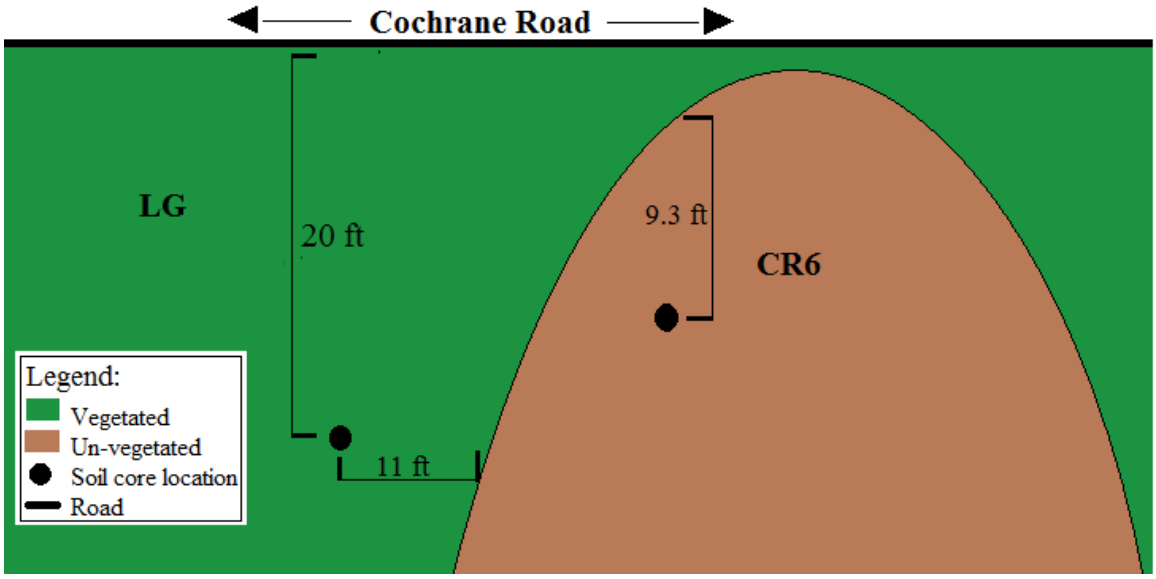

Figure 3.28: Location of the 3 inch diameter soil cores at the Lemongrass Site.

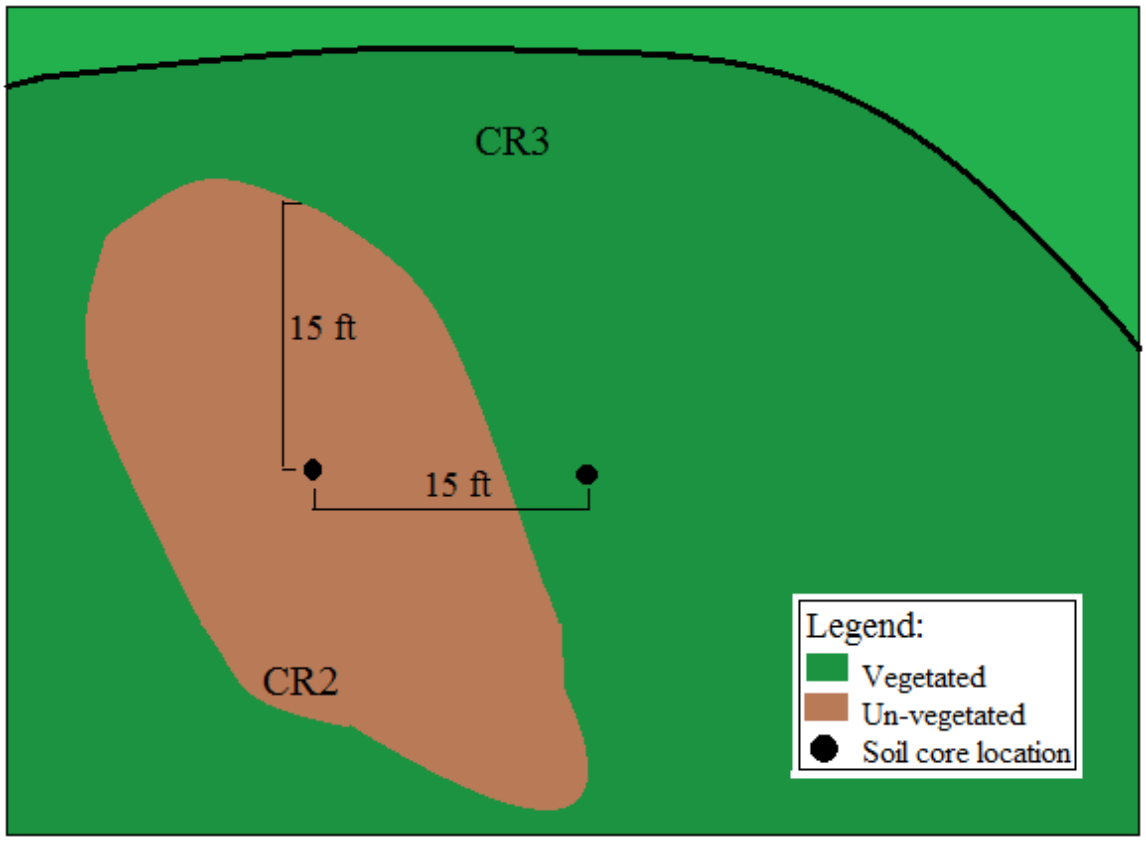

Figure 3.29: Location of the 3 inch diameter soil cores at the Forested Site.

At the Lemongrass Site, shear vane tests were done at the same locations as the ½ inch diameter soil cores. The purpose of a vane shear test is to determine the in-situ strength of soils, which is normally related to the undrained shear strength of the soil. A standard vane of 20x40 mm was used and measurements were taken at depths of up to 8 ft in order to detect relative changes in shear strength. Measurements were taken every foot. Very firm clay at different depths made it too difficult to push the vane deeper into the ground at sites LGb, LGc and LGd. Where it was difficult to advance the shear vane, the vane was removed and the coring tool was used to clear out the hole. The vane was reinserted and pushed 6" below the depth cleared by the coring tool. Removing the

overlying soil reduces the friction load when advancing the vane tubing but does not affect the in-situ measurement. Even by doing this, depths of 8 ft weren't reachable at LGa, LGb, LGc, and LGd. Vane shear measurements were also attempted at the forested site, but again, due to large clasts and roots, it was impossible.

Back in the lab, soil characterization was conducted on the soil samples from both the Lemongrass and Forested Sites (Figure 3.30). Using the USDA Soil Texturing Field Flow Chart, the plasticity, Munsell soil color, and soil name were determined. At the Lemongrass Site, characterization was done on samples from about 0 to 1 ft depth, as well as on samples from about 7 to 8 ft depths, in order to see if there was a change in material with depth. Since 8 ft depth soil cores could not be taken at the Forested Site due to the roots and large clasts, only one sample from about 1.4 ft depth was analyzed.

Figure 3.30: Samples laid out for soil characterization.

Clay Determination using X-Ray Diffraction (XRD)

The minerals present in a soil sample can be determined by X-ray diffraction (XRD). During XRD analysis X-rays are generated and directed through the sample producing interference and a diffracted ray. A unique x-ray diffraction pattern is generated and identification of the crystalline form can be accomplished by comparing the pattern to standard patterns and measurements. By determining the minerals present, the soil type present in the study areas can be deduced. For example, if the results from the XRD indicate that montmorillonite is present in the sample then a smectoid soil type could be assigned to that location. Unfortunately, using XRD analysis to identify soil mineralogy is not an exact process. Singh and Agrawal (2012) point out that swelling interlayers, thickness of diffracting domains, particle size, sample weight, sample preparation and other phenomena can all contribute to the complexity of XRD testing. They, along with Siqueira et al. (2011), point out that silica, specifically quartz, has high intensity peaks that often overlap the lower intensity peaks of minor elements making identification and determination difficult.

Sample preparation for XRD analysis involved drying, grinding, and sieving samples from each site. LGa samples from 0 to 1 ft depth and from 7 to 8 ft depth were chosen for the lemongrass site. The CR3 sample from 1.4 ft depth was chosen for the Forested Site.

Samples were initially dried in an oven over night at 105 degrees Celsius. All organic material was removed and lumps were pressed out using a mortar and pestle. The soil was then shaken through a No. 200 sieve in order to retain the finer clay materials

and remove as much quartz as possible. Finally, a powdered sample was placed on a glass slide and inserted into the XRD machine for analysis. Initial results showed interference and high intensities which can make mineral identification more difficult, so a second set of samples was prepared using the same technique as above, but instead of making a powder sample the material was made into a slurry, allowed to settle, and then placed on the glass side using an eye dropper. These samples were allowed to dry completely (at least 5 hours) prior to XRD analysis. After the samples were x-rayed, the 2-theta peaks were compared to known peaks of different clays in order to determine the clay minerals.

Direct Shear Testing

Direct shear testing began by trimming the 3 inch diameter cores collected at LG, CR6, CR2, and CR3. The core diameter needed to be reduced to fit in the circular shear ring inside the direct shear box (Figure 2.5), so the cores were trimmed into a cylindrical sample with a diameter of 2.5 inches and a height of 1 inch. The average height and diameter of each sample were measured with a Vernier caliper and recorded. The weight and gravimetric moisture content were also measured and recorded. Moisture content is the ratio of the mass of water in a sample to the mass of solids in the sample and is expressed as a percentage. It is measured by weighing a soil sample, drying the sample to remove the water, and then weighing the dried sample. The moisture content before testing was found by using the soil trimmings from the PVC core tube, while moisture content after testing was found using the direct shear sample. These two numbers can be compared to see how the sample changed with direct shear testing.

Direct shear testing was accomplished using a GeoTAC computer-controlled testing system run by DigiShear software (Figure 3.31). Once a sample was prepared, it was placed into the direct shear machine to perform a cyclic drained direct shear test. A cyclic test determines a shear stress value for each cycle performed (Figure 3.32a). The average of these values is used to plot to shear strength vs effective normal stress (Figure 2.6)

For each sample, a series of three tests were done at normal stresses of 500 lb/ft^2, 1000 lb/ft^2, and 2000 lb/ft^2. A test consisted of two phases: consolidation and shearing. During the consolidation phase, a sample was compressed at a certain normal stress until the consolidation plot of deformation vs time reached a constant value (Figure 3.32b). After consolidation the displacement rate, the rate at which shearing will occur, was determined using ASTM standard D3080:

$$t_F = 50t_{50} \tag{3.1}$$

$$Rate = \frac{d}{t_F} \tag{3.2}$$

where t_F is the time to failure, t_{50} is the time to achieve 50% consolidation, and d is the horizontal displacement. The displacement d was set at 0.25 inches and was the same for each test, while t_{50} varied during the test and depended on the constant value that each sample reached during consolidation. After the displacement rate was found, the shearing phase of the test was conducted to determine the shear strength at the same normal stress used in the consolidation phase. After both phases were completed, the next test was run and the same steps were followed until all three normal stresses listed above were tested. The results were used to plot shear strength vs effective normal stress (Figure 2.6) in

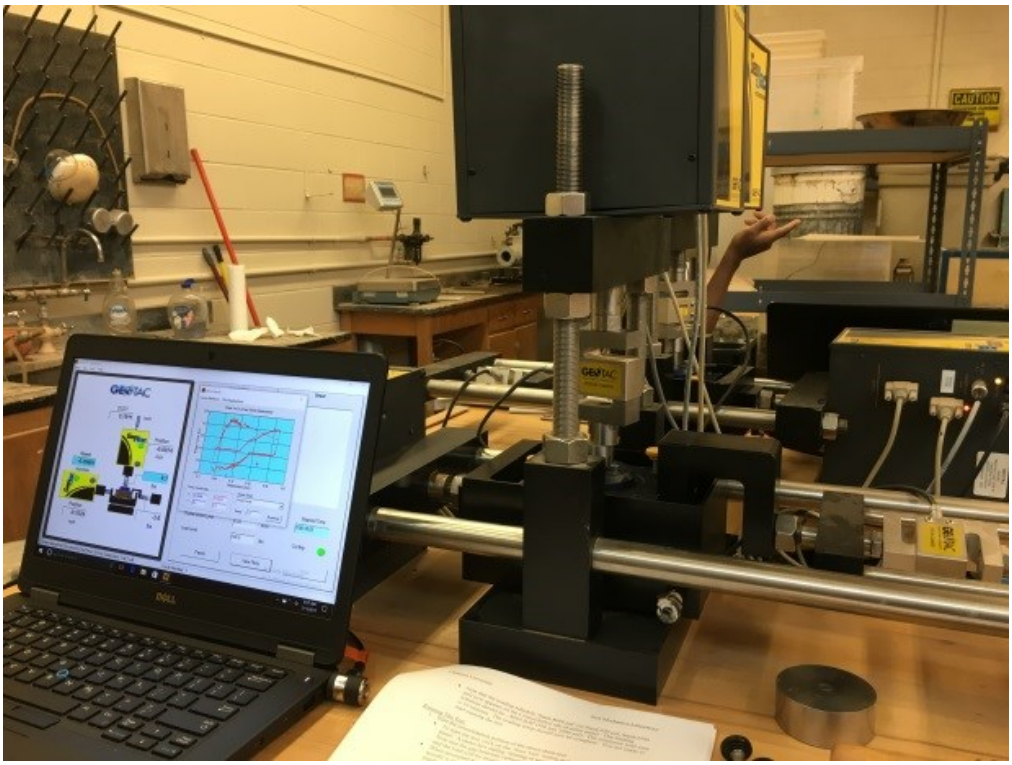

Figure 3.31: Direct shear test machine shown with the computer running the DigiShear software.

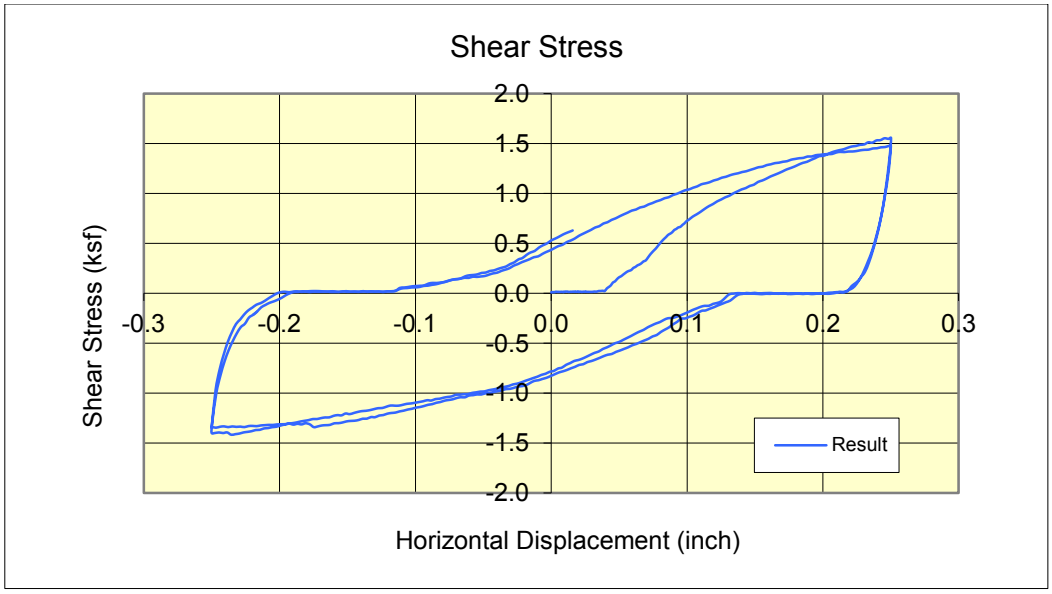

(a)

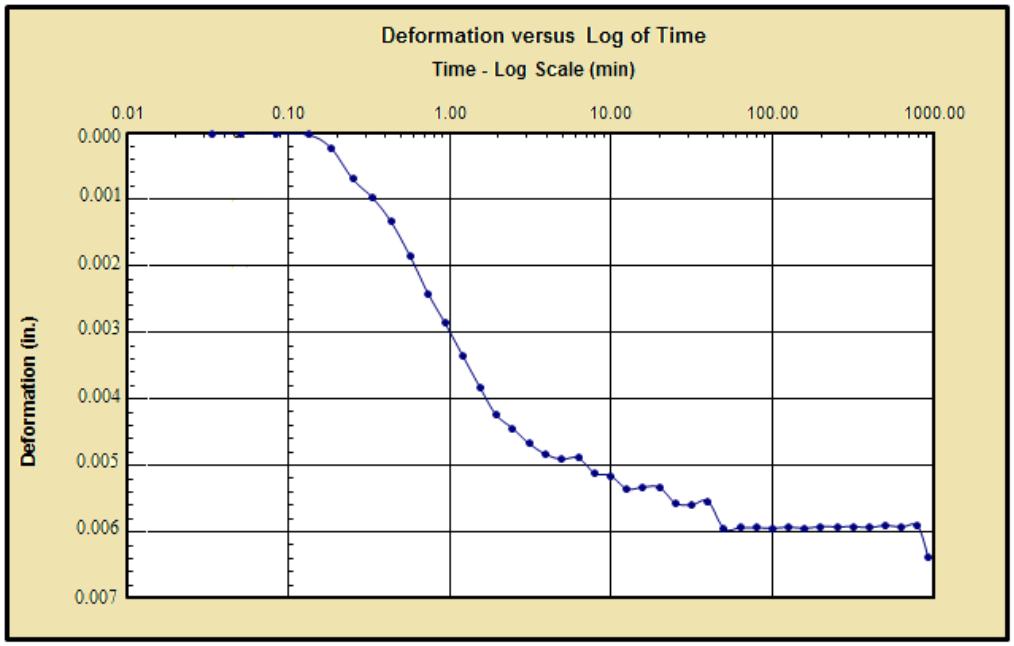

(b)

Figure 3.32: Examples of plots generated during direct shear testing. This specific data is for sample CR2 with a vertical load of 1000 lb/ft^2. Shear stress versus horizontal displacement (a) and deformation (vertical displacement) versus time (b).

order to find the friction angle (slope) and cohesion (y-intercept) values, which were used in the limit equilibrium analysis.

Limit Equilibrium Analysis

Limit equilibrium analysis was done using the infinite slope method. The infinite slope method is useful for very shallow, translational slides like those on Dominica (Reading, 1991; Rouse et al., 1986). Since a drained shear test was performed, the infinite slope equation for effective stress will be used and is listed in Formula 2.7.

Since LG is the only slope that hadn't failed in the study, it is the only slope that a forward calculation can be done on in order to find the factor of safety and predict failure or stability. This analysis uses Formula 2.7 and the effective friction angle and effective cohesion are those found in the direct shear test results. Since the other slopes have already failed, forward calculations will not be done, but instead two different back calculations will be done to find the friction angle needed for the current slope to stay stable under different conditions and the depth above or below the failure surface that the water table reached before the initial failure occurred (z_w). Certain assumptions must be made for the back calculations and are as follows:

- $c' = 0$
    - These soils have residual strength, and soils with residual strength typically have a c' value at or close to 0.
- $u = 0$ OR $u = \gamma_w z cos^2 \beta$

    - $u = 0$ is used for general conditions in instances where the water table is at the same elevation as the failure plane.
    - $u = \gamma_w z cos^2 \beta$ is used for seepage conditions in instances where there is seepage parallel to the slope (i.e. the water table is equal to the ground surface). γ_w is the density of water.
- The slope is made of homogeneous materials
- $\beta = 36°$
    - Measured in the field
- z = 2 to 5 feet
    - Depends on the site
- γ = 96 to 105 lb/ft^3
    - Depends on the site
    - It is calculated by dividing the mass of the direct shear test sample by its volume
- FS = 1
    - Condition at failure

Since *c'* is assumed to be 0, Formula 2.7 can be simplified to

$$FS = \left[cot\beta - \frac{u}{\gamma z}(cot\beta + tan\beta)\right] tan\phi' \quad (3.3)$$

Using Formula 3.3 and the two different values for *u*, the friction angle ϕ' needed to stay stable for both seepage (3.4) and general (3.5) conditions can be determined:

$$\phi' = tan^{-1}\left[\frac{FS}{cot\beta - \frac{\gamma_w z cos^2\beta}{\gamma z}(cot\beta - tan\beta)}\right] \quad (3.4)$$

$$\phi' = tan^{-1}\left[\frac{FS}{cot\beta}\right] \quad (3.5)$$

Additionally, by rearranging Formula 3.3 to solve for z_w, the depth above or below the failure surface that the water table reached during the initial failure can be determined. In order to do this, *FS* is assumed to be 1 and the ϕ' value is derived from direct shear testing. Lastly, the pore pressure value is for seepage conditions, but the depth *z* becomes the depth of the water table z_w:

$$FS = \left[cot\beta - \frac{u}{\gamma z}(cot\beta + tan\beta)\right] tan\phi'$$

$$1 = \left[cot\beta - \frac{\gamma_w z_w cos^2\beta}{\gamma z}(cot\beta + tan\beta)\right] tan\phi'$$

$$z_w = \frac{\gamma z(tan\phi' cot\beta - 1)}{\gamma_w cos^2\beta tan\phi'(cot\beta + tan\beta)} \quad (3.6)$$

Site	Soil Density ϒ (lb/ft^3)	Depth of Failure *z* (ft)
LG	102	5
CR6	105	5
CR2	101	2
CR3	96	2

Table 3.1: Site specific variables for slope failure assessment.

CHAPTER FOUR

RESULTS

Landslide Characteristics

All slope failures occurred on a hillside and all have un-vegetated surfaces except for slides CR3 and CR5, which pre-dated Hurricane Erika. Slides further up the road (CR6, CR7, and CR8) contained finer grained material than lower down the road (CR1 to CR5). CR2, CR3, and CR6 had similar slope angles at 36 degrees while the remaining

Site	Length (ft)	Width (ft)	Slope Angle (deg.)	Avg. depth to failure surface (ft)	Material on Failure Surface	Setting	Current Conditions
CR1	53	40	40-45	2 to 3	boulders to clay-sized ash	hillside	un-vegetated
CR2	43	18	36	2	clay size to cobble	hillside	un-vegetated
CR3	NA	NA	36	2	clay size to cobble	hillside	vegetated (tropical plants)
CR4	20	19	40-45	2 to 3	cobbles < 20cm clay clasts < 5cm	hillside	un-vegetated
CR5	NA	NA	40-45	NA	cobbles < 20cm clay clasts < 5cm	hillside	vegetated (tropical plants and tall brush)
CR6	44	70	36	5	clay clasts and rocks > 3cm	hillside	un-vegetated
CR7	64	48	52	5	clay clasts and rocks > 3cm	hillside	un-vegetated
CR8	NA	NA	50	5	loose material, no boulders or cobbles	hillside	un-vegetated

Table 4.1: Results from landslide characterization.

slides were much steeper at 40 to 50 degrees. Length and width measurements could not be taken for CR3 and CR5 due to the more recent slides (CR2 and CR4) that cut into them. CR5 was also highly vegetated and not easily accessible, making the depth of the slide unmeasurable. Measurements for CR8 are scarce due to accessibility issues (too dangerous to descend the slope). See Table 4.1 below.

Soil Characterization

Soil at the Lemongrass Site was found to have medium high to high plasticity and typically ranged from silty clay to sandy clay. The sandy clays were very gritty and the silty clays only slightly gritty. The soil color was a consistent hue of 7.5YR and ranged from 3 to 5 in value. Soil at the Forested Site is highly plastic clay with coloring also in the 7.5YR hue (Table 4.2).

Sample	Depth (ft)	Plasticity	Ribbon Length (cm)	Name	Munsell soil color
LG-a	0-1.0	Med. High	> 5	Sandy Clay	7.5YR 4/3
	7.0-8.0	Med. High	> 5	Sandy Clay	7.5YR 5/4
LG-b	0-2.0	High	~ 7	Silty Clay	7.5YR 3/2
	6.5-8.0	High	~ 7	Silty Clay	7.5YR 4/2
LG-c	0-0.8	High	> 8	Silty Clay	7.5YR 3/2
	7.5-8.0	Low	~ 3	Silty Clay Loam	7.5YR 4/6
LG-d	0-0.8	High	~ 7	Clay	7.5YR 3/1
	7.0-7.5	Low	~ 3	Silty Clay Loam	7.5YR 4/6
CR3	1.4	High	~ 10	Clay	7.5YR 3/4

Table 4.2: Results from soil characterization.

Clay Determination using X-Ray Diffraction (XRD)

XRD analysis yielded similar results for all three samples. The untreated tests and the slurry treated tests had peaks at the same 2-theta values, but the slurry treated tests had lower intensities (Figures 4.1, 4.2, and 4.3). By comparing the peaks from the results to typical peaks of halloysite, montmorillonite, kaolinite, and allophane, the clay minerology present at the study area could be determined. Both samples from the Lemongrass Site, as well as the sample from the Forested Site, had large peaks at 12 Å and 20 Å. Smaller peaks tended to occur at 25, 27, 35, 55, and 63 Å. The mineral halloysite has large peaks at 12 and 20 Å, with smaller peaks at 25, 27, 35, 50, 55, and 63 Å (Figures 4.4 and 4.5). The mineral kaolinite has a large peak at 12 Å with smaller peaks at 20, 22, 23, and 25 Å (Figure 4.6). The mineral montmorillonite can have a large peak somewhere between 5 and 9 Å, with smaller peaks at 15, 18, and 27 Å (Figure 4.7). The mineral allophane has large peaks at 20 and 25 Å with smaller peaks at 11, 18, and 40 Å (Figure 4.8). After deliberation, it was found that the peaks from the samples most closely match those of halloysite, which indicates the presence of kandoid soil at both study sites.

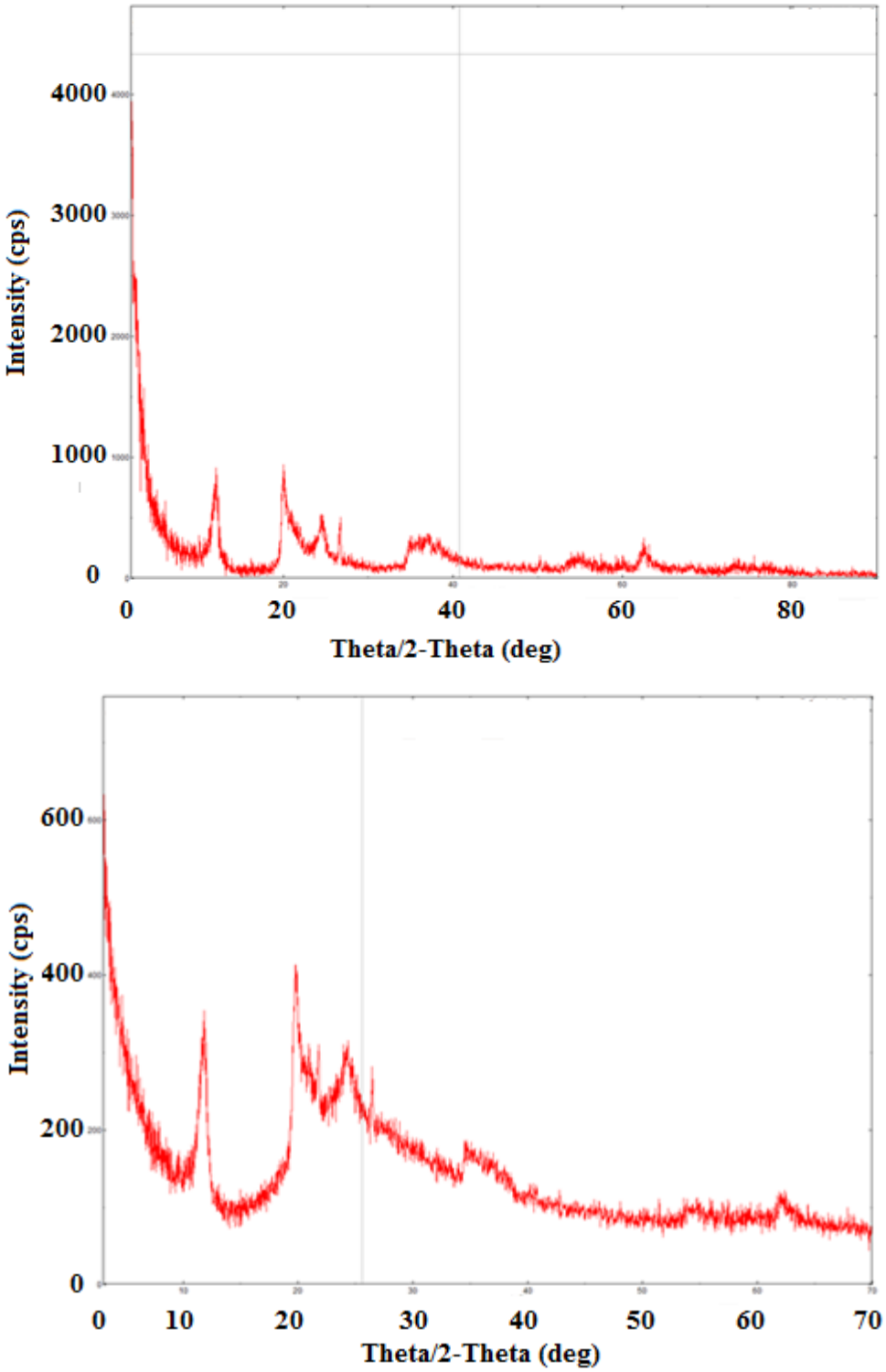

Figure 4.1: XRD results for both the untreated (top) and slurry treated sample (bottom) taken from a depth of 1-2 ft at LGa.

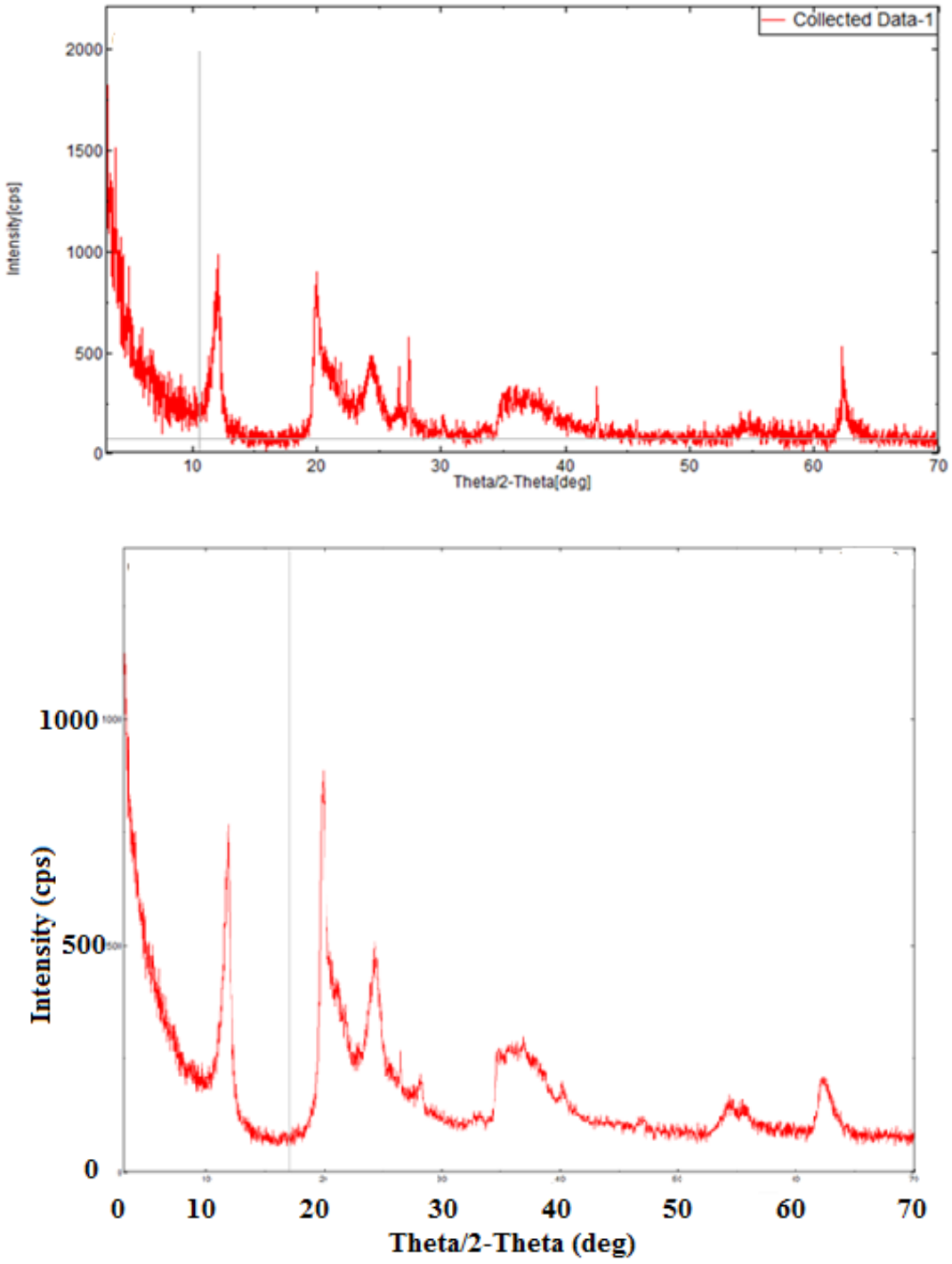

Figure 4.2: XRD results for both the untreated (top) and slurry treated sample (bottom) taken from a depth of 7-8 ft at LGa.

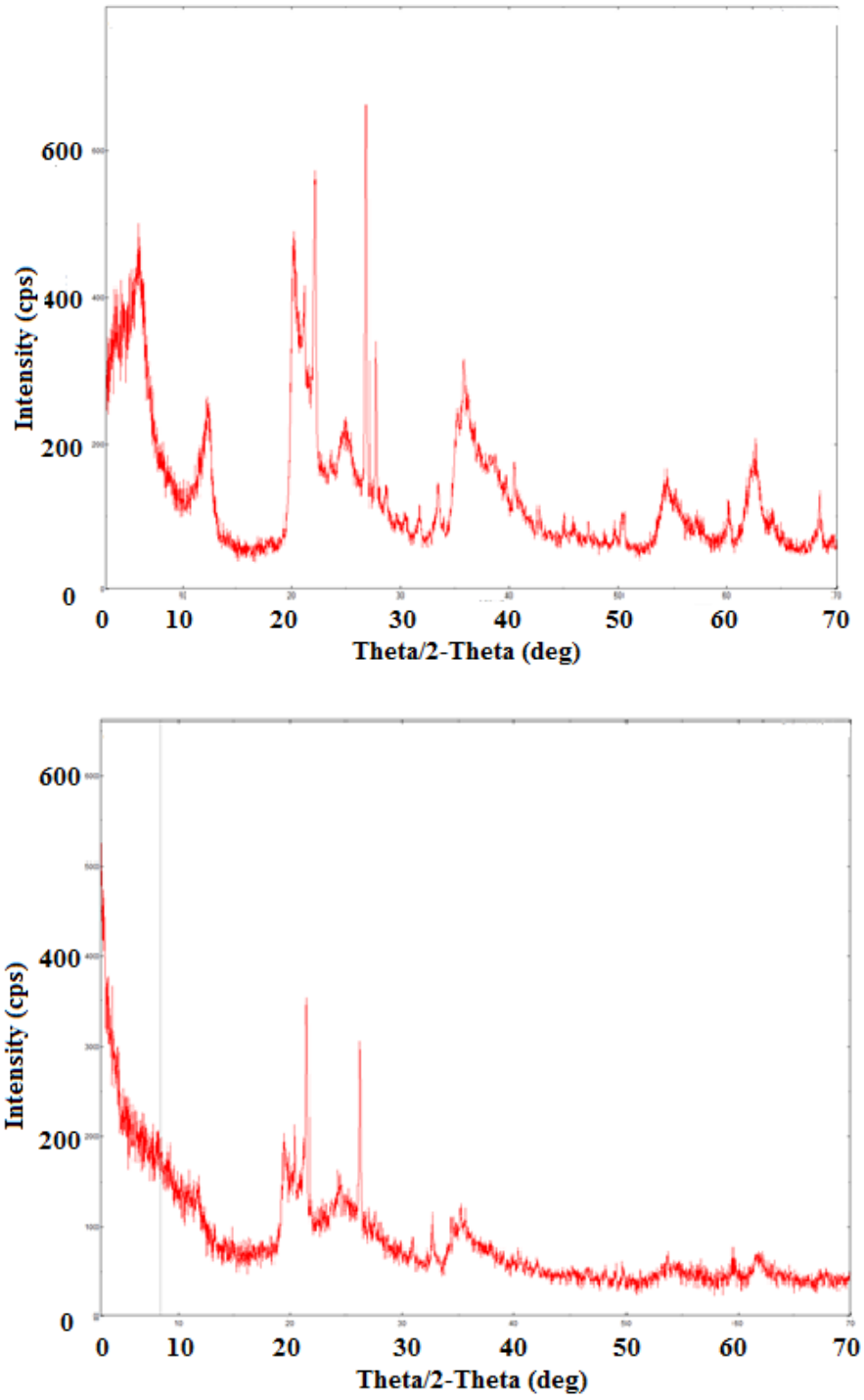

Figure 4.3: XRD results for both the untreated (top) and slurry treated sample (bottom) taken from a depth of 1.4 ft at CR3.

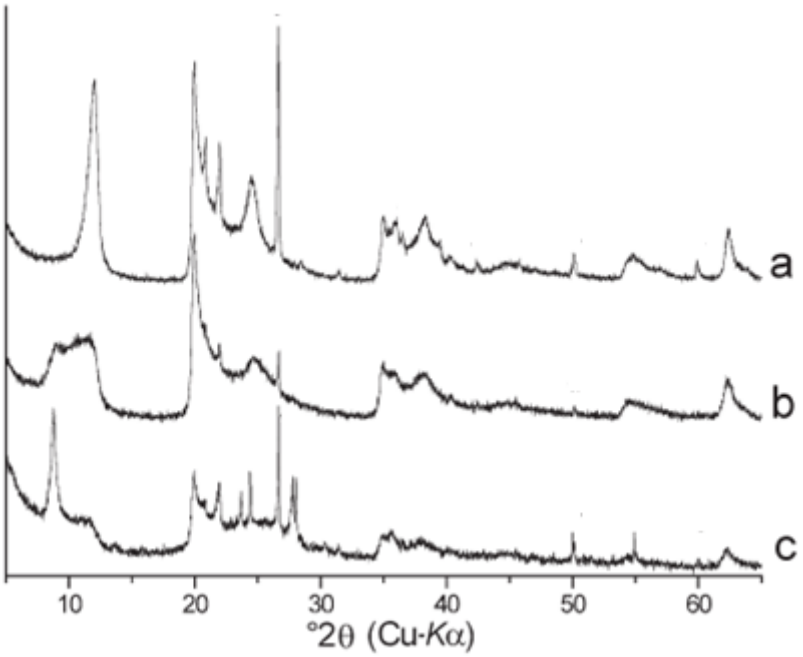

Figure 4.4: XRD powder patterns of the clay mineral Halloysite at three different locations in New Zealand (Modified from Joussein et al., 2005).

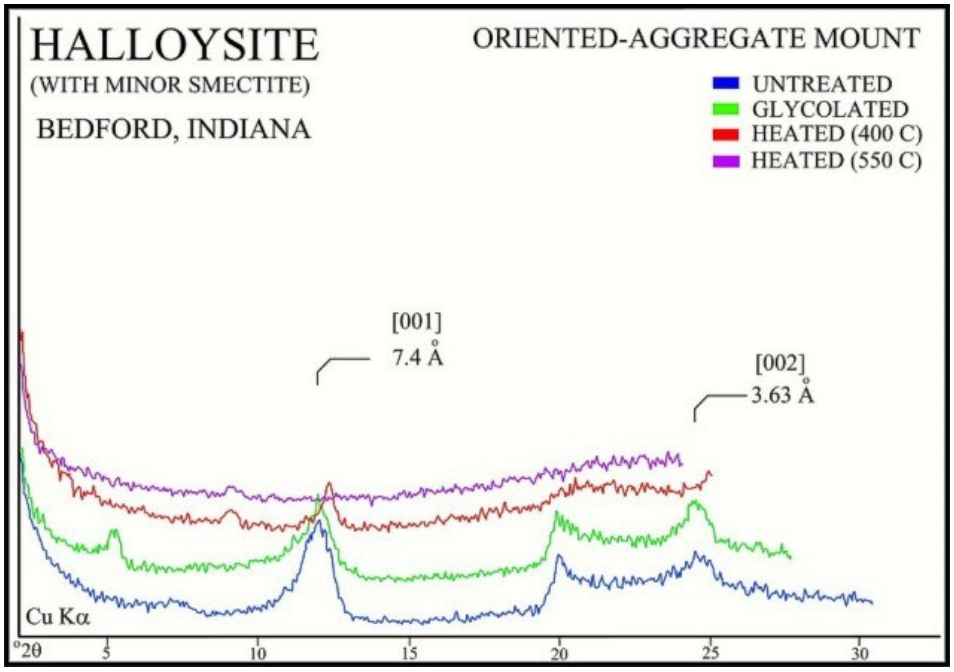

Figure 4.5: XRD patterns for the clay mineral halloysite (Poppe et al., n.d.).

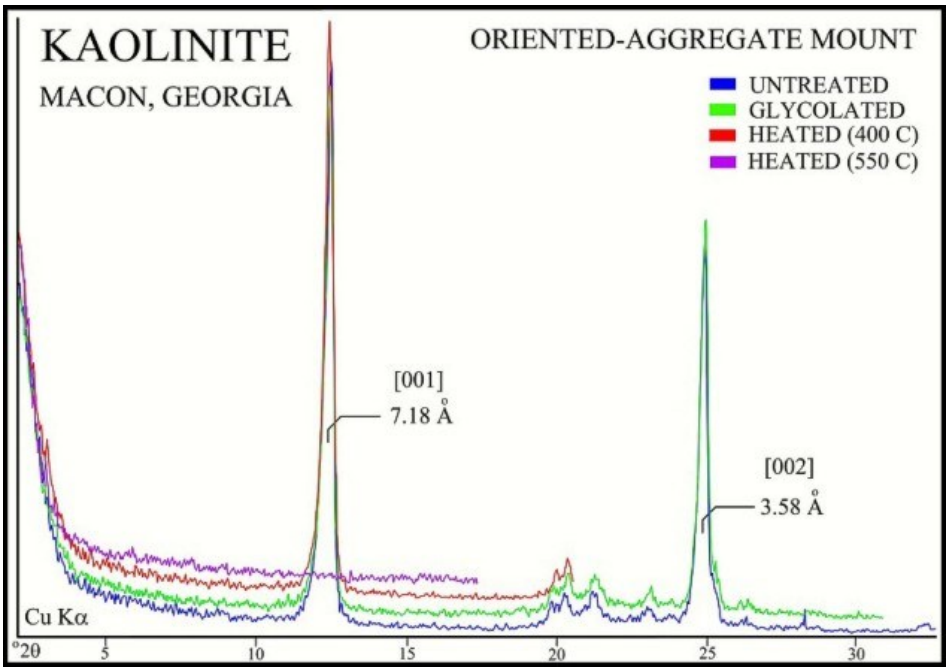

Figure 4.6: XRD patterns for the clay mineral kaolinite (Poppe et al., n.d.).

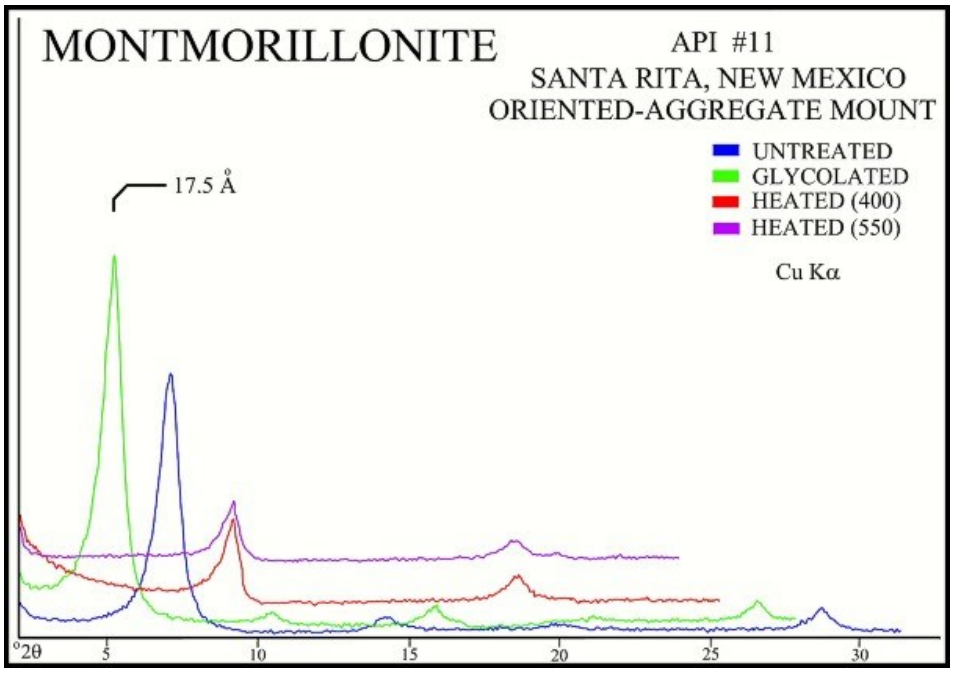

Figure 4.7: XRD patterns for the clay mineral montmorillonite (Poppe et al., n.d.).

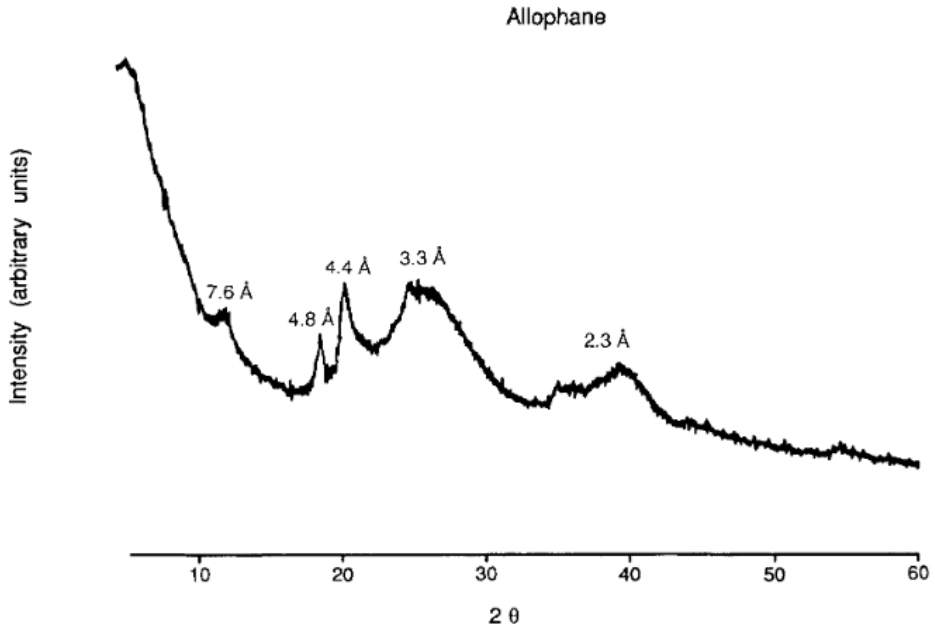

Figure 4.8: XRD pattern of Allophane from NM (He et al., 1995).

Vane Shear Testing

The results from vane shear testing in the field can be seen in Tables 4.3-4.6. Site LGa has average undrained shear strength values of around 1940 psf near the surface. The strength increased to 1655 psf at a depth of 3 ft, but then decreased to 1358 and 1389 psf at depths of 4 and 5 ft. At 6 ft depth, the shear strength increased again to about 2100 psf (Table 4.3). Site LGb had average strength values of about 1370 psf close to the surface. At 2 ft depth, this decreased to 940 psf. Depths of 3 to 5 ft had average strength values ranging from 2100-2420 psf, but they decreased to 1525 and 1744 psf at 6 and 7 ft depths before increasing again at 8 ft (Table 4.4). At site LGc, the vane shear could only

be used at depths of up to 4 ft. The strength ranged between 2500 and 2925 psf for depths of 1 to 3 ft before jumping to 4180 psf at a depth of 4 ft (Table 4.5). Site LGd showed strength values that steadily increased from about 2090 to 4390 from depths of 1 to5 ft. At depths of 6 and 7 ft there was a slight decrease to about 4280 (Table 4.6).

Site	Depth	Shear Strength									
		Hole 1		Hole 2		Hole 3		Hole 4		Avg.	
	ft	KPa	lb/ft^2	KPa	lb/ft^2	KPa	lb/ft^2	KPa	lb/ft^2	KPa	lb/ft^2
LG-a	1	85	1775	130	2715	110	2297	46	961	96	1937
	2	102	2130	84	1754	84	1754	102	2130	91	1942
	3	64	1337	97	2026	70	1462	86	1796	77	1655
	4	50	1044	70	1462	82	1713	58	1211	68	1358
	5	60	1253	44	919	88	1838	74	1546	71	1389
	6	66	1378	126	2632	124	2590	89	1859	106	2115

Table 4.3: In-situ undrained shear strength results from vane shear testing at LGa.

Site	Depth	Shear Strength					
		Hole 1		Hole 2		Average	
	ft	KPa	lb/ft^2	KPa	lb/ft^2	KPa	lb/ft^2
LG-b	1	45	940	86	1796	65.5	1368
	2	30	627	60	1253	45	940
	3	103	2151	98	2047	100.5	2099
	4	110	2297	100	2089	105	2193
	5	128	2673	104	2172	116	2423
	6	76	1587	70	1462	73	1525
	7	97	2026	70	1462	83.5	1744
	8	108	2256	102	2130	105	2193

Table 4.4: In-situ undrained shear strength results from vane shear testing at LGb.

Site	Depth	Shear Strength	
		Hole 1	
	ft	KPa	lb/ft^2
LG-c	1	140	2924
	2	120	2506
	3	128	2673
	4	200	4177

Table 4.5: In-situ undrained shear strength results from vane shear testing at LGc.

Site	Depth	Shear Strength	
		Hole 1	
	ft	KPa	lb/ft^2
LG-d	1	100	2089
	2	122	2548
	3	170	3551
	4	210	4386
	5	210	4386
	6	205	4282
	7	205	4282

Table 4.6: In-situ undrained shear strength results from vane shear testing at LGd.

Direct Shear Testing

Data from direct shear testing can be seen in tables 4.7, 4.8, and 4.9. Graphs produced from the DigiShear software are shown in Figures 4.9-4.20. Figures 4.9, 4.10, and 4.11 are associated with sample CR2. Figures 4.12, 4.13, and 4.14 are associated with sample CR3. Figures 4.15, 4.16, and 4.17 are associated with sample LG. Figures 4.18, 4.19, and 4.20 are associated with sample CR6. The shear stress vs horizontal displacement graphs have units of ksf (kilopounds per square foot; 1ksf = 1000 psf).

These graphs show multiple shearing cycles. The stress values in table 4.9 are calculated by taking the average stress values at the max displacements. The effective normal stress in table 4.9 is the average normal stress that is applied during consolidation and is calculated in DigiShear. It should be noted that some of the tests were sheared at faster rates than the ASTM standard due to time constraints and limited access to the machine. These tests are noted in table 4.8. Data in table 4.9 were used to plot shear strength versus effective normal stress (units of psf; psf = pounds per square foot; 1000 psf = 1 ksf) for each selected site (Figures 4.21, 4.22, 4.23, and 4.24). A line of best fit was applied to each plot and from this line the effective cohesion (y-intercept of the line) and effective friction angle (slope of the line) were calculated.

Both LG and CR6 had similar *c'* values at 128 psf (pounds per square foot) and 159 psf respectively. CR2 had a much higher value at 319 psf. The line of best fit for CR3 initially showed a negative intercept, but cohesion cannot be negative, so the line was forced to an intercept of zero. LG and CR6 had lower values for ϕ' at 26˚ and 32˚, while CR2 and CR3 both had a higher value of 47˚. Maximum friction angles for clays and silty clays are typically around 30˚ so a friction angle of 47˚ is an anomalous. The Forested Site contained many rocks, clasts, and very stiff clay, which could possibly explain the larger friction angle.

Sample	Avg. Height (inches)	Avg. Diameter (inches)	Weight (grams)	Moisture Content	
				pre-testing	post-testing
LG	1.04	2.49	135.5	51.1%	52.5%
CR6	1.00	2.49	134.4	52.4%	58.1%
CR2	1.01	2.49	137.1	65.2%	59.6%
CR3	1.05	2.48	128.5	45.6%	54.1%

Table 4.7: Average height, average diameter, weight, and moisture content of direct shear test samples.

Sample	Consolidation (lb/ft^3)	t_{50} (min)	t_F (min)	Disp. Rate (in/min)
LG	500	60	*600	0.00042
	1000	1.5	75	0.0033
	2000	0.52	26.2	0.00954
CR6	500	60	*600	0.00042
	1000	1.5	75	0.0033
	2000	0.43	21.5	0.01163
CR2	500	0.93	46.5	0.00538
	1000	1	50	0.005
	2000	0.4536	22.68	0.01102
CR3	500	11	550	0.000455
	1000	3.93	196.5	0.00127
	2000	9.95	*99.5	0.002513

*Used $t_F=10*t_{50}$ instead of ASTM standard $t_F=50*t_{50}$ due to time constraints. If the standard rate was used, the time to shear the sample over multiple cycles would have been weeks instead of days.

Table 4.8: Shearing rate data for different normal stresses during direct shear testing.

Sample	Consolidation (lb/ft^2)	Shear Strength (psf)	Eff. Normal Stress σ' (psf)	Eff. Friction Angle ϕ' (degrees)	Eff. Cohesion c' (psf)
LG	500	408	500	32	128
	1000	791	1000		
	2000	1351	2000		
CR6	500	386	500	26	159
	1000	660	1000		
	2000	1114	2000		
CR2	500	846	501	47.0	320
	1000	1418	1011		
	2000	2459	2000		
CR3	500	296	556	47.0	*0
	1000	747	1000		
	2000	1337	2000		

*Had to force the intercept (c') to zero because c' can't be negative

Table 4.9: Results from direct shear testing including shear strength, effective normal stress, effective friction angle, and effective cohesion.

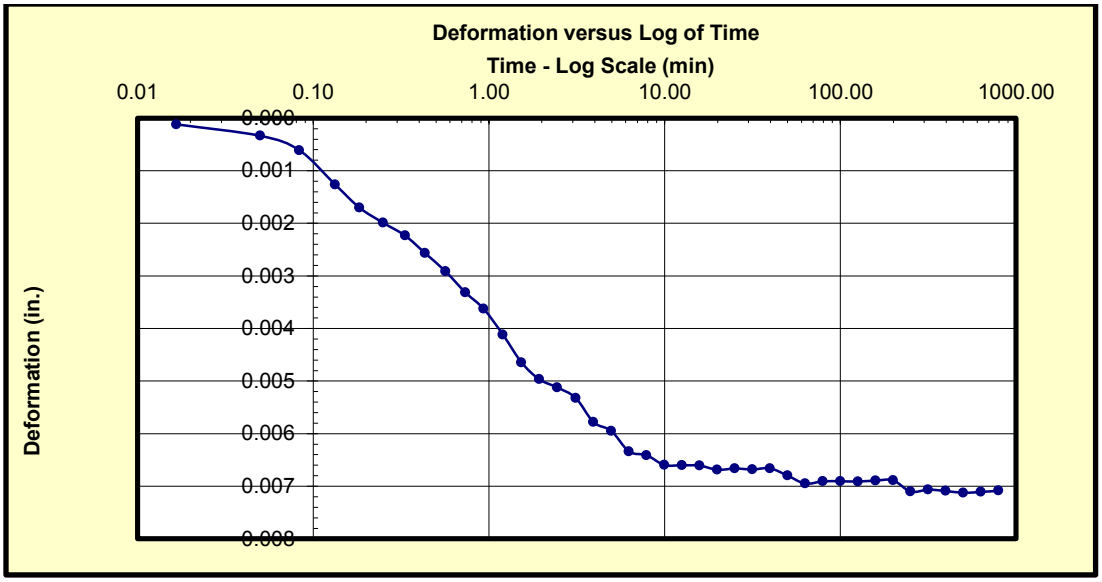

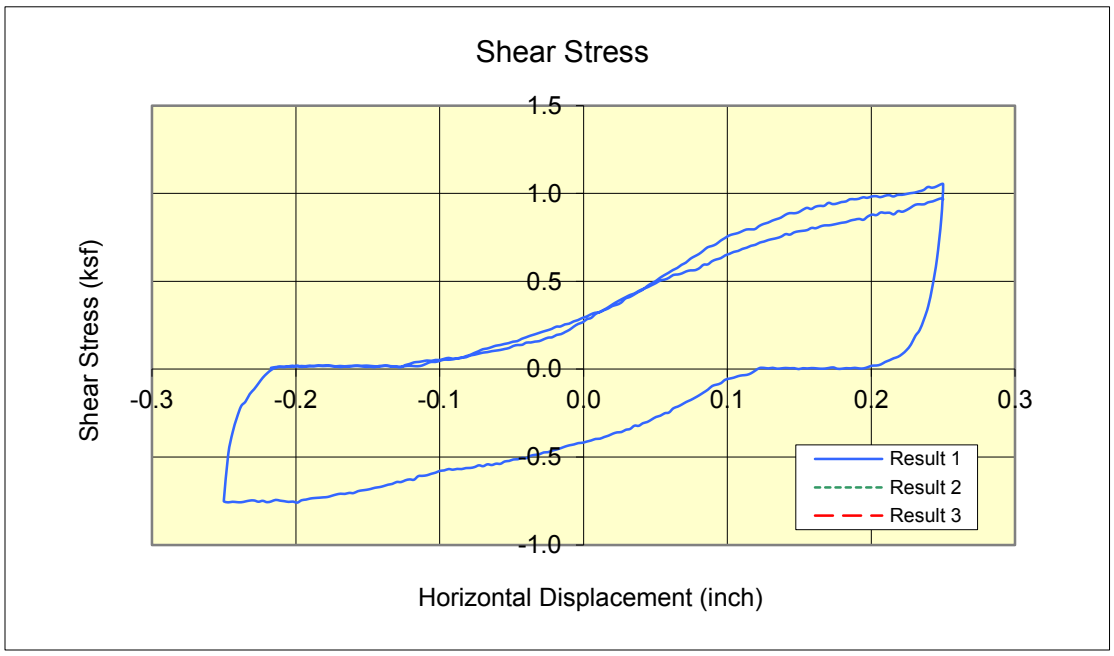

Figure 4.9: Deformation vs time and shear stress vs horizontal displacement graphs produced during direct shear testing of sample CR2 with a normal load of 500 lbs/ft^2 (lbs/ft^2 = psf and 1000 psf = 1 ksf).

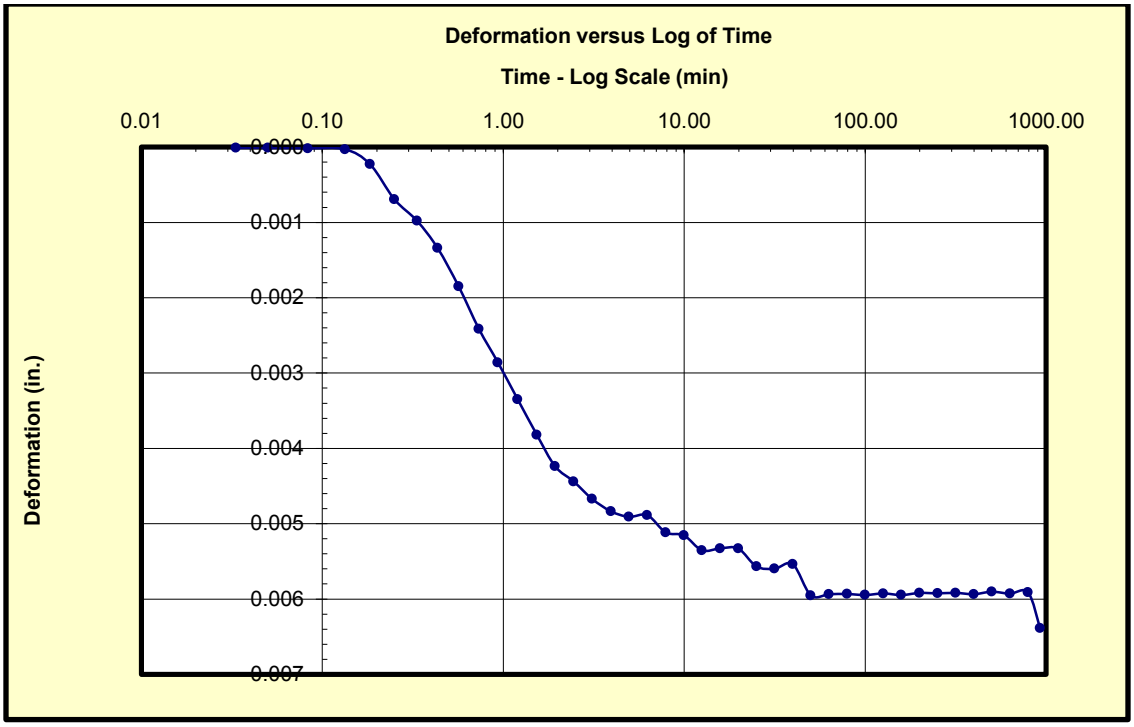

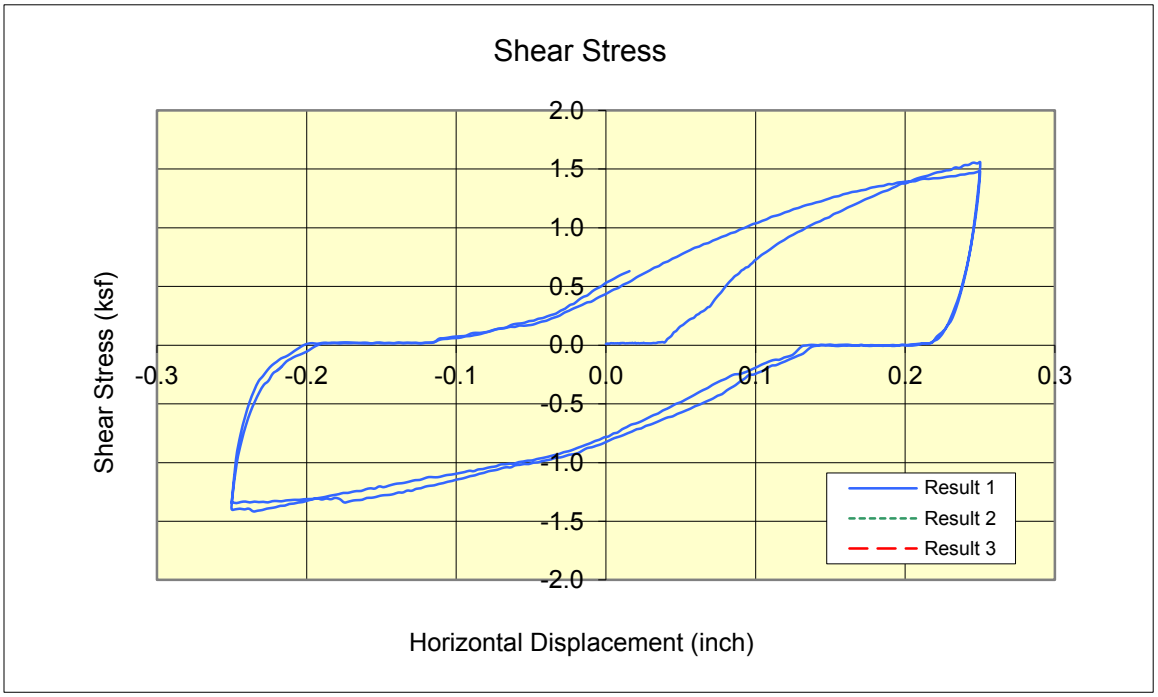

Figure 4.10: Deformation vs time and shear stress vs horizontal displacement graphs produced during direct shear testing of sample CR2 with a normal load of 1000 lbs/ft^2 (lbs/ft^2 = psf and 1000 psf = 1 ksf).

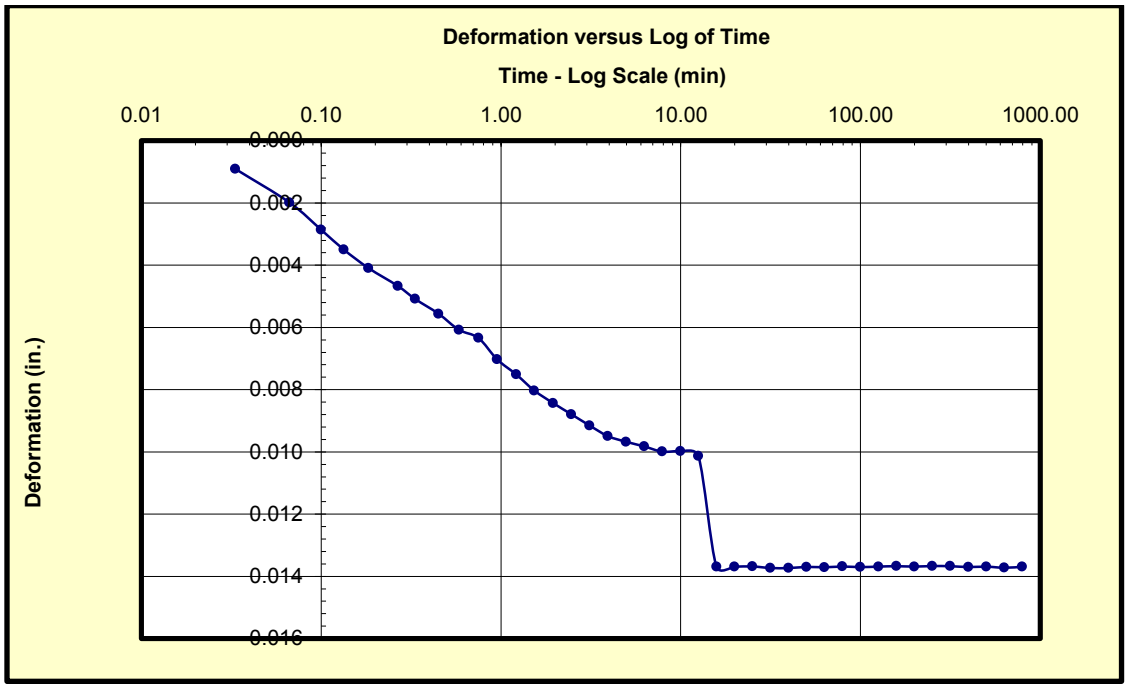

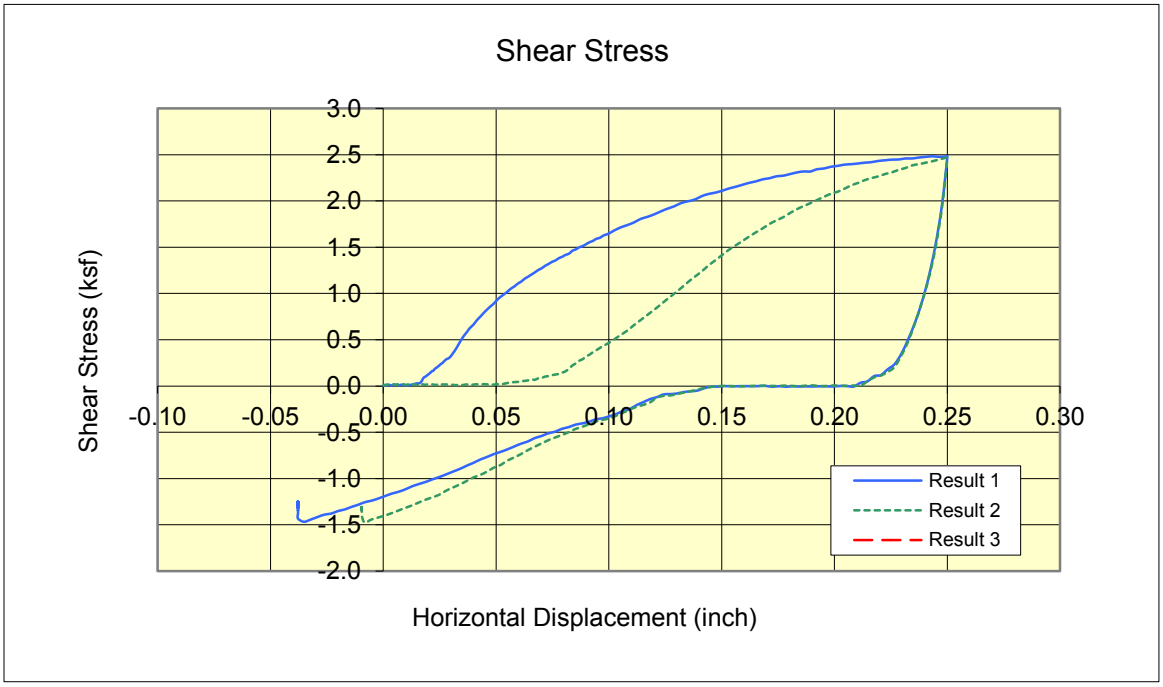

Figure 4.11: Deformation vs time and shear stress vs horizontal displacement graphs produced during direct shear testing of sample CR2 with a normal load of 2000 lbs/ft^2 (lbs/ft^2 = psf and 1000 psf = 1 ksf).

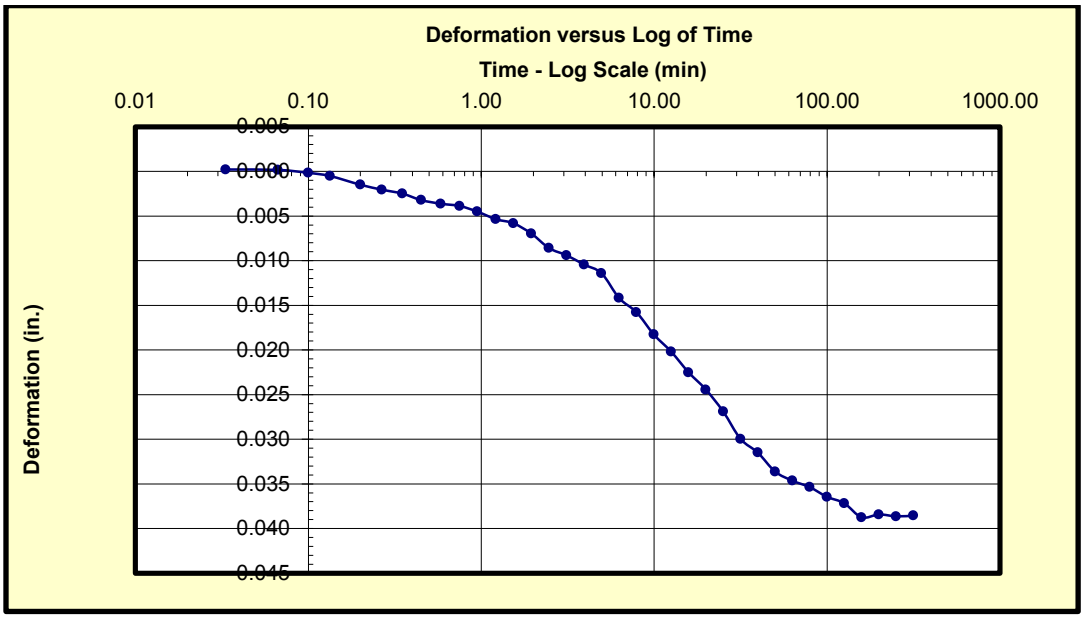

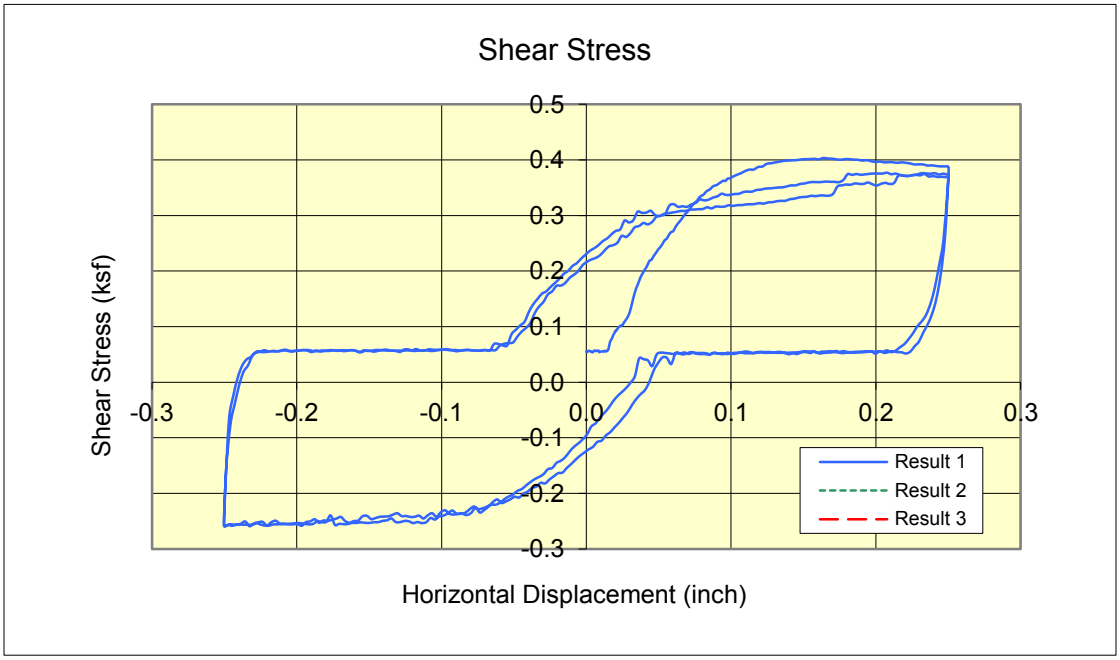

Figure 4.12: Deformation vs time and shear stress vs horizontal displacement graphs produced during direct shear testing of sample CR3 with a normal load of 500 lbs/ft^2 (lbs/ft^2 = psf and 1000 psf = 1 ksf).

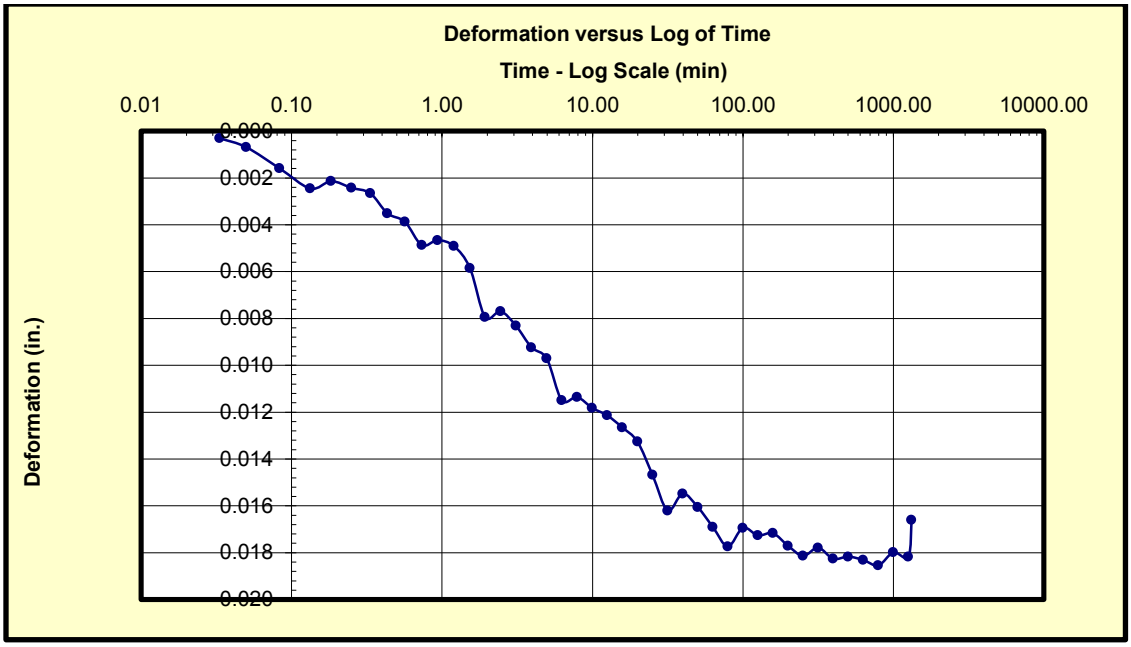

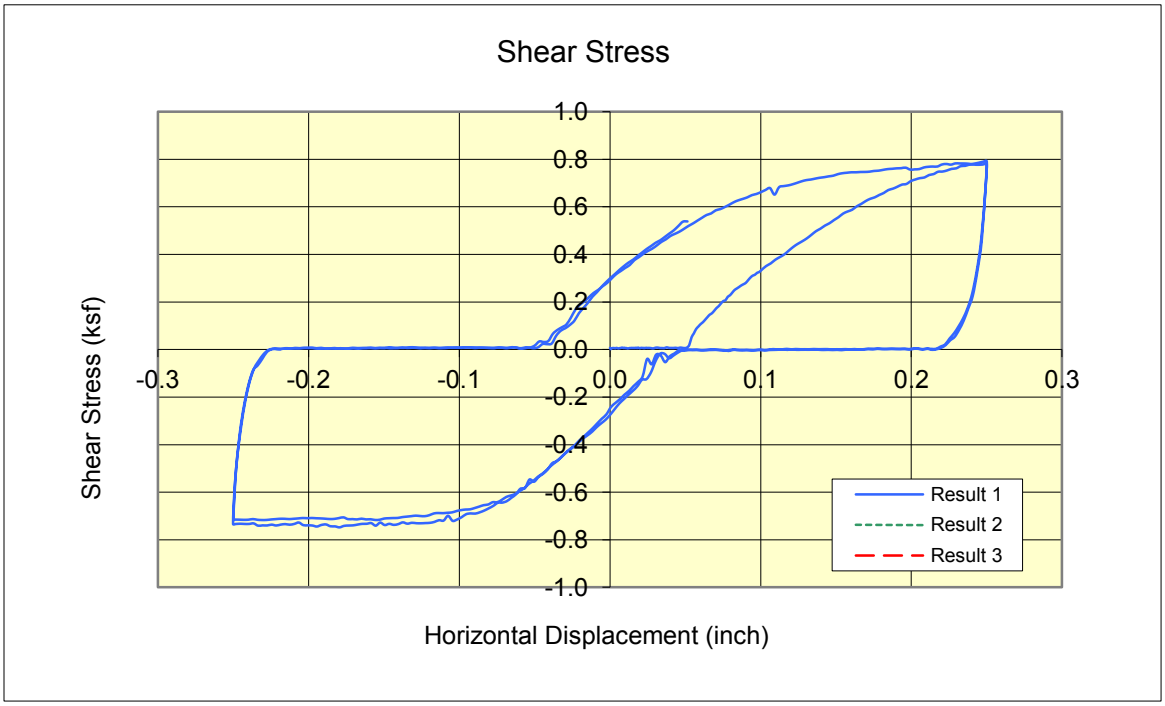

Figure 4.13: Deformation vs time and shear stress vs horizontal displacement graphs produced during direct shear testing of sample CR3 with a normal load of 1000 lbs/ft^2 (lbs/ft^2 = psf and 1000 psf = 1 ksf).

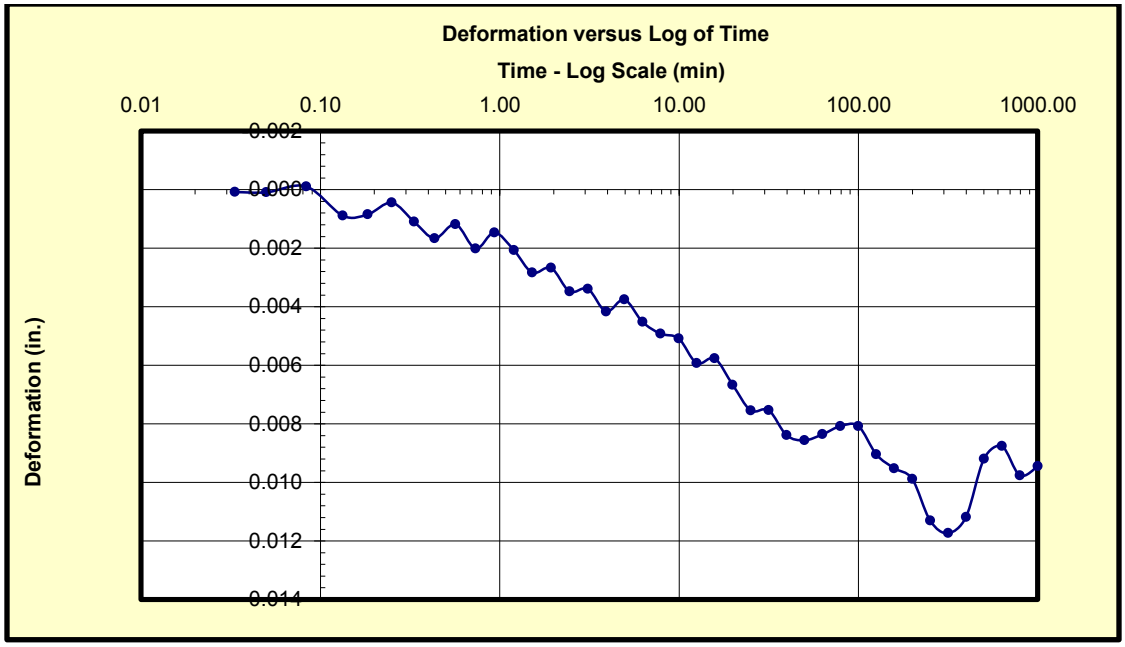

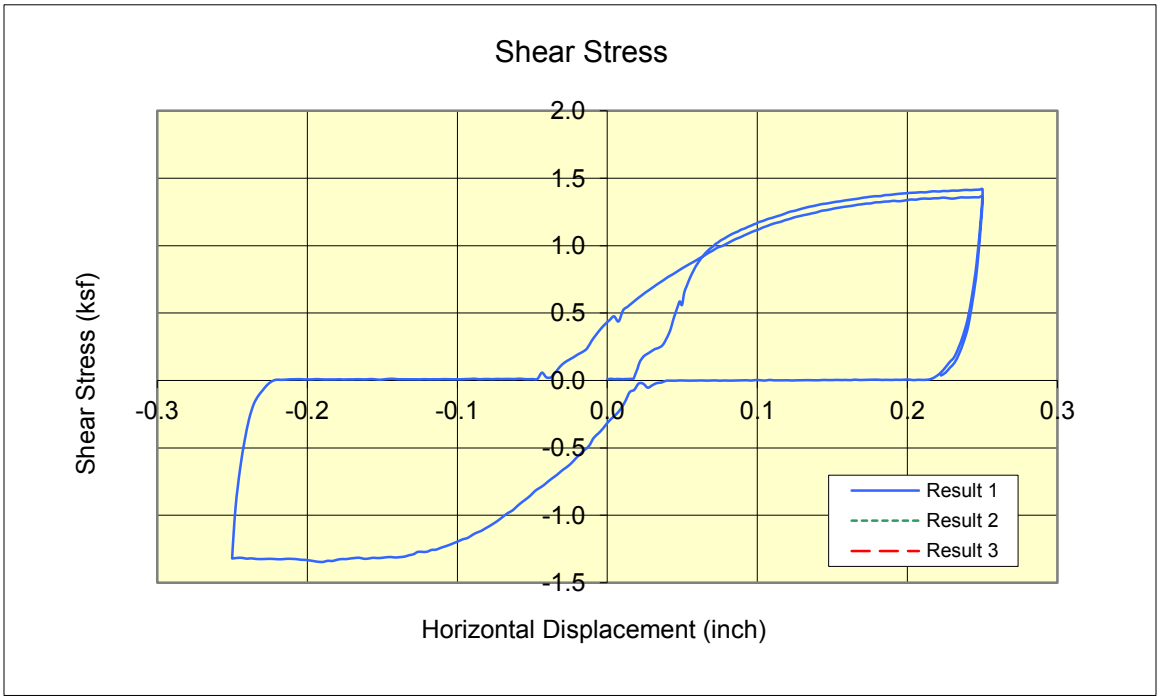

Figure 4.14: Deformation vs time and shear stress vs horizontal displacement graphs produced during direct shear testing of sample CR3 with a normal load of 2000 lbs/ft^2 (lbs/ft^2 = psf and 1000 psf = 1 ksf).

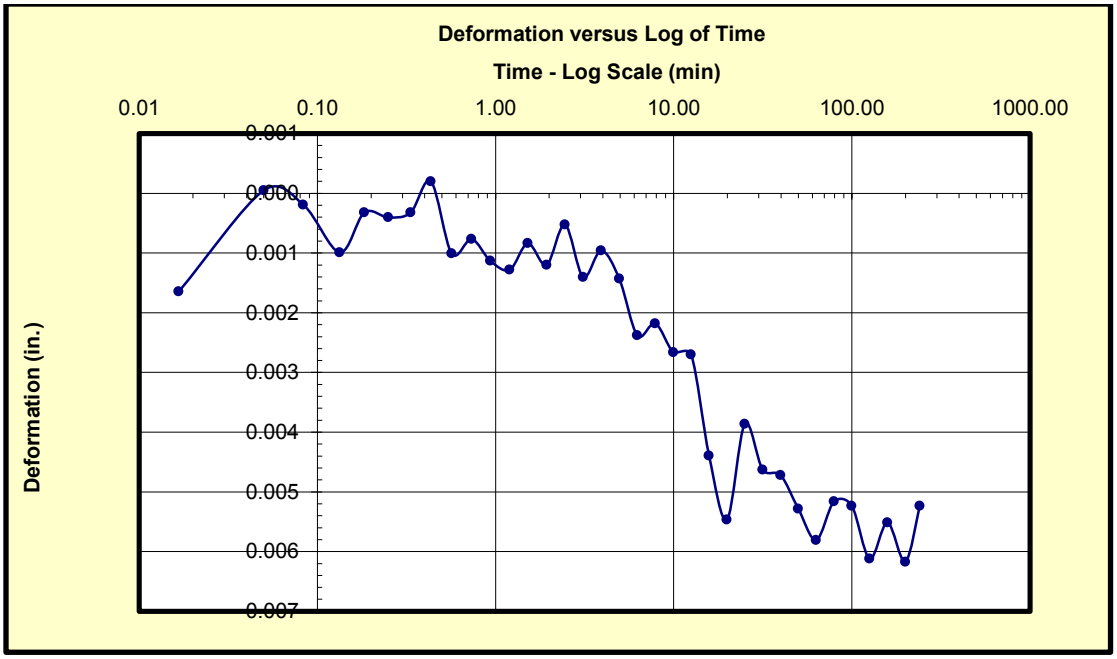

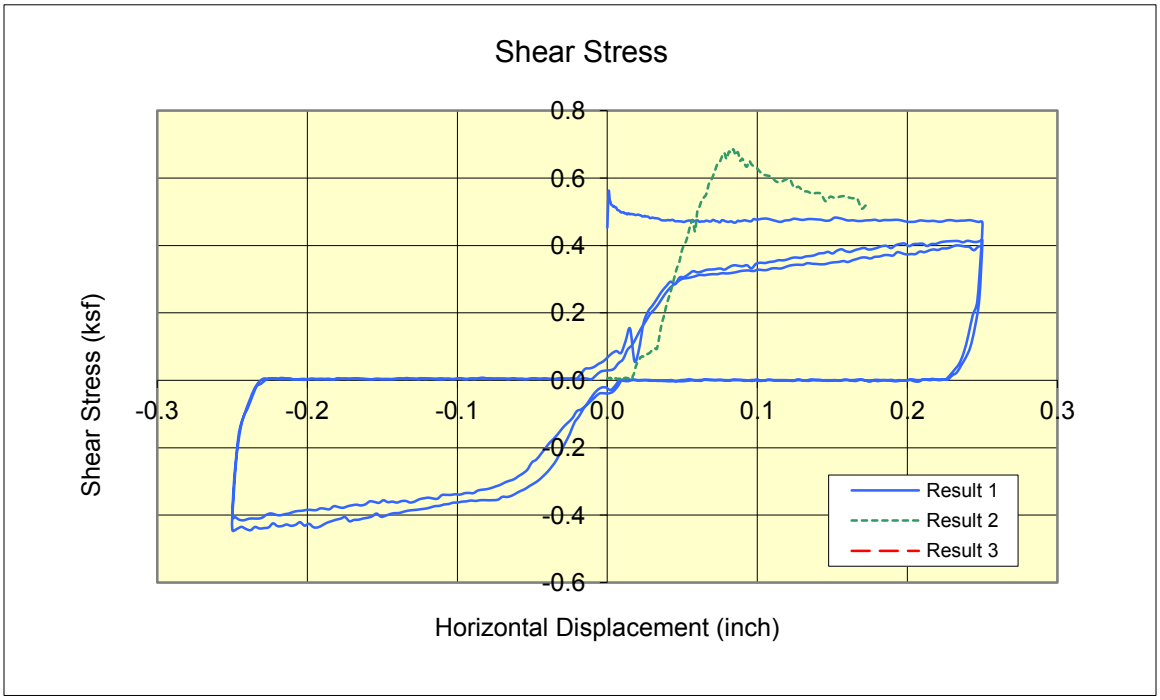

Figure 4.15: Deformation vs time and shear stress vs horizontal displacement graphs produced during direct shear testing of sample LG with a normal load of 500 lbs/ft^2 (lbs/ft^2 = psf and 1000 psf = 1 ksf).

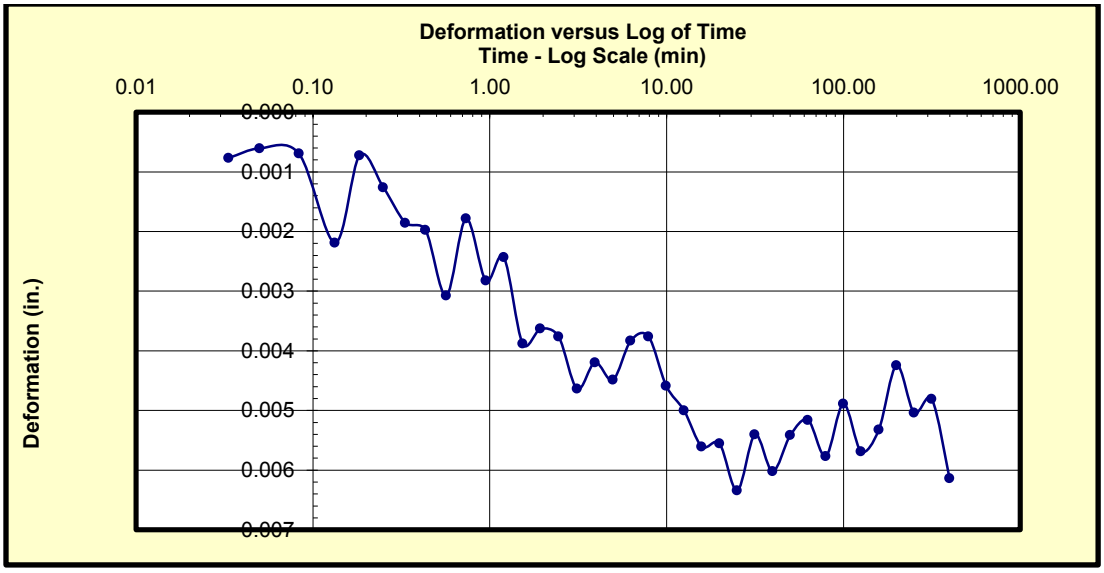

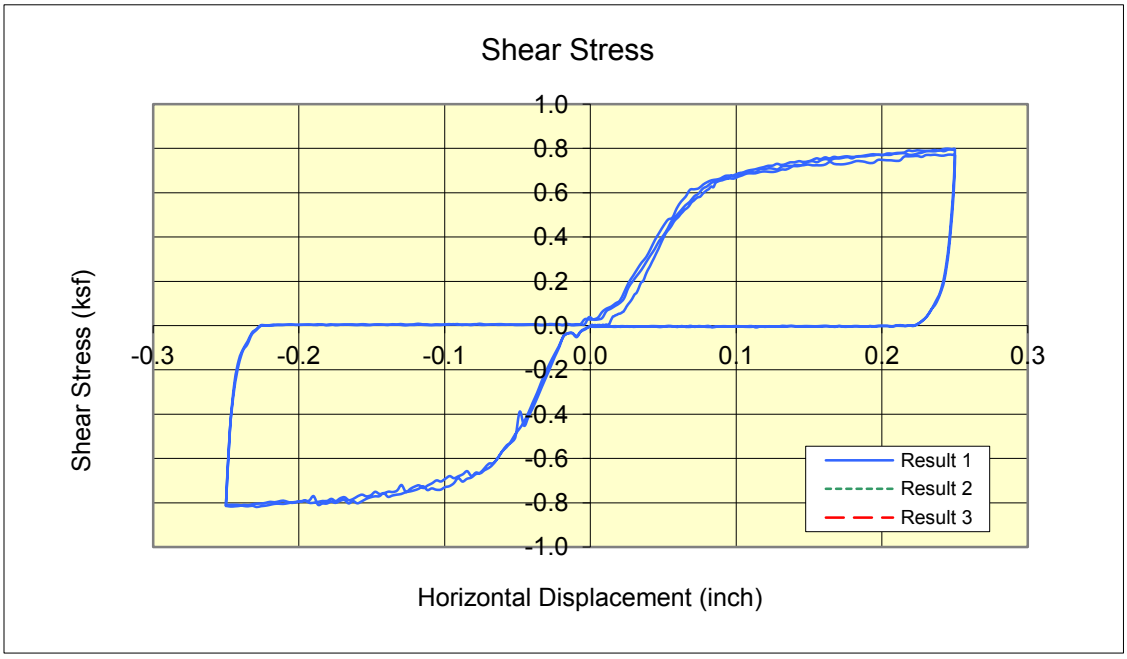

Figure 4.16: Deformation vs time and shear stress vs horizontal displacement graphs produced during direct shear testing of sample LG with a normal load of 1000 lbs/ft^2 (lbs/ft^2 = psf and 1000 psf = 1 ksf).

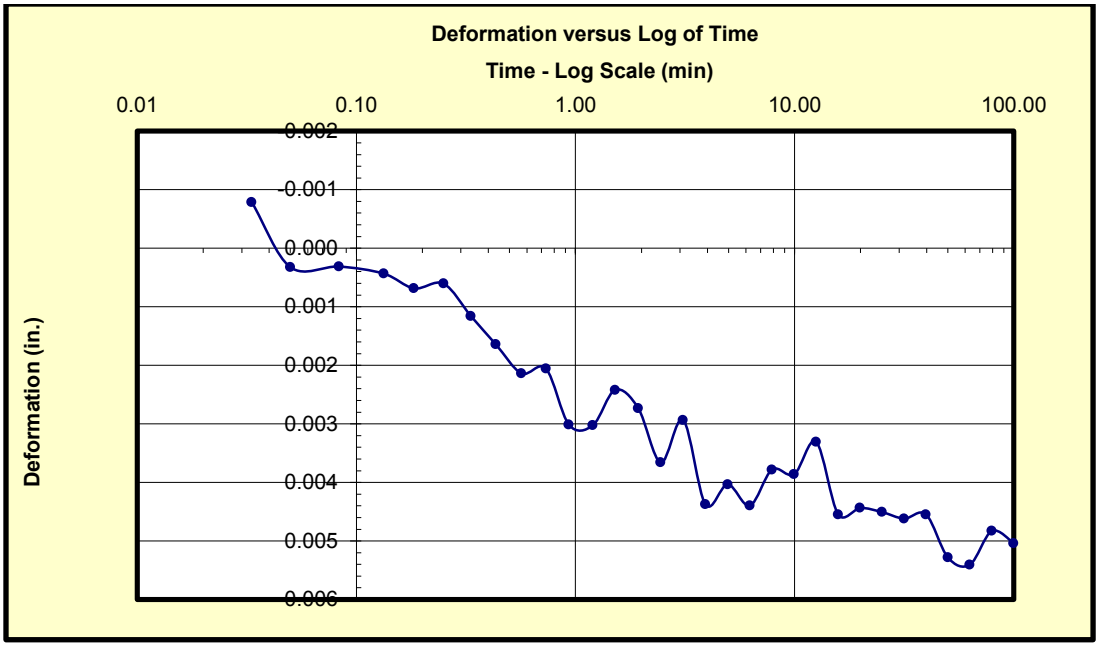

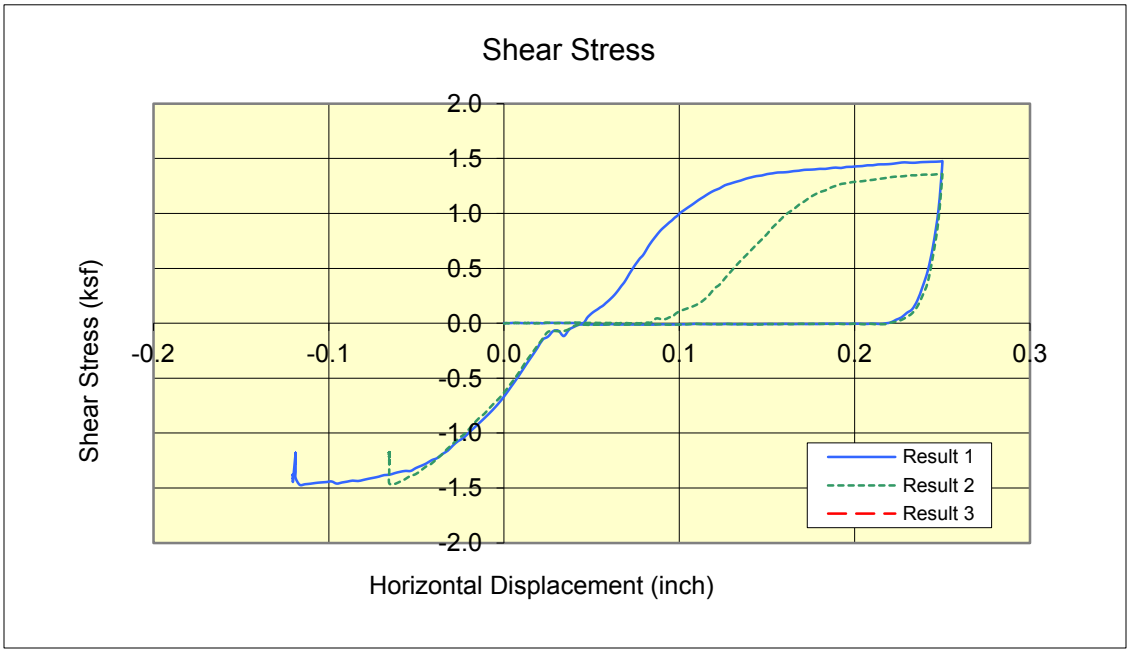

Figure 4.17: Deformation vs time and shear stress vs horizontal displacement graphs produced during direct shear testing of sample LG with a normal load of 2000 lbs/ft^2 (lbs/ft^2 = psf and 1000 psf = 1 ksf).

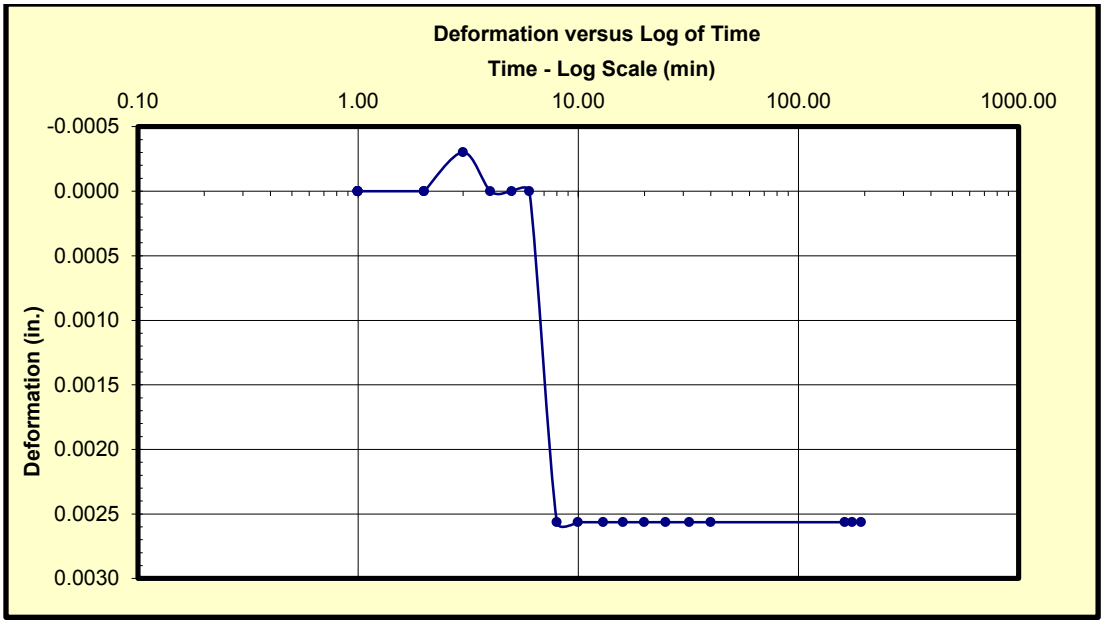

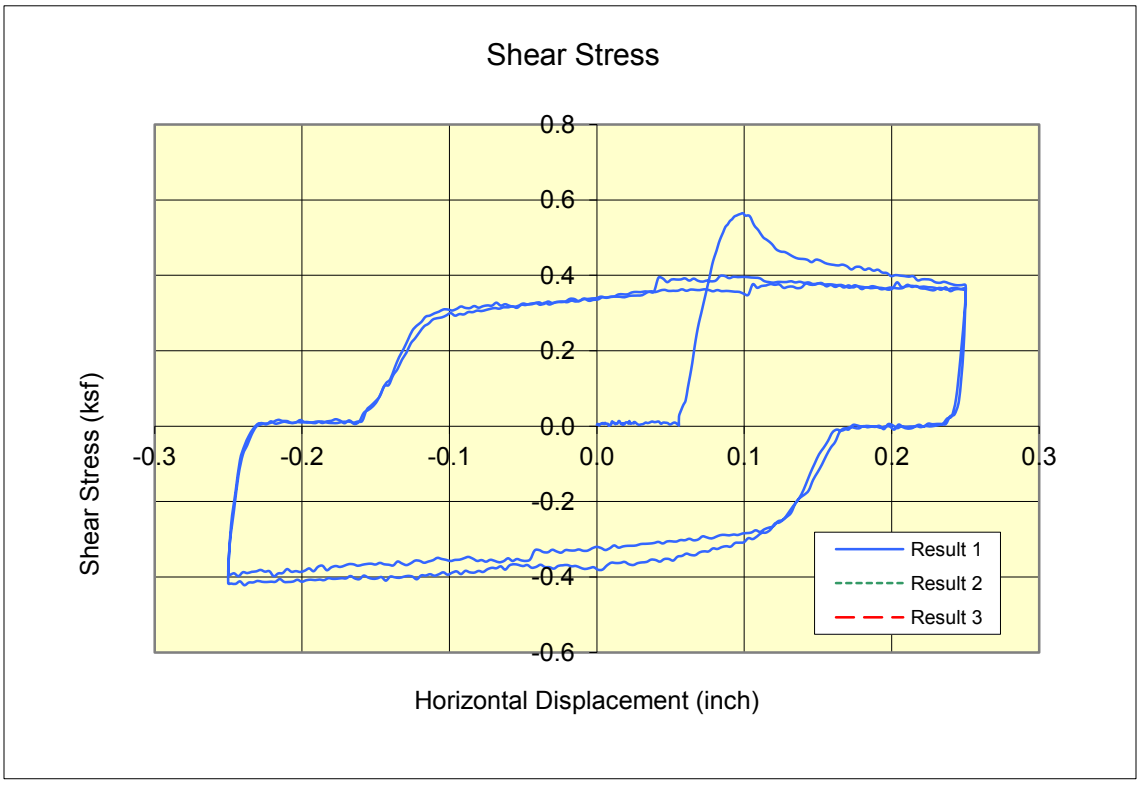

Figure 4.18: Deformation vs time and shear stress vs horizontal displacement graphs produced during direct shear testing of sample CR6 with a normal load of 500 lbs/ft^2 (lbs/ft^2 = psf and 1000 psf = 1 ksf).

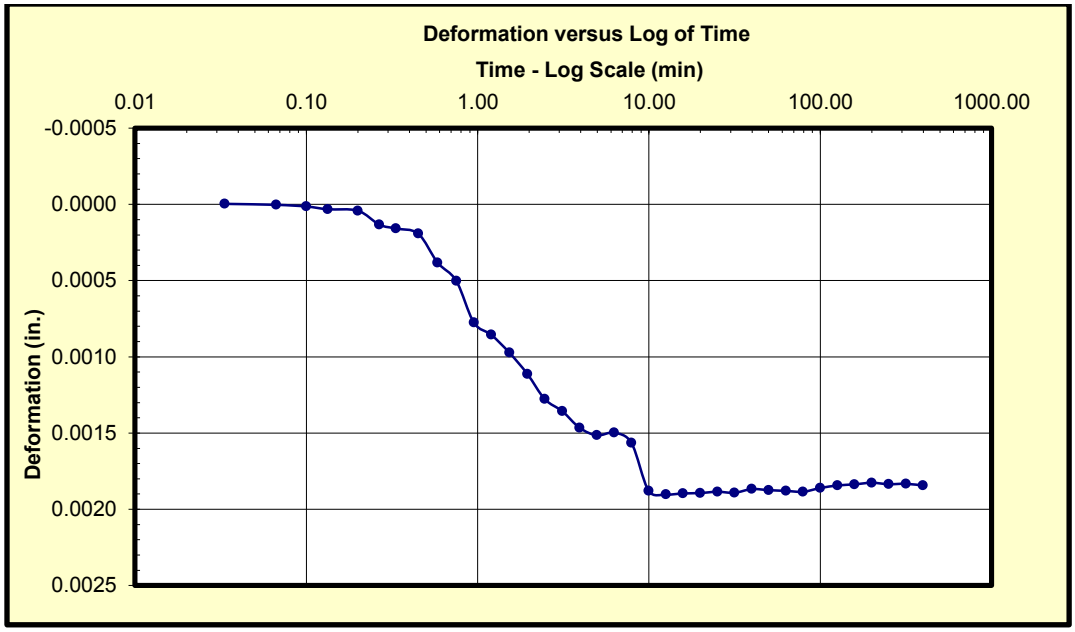

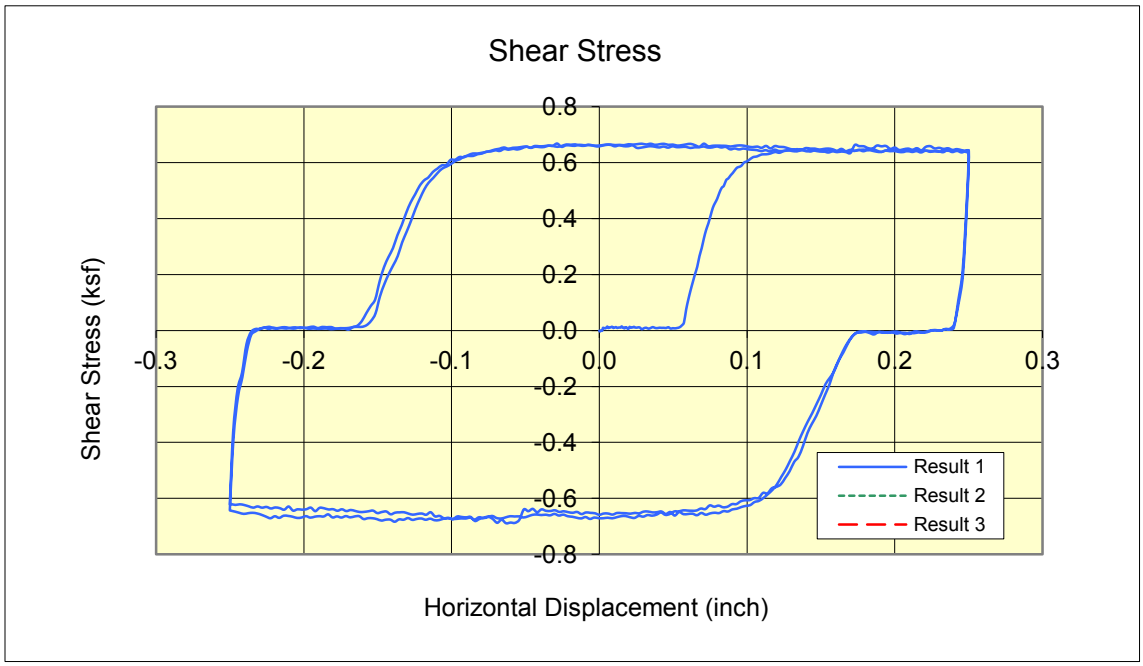

Figure 4.19: Deformation vs time and shear stress vs horizontal displacement graphs produced during direct shear testing of sample CR6 with a normal load of 1000 lbs/ft^2 (lbs/ft^2 = psf and 1000 psf = 1 ksf).

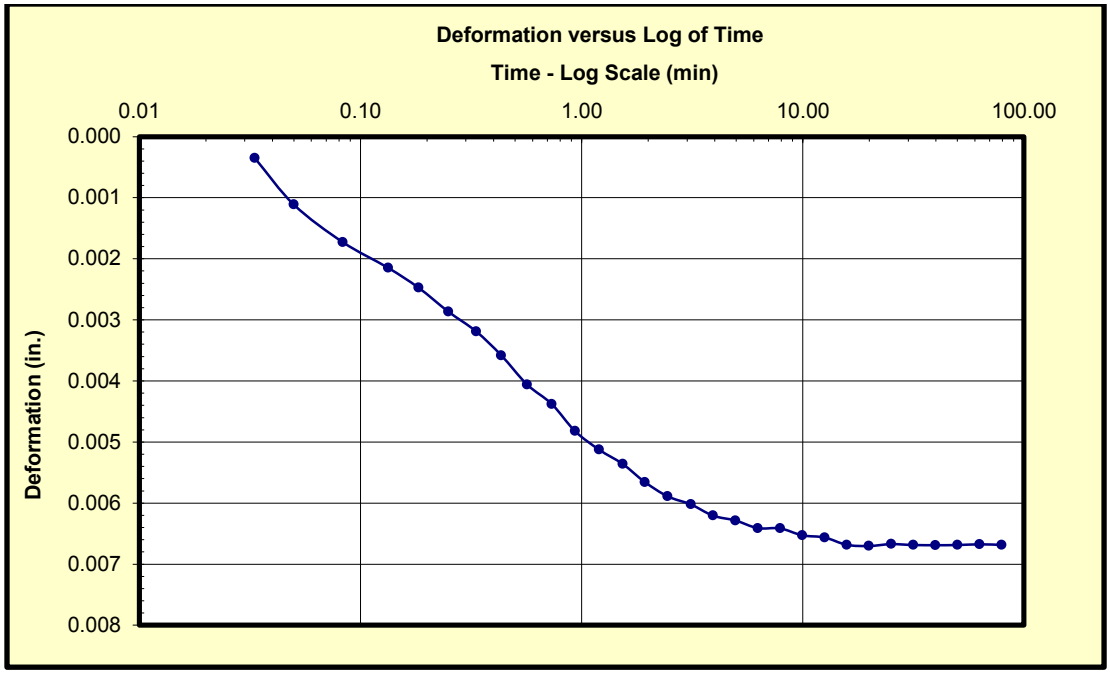

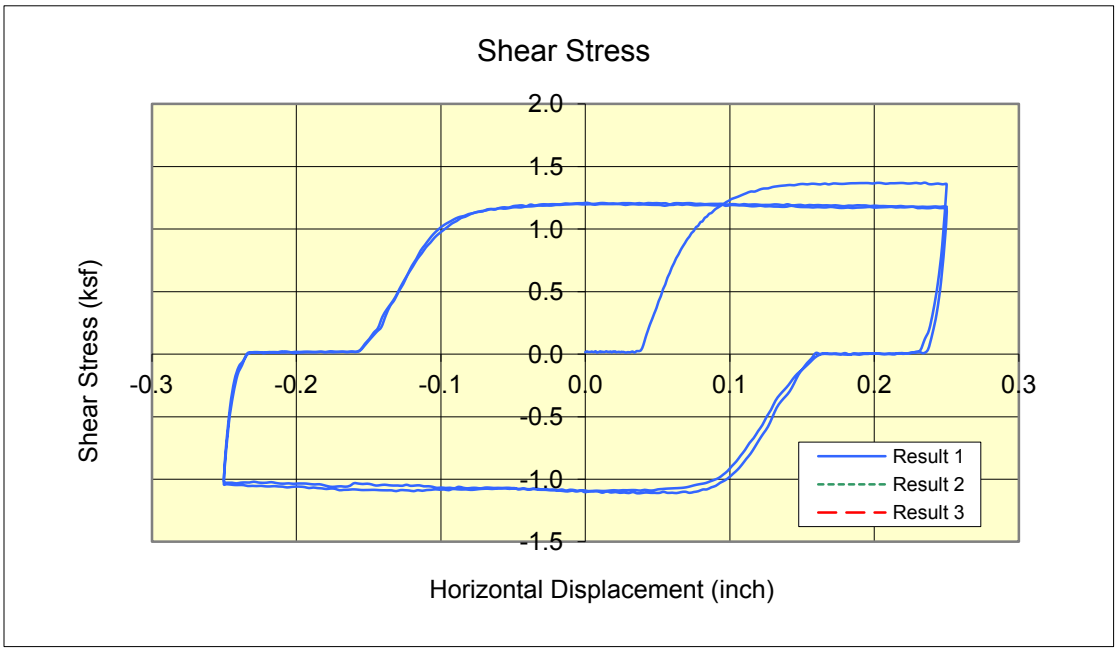

Figure 4.20: Deformation vs time and shear stress vs horizontal displacement graphs produced during direct shear testing of sample CR6 with a normal load of 2000 lbs/ft^2 (lbs/ft^2 = psf and 1000 psf = 1 ksf).

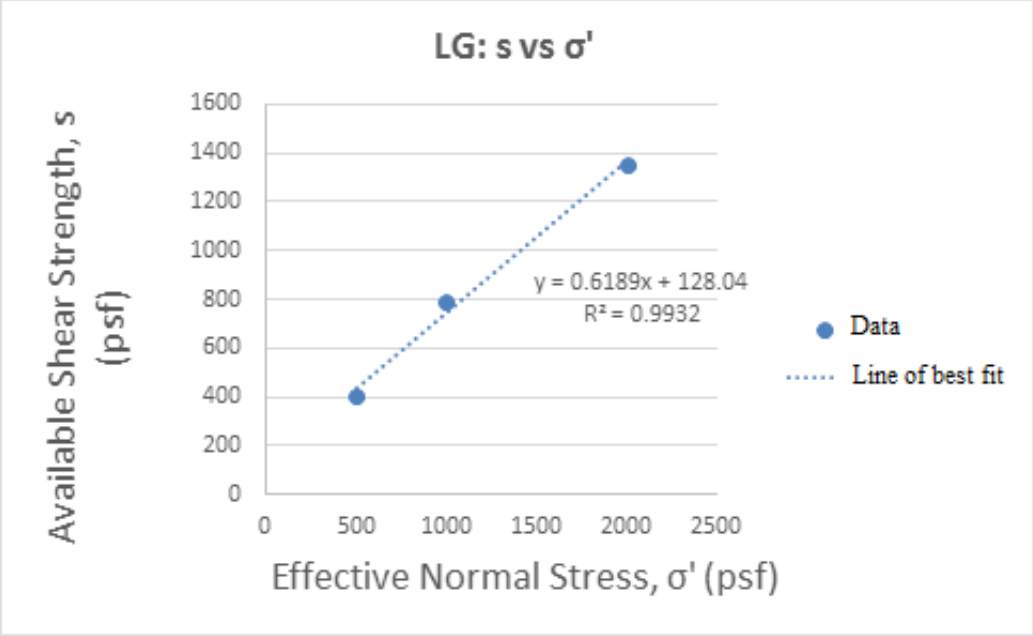

Figure 4.21: Plot of shear strength versus effective normal stress for LG.

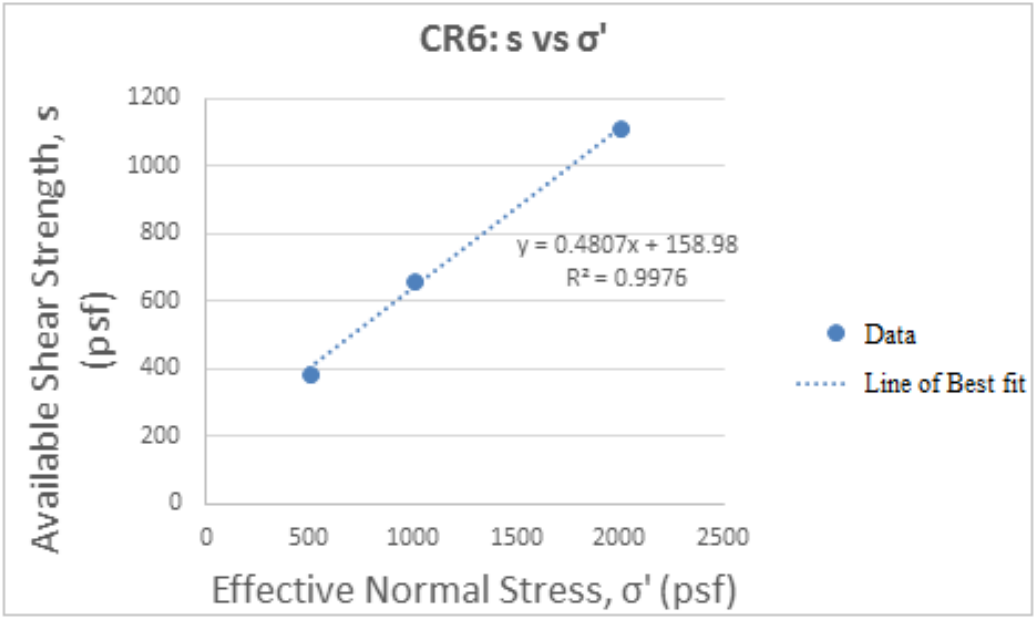

Figure 4.22: Plot of shear strength versus effective normal stress for CR6.

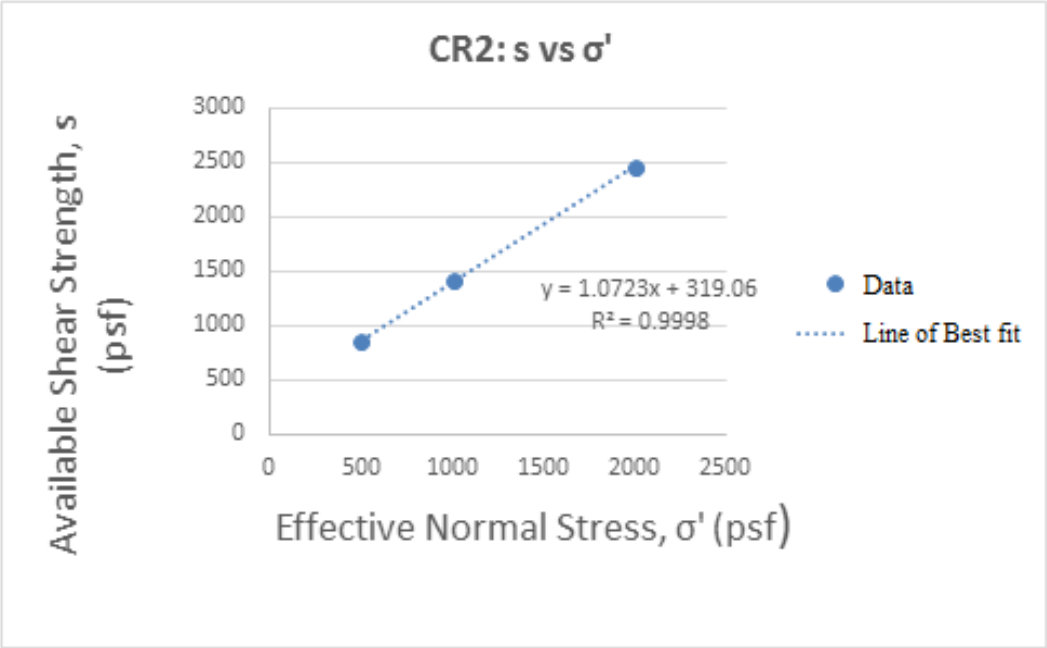

Figure 4.23: Plot of shear strength versus effective normal stress for CR2.

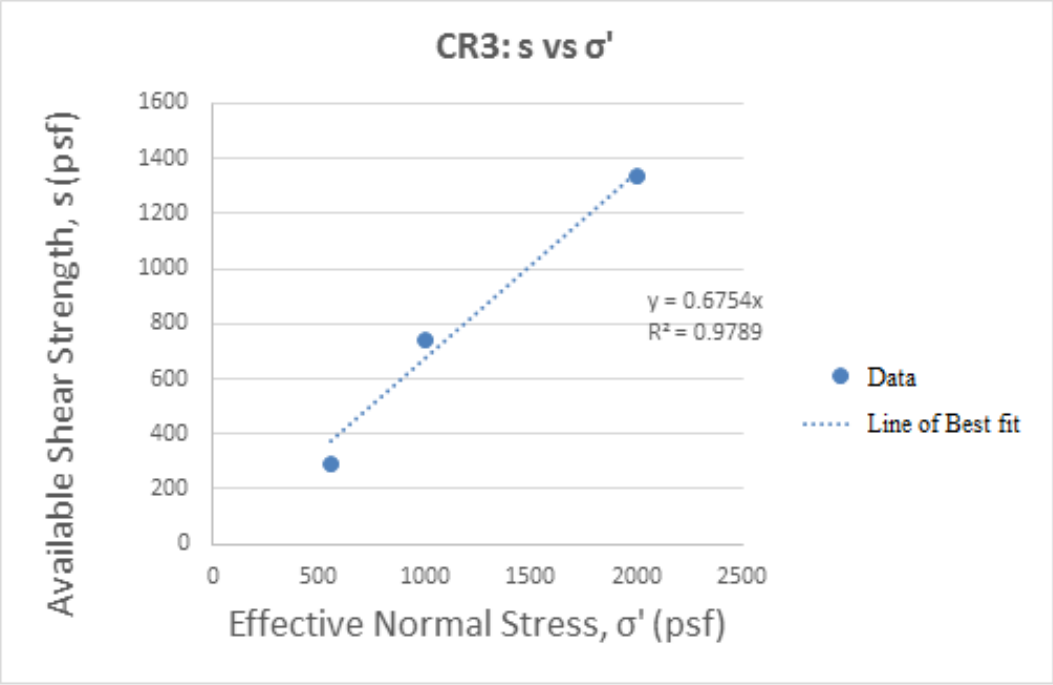

Figure 4.24: Plot of shear strength versus effective normal stress for CR3.

Limit Equilibrium Analysis

Forward calculation during the infinite slope analysis for LG yielded a FS value much greater than 1 under seepage conditions, so failure is not predicted for LG. LG will still be included in the back calculations and the ϕ' and z_w results will be treated as a prediction for if LG ever does fail. Back calculations yielded friction angles of 36˚ for all four slopes under general conditions and an average friction angle of 62˚ for seepage conditions (Table 4.10). The depth above or below the failure surface that the water table reached before failure, z_w, differed for each site, but results show that when failure occurred, the water table was above the failure surface at the Forested Site but below the failure surface at the Lemongrass Site (Table 4.10). Since LG is the only slope that had not recently failed in this study, the z_w value is a prediction of where the water table might be if failure occurs. The failure depth, z, used in that calculation is also a prediction based off of the failure depth for CR6. Since CR6 and LG are adjacent to each other, composed of similar material, and covered in the same vegetation then it is plausible to assume that LG would fail in a similar way to CR6.

Site	ϕ' when u= 0	ϕ' when $u= \gamma_w z\cos^2\beta$	ϕ' from direct shear	Depth to failure, z	Depth to water table, z_w	Study Site
LG	36˚	61.8˚	31.8˚	5 ft	-1.18 ft	Lemongrass
CR6	36˚	60.75˚	25.7˚	5 ft	-4.30 ft	Lemongrass
CR2	36˚	62.39˚	47˚	2 ft	+1.04 ft	Forested
CR3	36˚	64.22˚	47˚	2 ft	+0.99 ft	Forested

Table 4.10: The results of ϕ' and z_w from the slope stability analysis.

CHAPTER FIVE

DISCUSSION AND CONCLUSION

The soil at the study sites is halloysite rich, thus they belong to the kandoid soils group. Using the classification of Rouse et al. (1986), this soil would be expected to have moderate and continuous leaching with relatively high permeability for clay soils. These soils are also associated with the oldest volcanic areas of the island and that was confirmed by the presence of basalt bedrock along Cochrane Road. Soil characterization determined that the soil at both sites had a medium to high plasticity and a consistent color hue of 7.5YR

Vane shear testing of slope LG at the Lemongrass Site determined that the in-situ undrained shear strength varies with depth. After examining the data from sample sites LGa, LGb, and LGd, a noticeable pattern emerged. Between depths of 4 and 6 ft, there was a drop in shear strength which suggests a zone within the slope that is weaker than the zones above and below it. This depth of 4-6 ft coincides with the depth of the failure surface (about 5 ft) at CR6, which is directly adjacent to LG. It is therefore plausible to assume that before CR6 failed, it also had a weaker zone between 4 and 6 ft depths. This depth also coincides with the bottom of the lemongrass root mat which would cause a reduction in soil strength.

At the Lemongrass Site, LG and CR6 samples were collected about 11 feet apart and at the Forested Site, CR2 and CR3 samples were collected about 15 feet apart. Given their close proximity and similar clay mineralogy, it was anticipated that the samples from the respective sites would have similar direct shear results, but this was not the case.

When comparing results from the LG and CR6 samples, the LG sample had slightly higher shear strength which resulted in a higher effective friction angle. When comparing shear strength values for the CR2 and CR3 samples, the CR2 sample had twice as high shear strength values as CR3. The CR2 slide occurred on and cut into the CR3 slide, and the CR2 sample was collected at a lower relative depth than the CR3 sample. The higher shear strength of the CR2 sample could suggest that the material underneath the CR2 slide surface is stronger than the material on the CR3 slide surface and the material that failed at CR2. The line of best fit on the shear strength vs effective normal stress graph for CR3 was initially showing a negative y-intercept and therefore negative effective cohesion. Cohesion cannot be negative, so the line was forced to an intercept of zero and cohesion of zero. The slope of this line ended up being the same as the CR2 slope, so both sites have the same effective friction angle. Since the line had to be forced to zero, the effective friction angle for CR3 is uncertain and so are the results for the CR3 infinite slope analysis. There were problems with the CR2 sample during the direct shear test. The sample compressed non-uniformly (more on one side than the other) which might explain why the shear strength values were considerably different from the CR3 values. Another possible source of uncertainty is that during direct shear testing, some tests (noted on Table 4.8) were sheared at a faster rate than the recommended ASTM standards due to time constraints and problems with the machine. If the shear rate is too fast, the soil can expand and shear strength can be overestimated (Wright, 2005). Reading (1991) concludes that laboratory values of residual shear strength are inconsistent, frequently low, and easily affected by test type and sample preparation. Additional work might

resolve the uncertainty by conducting the direct shear tests at the recommended ASTM rate. This was not done due to time constraints and limited access to the testing equipment.

The slope failure analysis indicates that under general conditions (water table is at the same elevation as the failure surface) the effective friction angle for all slopes must be greater than 36˚ for the slope to remain stable. Under seepage conditions (water table is at the same elevation as the ground surface), the effective friction angle must be on average greater than 62˚ for the slope to remain stable. It is highly unlikely that any slope would have a friction angle as high as 62˚, so it is concluded that the slopes would fail under seepage conditions. If slope failure occurs after prolonged rain but the water table did not reach the ground surface, then ϕ' is between 36˚ and 62˚. At the Lemongrass Site, the water table reached a depth around 4.3 ft below the failure surface when failure occurred. It can be inferred that failure occurred before general conditions (water table is at the failure surface) were reached. At the Forested Site, the water table reached an average depth of 1 ft above the failure surface when failure occurred. For this site, it can be inferred that failure occurred somewhere between general conditions and seepage conditions. In other words, failure occurred when the water table had risen to an elevation between the failure surface and ground surface. Sources of uncertainty in the infinite slope analysis could be from the soil density measurements. These numbers were calculated from the direct shear soil samples, which may not be indicative of the entire slope, just the specific area around where the sample was taken from. Additionally, these

samples were taken from directly beneath the failure surface in the field and that material may have been different than the failed material.

In mid-September of 2017 after this study was completed, Dominica was hit by Hurricane Maria, a category 5 hurricane that devastated the island with up to 160 mph winds and intense flooding. A report from NOAA (National Oceanic and Atmospheric Administration) said expected total rain accumulations in the area of the Windward Islands were 2 to 4 inches with maximum amounts of 8 inches in some isolated areas. This is comparable to Hurricanes David and Frederic that passed over Dominica in 1979. Both of those storms caused many landslides. Hurricane Maria impacted the study area as indicated by aerial photographs taken after the storm.

REFERENCES

Andereck, Z.D. (2007). Mapping vulnerability of infrastructure to destruction by slope failures on the island of Dominica, WI: A case study of Grand Fond, Petite Soufriere, and Mourne Jaune. (Electronic Thesis). Retrieved from http://etd.ohiolink.edu/

Anderson, M.G., Holcombe, E., Blake, J.R., Ghesquire, F., Holm-Nielsen, N., & Fisseha, T. (2011). Reducing landslide risk in communities: Evidence from the Eastern Caribbean. *Applied Geography*, 31(2): 590-599.

Cooper, R.G. (2007) Mass Movements in Great Britain, Geological Conservation Review Series, No. 33, Joint Nature Conservation Committee, Peterborough, 348 pp.

Corps of Engineers. (1970). "Laboratory Soils Testing." *Engineer Manual EM 1110-2-1906*, Department of the Army, U.S. Army Corps of Engineers, Washington, D.C., November 1970 with Change 1 dated May 1980.

Crunden, D.M. (1991). A simple definition of a landslide. *Bulletin of the International Association of Engineering Geology.* 43: 27-29

DeGraff, J. V., Bryce, R., Jibson, R. W., Mora, S., & Rogers, C. T. (1989). "Landslides: their extent and significance in the Caribbean." *Landslides: Extent and economic significance*, *68*.

Faugeres, M.L. (1966). Obsercations dur le modele des versants dans la refion des Pitons du Garbet (Martinique). Assoc. Geographes Francais Bull. 342-343: 52-63.

Google Maps. (2017). "*Archibold Tropical Research and Education Center*." Retrieved from https://www.google.com/maps/place/Archbold+Tropical+Research+and+Education+Center+(ATREC)/@15.4160898,-61.1954148,10.7z/data=!4m12!1m6!3m5!1s0x8c14d48b6e15c8f3:0x3c33c1f878e55a3b!2sArchbold+Tropical+Research+and+Education+Center+(ATREC)!8m2!3d15.3466901!4d-61.3686985!3m4!1s0x8c14d48b6e15c8f3:0x3c33c1f878e55a3b!8m2!3d15.3466901!4d-61.3686985

He, H., Barr, T., Klinowski, J. (1995). ESCA and solid-state NMR studies of allophane. *Clay Minerals*, 30: 201-209.

Huang, Y.H. (2014). *Slope stability analysis by the limit equilibrium method*. Reston, VA: ASCE Press.

Joussein, E., Petit, S., Churchman, J., Theng, B., Righi, D., & Delvaux, B. (2005). Halloysite clay minerals- a review. *Clay Minerals*, 40: 383-426.

Matthews, C., Farook, Z. & Helm, P.R. (2014). Slope stability analysis – limit equilibrium or the finite element method? Technical Paper. *Ground Engineering*. May. pp. 22-28.

Mesri, G. & Huvaj-Sarihan, N. (2012). Residual shear strength measured by laboratory tests and mobilized in landslides. *Journal of Geotechnical and Geoenvironmental Engineering*, Vol. 138, Issue 5.

Moore, D. M., & Reynolds, R. C. (1997). X-ray diffraction and the identification and analysis of clay minerals. Oxford: *Oxford Univ. Press*.

Ogden, F.L. (2016). Evidence of equilibrium peak runoff rates in steep tropical terrain on the island of Dominica during Tropical Storm Erika, August 27, 2015. *Journal of Hydrology*, 542: 35-46.

Poppe, L., Paskevich, V., Hathaway, J., Blackwood, D. (n.d.). A Laboratory Manual for X-Ray Powder Diffraction. Retrieved January 05, 2018, from https://pubs.usgs.gov/of/2001/of01-041/index.htm

Prior, D.B. & Ho, C. (1972). Coastal and mountain slope instability on the islands of St. Lucia and Barbados. *Eng. Geol.*, 6: 1-18.

Reading, A.J. (1991). Stability of tropical residual soils from Dominica, West Indies. *Eng. Geol.,* 31: 27-44.

Rouse, C. (1990). The mechanics of small tropical flowslides in Dominica, West Indies. *Eng. Geol.,* 29: 227-239.

Rouse, W.C., Reading, A.J., & Walsh, R.P.D. (1986). Volcanic soil properties in Dominica, West Indies. *Eng. Geol.,* 23: 1-28.

Schematic diagram of a direct shear box. Digital Image. *IIT Gandhinagar*. N.d. Web.. 5 Dec 2017. < iitgn.ac.in >.

"shear strength." A Dictionary of Earth Sciences. Retrieved November 02, 2017 from Encyclopedia.com: http://www.encyclopedia.com/science/dictionaries-thesauruses-pictures-and-press-releases/shear-strength

Singh, V. & Agrawal, H.M. (2012). Qualitative soil mineral analysis by EDXRF, XRD, and AAS probes. *Radiation Physics and Chemistry*, 81:1796-1803.

Siqueira, R.E., Andrade, M.M., Valezi, D.F., Carneiro, C.E.A., et al. (2011). EPR, FT-IR and XRD investigation of soils from Parana, Brazil. *Applied Clay Science*, 53: 42-47.

Six, J., Feller, C., Denef, K., Ogle, S., de Moraes Sa, J.C., et al. (2002). Soil organic matter, biota and aggregation in temperate and tropical soils - Effects of no-tillage. Agronomie, *EDP Sciences*, 22 (7-8): 755-775. <10.1051/agro:2002043>. <hal-00885974>

Thiel, R.T. (2001). Peak versus residual shear strength for landfill bottom liner stability analyses. *Proceedings 15th GRI conference, Houston*: 40-70.

Van Westin, C.J. (2016). National scale landslide susceptibility assessment for Dominica. CHARIM Caribbean Handbook on Risk Information Management, World Bank GFDRR, ACP-EU Natural Disaster Risk Reduction Program.

Wallace, K.B. (1973). Structural behavior of residual soils of the continually wet highlands of Papua New Guinea. *Geotechnique*, 23: 203-18

Walsh, R.P.D. (1985). The influence of climate, lithology, and time on drainage density and relief development in the volcanic terrain of the Windward Islands. In I. Douglas & T. Spencer (eds.), *Environmental Change and Tropical Morphology*, p. 93-122. London: Allen & Unwin.

Wesley, L.D. (1977). Shear strength properties of halloysite and hallophane clays in Java, Indonesia. *Geotechnique*, 73: 125-36.

Wright, S.G. (2005). Evaluation of soil shear strengths for slope and retaining wall stability analyses with emphasis on high plasticity clays (Report No. FHWA/TX-06/5-1874-01-1). Austin, TX. Texas Department of Transportation Services.

Yifru, J. (2015). National scale landslide hazard assessment along the road corridors of Dominica and Saint Lucia. Master of Science, University of Twente.